MESOSCOPIC STRUCTURES AND QUANTUM OPTICAL PROPERTIES OF InAs/GaAs AND $Al_xGa_{1-x}P/Al_yGa_{1-y}P$ SEMICONDUCTORS

FEBRUARY 1996

YOICHI NABETANI

Acknowledgments

The author would like to express his sincere gratitude to Prof. Akio Sasaki for providing the opportunity and continuous support to this work. The author also deeply acknowledges to Prof. Hiroyuki Matsunami and Prof. Shigeo Fujita for their valuable comments, suggestions and corrections on this manuscript. He is grateful to Associate Prof. Susumu Noda and Dr. Akihiro Wakahara for their helpful suggestions and fruitful discussions throughout of this work. He is also grateful to Mr. Toyotsugu Ishibashi for his support.

Special thanks are due to Mr. Masao Tabuchi at Nagoya University for his helpful advice and pioneering work, from which this work has originated.

The author is also grateful to Associate Prof. Shizuo Fujita for his valuable discussion and advice on TEM observation.

The author would like to thank to Prof. Jack Washburn, Prof. Zusanna Liliental-Weber, Prof. Eicke. R. Weber and Dr. X. Wei Lin at Lawrence Berkeley Laboratory for their fruitful discussions on TEM observation.

He is also much obliged to Messrs. Tsutomu Ishikawa, Noritugu Yamamoto and Takashi Tokuda for their contribution to this work. He also wishes to express gratitude to Dr. Xue Lung Wang for his advice on OMVPE apparatus. He also thanks to Messrs. Kazuyuki Uno and Yoshitaka Hasegawa for their fruitful discussions on disordered superlattices. He is grateful to Messrs. Takashi Asano, Yuzo Furukawa and all other members of Sasaki Laboratory.

This work was partly supported by a Grant-in-Aid #04227107 for Scientific Research on Priority Areas "Crystal Growth Mechanism in Atomic Scale" from the Ministry of Education, Science and Culture of Japan.

Finally, the author really would like to thank his parents for their heartful encouragements and supports.

Contents

Chapter 1

Introduction

Mesoscopic structure of semiconductor has been extensively interested in fabricating new devices based on quantum confinement effects. It is well known that electrons and holes cannot move freely and their energy states are quantized in a mesoscopic structure, in other words, quantum structure [1]. Modified energy state in a quantum structure of semiconductor leads to optical and electrical properties which are different from bulk semiconductor. This means that energy state can be tailored for desired devices specification by controlling the structure size and selecting suitable materials as having appropriate band structures. It has been theoretically and experimentally shown that the threshold current of laser diode(LD) with quantum well(QW) as an active layer is much lower than that of conventional LD [2,3]. Frequency fluctuations and threshold current variations dependence on temperature can be stabilized by quantum effects, because the density of states(DOS) becomes sharper in the quantum structures [4,5]. The change in DOS is especially remarkable in low dimensional quantum structures such as quantum well wire(QWW) and quantum dot(QD).

Fabrication of quantum structures has employed mainly III-V semiconductors. Since III-V semiconductors are composed of two chemical elements, several varieties of III-V semiconductors can be made by changing the combination of group III and group V elements. Furthermore, it is possible to make up alloy

semiconductors which are compound solid solutions of more than two kinds of semiconductors. Optical and electrical properties of alloy semiconductor can be continuously changed by controlling composition of group III and/or group V elements. From a view point of device application, large variation and flexibility of properties are attractive for material selection. Another advantage of III-V semiconductors is their band structures. They can be utilized for light-emitting devices, since some of III-V semiconductors have direct band gap structures.

Thus far, III-V semiconductor QWs have been extensively fabricated and investigated their optical and electrical properties since novel growth techniques were developed. There are two typical crystal growth techniques that can control the interface as precise as monolayer(ML) order. One method is molecular beam epitaxy(MBE) [6] and another is organometallic vapor phase epitaxy(OMVPE) [7]. Because the material composition is modulated along only one dimension in QW, fabrication of QW is much easier than other quantum structures.

Although MBE and OMVPE can control the composition in the growth direction, it is impossible to change composition in a growth plane which means that the fabrication of QWW and QD is considerably difficult. Some preparations to pattern a substrate surface must be involved before growth to make quantum structures which have lateral confinement ability. For example, wet or dry etching is required to pattern a substrate on which an epitaxial layer is grown [8,9]. Ion beam implantation is also used [10]. These methods, however, bring contamination or mechanical damage induced during the surface process stage. Moreover, the size of quantum structures fabricated by these methods is limited by the spatial resolution of lithographic techniques or ion beam diameter that is mostly sub-micro meter. Quantum effect is hardly expected by such a large size structure. Another growth method of low dimensional structure called fractional layer superlattice(FLS) were suggested [11,12]. FLS is a kind of QWW structures and grown on misoriented substrate using step flow growth mode. By growing epitaxial layer at the surface step, one can control the composition in the lateral direction. However, this growth method is applied only for QWW.

Some experiments to make QD by growing on misoriented substrate have been reported [13]. However, no expected results were obtained because appropriate surface step structure for QD formation does not exist.

Another important problem in the present crystal growth techniques is lattice-mismatch. In a lattice-mismatched system, it is known that epitaxial layer does not grow two-dimensionally but three-dimensionally and then island is formed. The island formation is not desirable to control abrupt interface. Moreover, misfit dislocation is generated when the epitaxial layer thickness exceeds the critical thickness to release the strain accommodated in epitaxial layer [14]. Since most of misfit dislocations deteriorate the optical and electrical properties of semiconductor, the epitaxial layer for device applications should be free from dislocation. As a result, selectivity of the epitaxial layer becomes very small once the substrate is fixed. From this back ground, many works to investigate initial growth stage of lattice-mismatched heteroepitaxy have been carried out. It is also investigated that the suppression of dislocation generation by patterning the substrate [15,16] or of dislocation propagation by inserting strained layer superlattices [17-19].

Although island growth becomes an obstacle to obtain smooth interface, this three-dimensional structure can be used as a QD by changing point of view. Our group have suggested the utilization of coherently grown island in lattice-mismatched heteroepitaxy as a QD for the first time [20]. Not only suggestion, but also we have grown defect free nano-scale island and investigated its optical property [20-22]. Merits of QD formation by island growth are followings:

1. QDs are formed without any complicated processes and free from contamination.

2. Size of QD is as small as several hundred Å , hence the spatial filling factor becomes as large as $10^{11}cm^{-2}$.

3. QD plane can be stacked easily.

Comparing QWW or QD, quantum effect expected from QW or superlattice(SL) is not high, because carriers are quantized in only one dimension. How-

ever, A. Sasaki et al. has proposed a completely different type of quantum structure called disordered crystalline semiconductor to enhance quantum effect [23]. A disordered superlattice(d-SL) is an example of disordered crystalline semiconductor and has ability to improve the luminescence efficiency of indirect band gap semiconductors, such as SiGe, AlGaAs and AlGaP [24-33]. In a d-SL, two constituent materials have a random arrangement in the layer thickness in contrast to a conventional ordered superlattice(o-SL) in which the arrangement of two materials are regularly ordered. The enhanced luminescence efficiency of d-SL has been discussed in terms of carrier localization induced by a disordered material arrangement. The carrier localization caused by artificially disordered structure is not only unique and interesting physical phenomena but also important for device application. Especially, AlGaP has the largest band gap in the zincblende structured III-V semiconductors and expected for the material of light-emitting device of green to orange region(506~600nm). It is necessary to enhance the luminescence efficiency of AlGaP to utilize for the light-emitting devices because of the indirect band gap. AlP/GaP short period o-SL using zone-folding and band-mixing effects is one of the method to improve luminescence efficiency. Theoretical prediction indicated that band structure of AlP/GaP o-SL becomes direct band gap [34-37]. Some experimental approaches have shown the luminescence from AlP/GaP o-SL [38-51]. On the other hands, the former investigation of AlP/GaP d-SL revealed that the luminescence intensities from d-SLs are several times larger than those from o-SLs [30]. However, the luminescence wavelength of pure green region was not realized due to type-II structure. Since band gap of AlGaP system is large enough to emit pure green light, further improvement of luminescence efficiency and reduction of luminescence wavelength of AlGaP semiconductor by d-SL structure are considerably stimulative.

The purpose of this thesis is to realize new quantum optical properties by new approach of mesoscopic structures in semiconductor. Two mesoscopic quantum structures are investigated: 1) investigation of structure and quantum optical

property of self-assembled QD in InAs/GaAs lattice-mismatched heteroepitaxy and 2) enhancement of luminescence efficiency and reduction of luminescence wavelength of AlGaP d-SL.

This thesis is constructed by eight chapters and divided into two parts by the kind of quantum structure. The first part is chapter 2~5 and is devoted to the fabrication and characterization of QD by island formation of InAs/GaAs lattice-mismatched heteroepitaxy. In chapter 2, the structure of initial growth layer of InAs/GaAs is characterized. The island shape and size are intensively investigated by various techniques. Theoretical approach of island formation is shown in chapter 3. The results become a guide for the selection of materials to fabricate a self-assembled QD. In chapter 4, optical property of InAs grown structure is investigated to examine whether the island has a nature of QD. Chapter 5 deals with the dislocation suppression by introducing misoriented substrates. The demonstration of dislocation suppression is shown both experimentally and theoretically by calculating the strain energy in epitaxial layer.

The second part is chapter 6 and 7, dealing with AlGaP d-SLs. In chapter 6, the period of AlP/GaP d-SL is changed and investigated the dependence of optical property on SL period. In chapter 7, $Al_xGa_{1-x}P/Al_yGa_{1-y}P$ o- and d-SLs are fabricated to obtain enhanced luminescence of shorter wavelength. The results of structural and optical characterization are described. Finally the conclusions and some suggestions are summarized in chapter 8.

References

1) For example, R. Dingle, *Semiconductor and semimetals* vol.24.

2) W.T. Tsang and R.L. Hartman, Appl. Phys. Lett. **38**, 502 (1981).

3) W.T. Tsang, Appl. Phys. Lett. **39**, 785 (1981).

4) Y. Arakawa and H. Sakaki, Appl. Phys. Lett. **40**, 939 (1982).sakaki

5) Y. Arakawa, K. Vahara, and A. Yariv, Appl. Phys. Lett. **45**, 950 (1984).

6) F.V. Williams, R.A. Ruehrwein, J. Electrochem. Soc. **108**, 177C (1961).

7) H.M. Manasevit and W.I. Simpson, J. Electrochem. Soc. **116**, 1725 (1969).

8) B.I. Miller, A. Shahar, U. Koren, and P.J. Corvini, Appl. Phys. Lett. **54**, 188 (1989).

9) K. Kash, A. Scherer, J.M. Worlock, H.G. Craighead, and M.C. Tamargo, Appl. Phys. Lett. **49**, 1043 (1986).

10) J. Cibert, P.M. Petroff, G.J. Dolan, S.J. Pearton, A.C. Gossard, and J.H. English, Appl. Phys. Lett. **49**, 1275 (1986).

11) T. Fukui and H. Saito, J. Vac. Sci. Technol. **B6**, 1373 (1988).

12) J.M. Gaines, P.M. Petroff, H. Kroemar, R.J. Simes, R.S. Geels, and H. English, J. Vac. Sci. Technol. **B6**, 1378 (1988).

13) O. Brandt, L. Tapfer, K. Ploog, R. Bierwolf, M. Hohenstein, E. Phillipp, H. Lage, and A. Heberle, Phys. Rev. **B44**, 8043 (1991).

14) J.H. Van der Merwe, J. Appl. Phys. **34**, 117 (1963).

15) N. Hayafuji, H. Kizuki, M. Miyashita, K. kadoiwa, T. Nishimura, N. Ogasawara, H. Kumabe, T. Murotani, and A. Tada, Jpn. J. Appl. Phys. **30**, 459 (1991).

16) K. Ismail, F. Legoues, N.H. Karam, J. Carter, and H.I. Smith, Appl. Phys. Lett. **62**, 2711 (1993).

17) R. Fischer, D. Neuman, H. Zabel, H. Morkoc, C. Choi, and N. Otsuka, Appl. Phys. Lett. **48**, 1223 (1986).

18) T. Nishimura, K. Mizuguchi, H. Hayafuji, and T. Murotani, Jpn. J. Appl. Phys. **27**, L1141 (1987).

19) Y. Okuno and T. Kawano, J. Cryst. Growth **145**, 338 (1994).

20) M. Tabuchi, S. Noda, and A. Sasaki, in *Science and Technology of Mesoscopic Structures*, edited by S. Namba, C. Hamaguchi, and T. Ando (Springer, Tokyo 1992), p.379, paper presented at 1st Int. Symp. Sci. and Technol. of Mesoscopic Structures (Nov.6-8, 1991, Nara, Japan) p.18.

21) Y. Nabetani, T. Ishikawa, S. Noda, and A. Sasaki, J. Appl. Phys. **76**, 347 (1994).

22) Y. Nabetani, N. Yamamoto, T. Tokuda, and A. Sasaki, J. Cryst. Growth **146**, 363 (1995).

23) A. Sasaki. M. Kasu, and S. Noda, Jpn. J. Appl. Phys. **28**, L1249 (1989).

24) M. Kasu, T. Yamamoto, S. Noda, and A. Sasaki, Jpn. J. Appl. Phys. **29**, 828 (1990).

25) M. Kasu, T. Yamamoto, S. Noda, and A. Sasaki, Jpn. J. Appl. Phys. **29**, L1055 (1990).

26) M. Kasu, T. Yamamoto, S. Noda, and A. Sasaki, Jpn. J. Appl. Phys. **29**, L1588 (1990).

27) T. Yamamoto, M. Kasu, S. Noda, and A. Sasaki, J. Appl. Phys. **68**, 5318 (1990).

28) M. Kasu, T. Yamamoto, S. Noda, and A. Sasaki, Appl. Phys. Lett. **59**, 800 (1991).

29) A. Sasaki, J. Cryst. Growth **115**, 490 (1991).

30) X.L. Wang, A. Wakahara, and A. Sasaki, Appl Phys. Lett. **62**, 888 (1993).

31) A. Wakahara, T. Hasegawa, K. Kuramoto, K.K. Vong, and A. Sasaki, Appl. Phys. Lett. **64**, 1850 (1994).

32) X.L. Wang, A. Wakahara, and A. Sasaki, Appl. Phys. Lett. **64**, 2016 (1994).

33) K. Uno, S. Noda, and A. Sasaki, J. Appl. Phys. **77**, 4693 (1995).

34) J.Y. Kim and A. Madhukar, J. Vac. Sci. Technol. **21**, 528 (1982).

35) M.F.H. Schuurmans, H.W.A.M. Rompa, and R. Eppenga, J. Lumin. **37**, 269 (1987).

36) M. Kumagai, T. Takagahara, and E. Hanamura, Phys. Rev. **B37**, 898 (1988).

37) C.H. Park and K.J. Chang, Phys. Rev. **B47**, 12709 (1993).

38) H. Asahi, K. Asami, T. Watanabe, J.Y. Soon, T. Kaneko, S. Emura, and S. Gonda, Appl. Phys. Lett. **58**, 1407 (1991).

39) A. Morii, I. Ohno, A. Kanda, K. Arai, K. Tokudome, K. Hara, J. Yoshino, and H. Kukimoto, Jpn. J. Appl. Phys. **30**, L1244 (1991).

40) K. Asami, H. Asahi, T. Watanabe, S. Gonda, H. Okumura, and S. Yoshida, Surf. Sci. **267**, 450 (1992).

41) A. Morii, H. Okagawa, K. Hara, J. Yoshino, and H. Kukimoto, J. Cryst. Growth **124**, 772 (1992).

42) K. Asami, H. Asahi, T. Watanabe, M. Enokida, S. Gonda, and S. Fujita, Appl. Phys. Lett. **62**, 81 (1993).

43) H. Asahi, M. Enokida, K. Asami, J.H. Kim, T. Watanabe, R.K. Soni, and S. Gonda, J. Cryst. Growth **136**, 268 (1994).

44) A. Morii, T. Takano, J. Kitamura, K. Hara, H. Kukimoto, J.Yoshino, and T. Yasuda, Solid-State Electron. **37**, 649 (1994).

45) K. Asami, H. Asahi, S.G. Kim, J.H. Kim, A. Ishida, S. Takamuku, and S. Gonda, Appl. Phys. Lett. **64**, 2430 (1994).

46) X.L. Wang, A. Wakahara, and A. Sasaki, J. Appl. Phys. **76**, 524 (1994).

47) X.L. Wang, A. Wakahara, and A. Sasaki, Appl. Phys. Lett. **65**, 2096 (1994).

48) J.H. Kim, H. Asahi, K. Asami, K. Iwata, S.G. Kim, and S. Gonda, Appl. Surf. Sci. **82**, 76 (1994).

49) A. Wakahara, Y. Nabetani, X.L. Wang, and A. Sasaki, J. Cryst. Growth **145**, 187 (1994).

50) E.G. Wang and C.S. Ting, Appl. Phys. Lett. **66**, 1400 (1995).

51) F. Issiki, S. Fukatsu, and Y. Shiraki, Appl. Phys. Lett. **67**, 1048 (1995).

Chapter 2

Growth of InAs on GaAs and epitaxial layer structure

2.1 Introduction

Lattice-mismatched heteroepitaxial growths such as GaAsP/GaAs and InGaAs/GaAs have been widely studied [1,2]. Especially InGaAs/GaAs has been intensively investigated because InGaAs possesses high electron mobility and suitable band gap for optical communication devices.

Several researches on the structural characterization of InAs/GaAs have been reported. Since reflection high energy electron diffraction(RHEED) pattern can be observed during MBE growth, i.e., *in-situ*, surface structure of InAs grown on GaAs can be easily investigated as a function of InAs layer thickness [3,4]. Although the intensive investigation, we can obtain only surface structure from RHEED. The quantitative island size nor existence of dislocation are not obtainable. On the other hands, transmission electron microscope(TEM) or surface prove microscope such as atomic force microscope(AFM) or scanning tunneling microscope(STM) observation can reveal such structural properties. However, because the lattice-mismatching between InAs and GaAs is as large as 7.2%(see Table 2-1), the change in growth mode and strain relaxation by misfit dislocation

Table 2-1 Lattice properties of InAs and GaAs [5]

	lattice constant(Å)	elastic moduli(10^{11}dyn/cm^2)		
		c_{11}	c_{12}	c_{44}
InAs	6.0583	8.329	4.526	3.959
GaAs	5.6533	11.9	5.38	5.99

occur at very early growth stage. Therefore most of previous reports on structural characterization of InAs/GaAs investigated well-formed island, in other words, the island formation process has not been clarified [6-13] Therefore, the dynamic island formation process has not been clarified. It is necessary to characterize the structure of epitaxial layer where the epitaxial layer thickness is systematically changed to investigate the dynamics of island formation, because the island formation process, island size, island shape and defect in island are important problems for self-assembled QD [14,15].

In this chapter, the growth and structural characterization of InAs/GaAs is described. The structural change of InAs grown on GaAs is investigated by RHEED, TEM, and AFM where InAs layer thickness is varied. The size and shape of island is measured from TEM and AFM images. The growth mechanism of InAs on GaAs is discussed with obtained structural properties.

2.2 Growth procedure and experimental setup

InAs was grown by MBE for III-V semiconductors. The MBE system used in this study is ANELVA MBE-831 and is illustrated in Fig.2-1. It is composed of three chambers; loading, exchange, and growth chambers. The utmost vacuum pressures are 10^{-7}, 10^{-9} and 10^{-10} Torr for loading, exchange, and growth chambers, respectively. Schematic structure of growth chamber is shown in Fig.2-2. Six Knudsen cells including two for dopant sources is attached in the growth

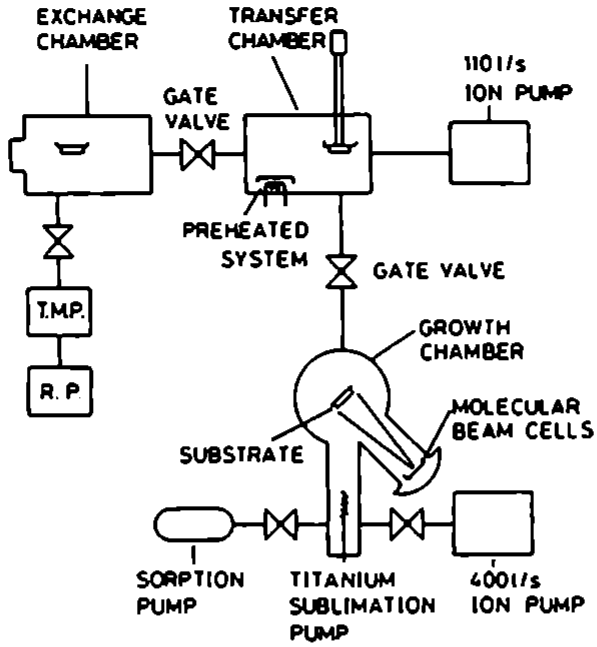

Fig.2-1 Schematic illustration of MBE system used in this study.

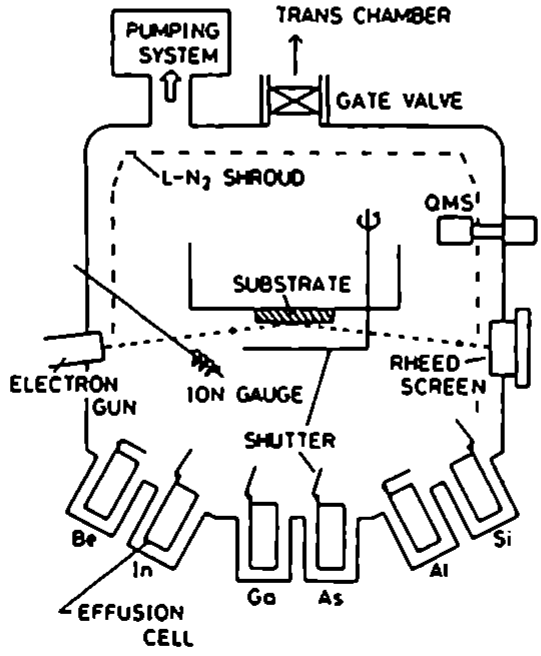

Fig.2-2 Schematic illustration of the growth chamber.

chamber. 30kV RHEED observation system is available. The beam pressure is monitored by ion gauge which is located near the substrate. Liquid nitrogen flows continuously in the shroud during growth.

The substrates were CrO doped semi-insulating GaAs nominally (001) just-oriented. Substrates were degreased by organic solvent followed by etching in H_2SO_4:H_2O_2:H_2O=5:1:1 solution for 1min at 60°C. Etching was stopped by pouring deionized water and the substrates were rinsed by flowing deionized water for 4min further. In the rinse process, oxide film which protects the substrate surface is formed. The substrate were soldered with indium on molybdenum holder and set in the loading chamber. Prior to the introduction of substrates into the growth chamber, the substrates were baked at 350~400°C for 1hour in the exchange chamber, in order to suppress carbon contamination introduction into the growth chamber. Then, the substrates were transfered to growth chamber, and heated at 620°C to eliminate the oxide film. The substrate temperature was controlled by heater current, which is calibrated by the eutectic points of Au-Si(370°C) and Al-Si(577°C). The main shutter was kept open and substrate was expose to As flux to avoid As desorption. The elimination of oxide film was confirmed by RHEED observation, where halo pattern which is caused by the oxide amorphous turned to normal diffraction pattern of (001) plane of GaAs. Even after halo pattern disappeared, the substrate temperature was kept 620°C for 10 min to eliminate the oxide film completely, and then, was lowered to 580°C for GaAs buffer layer growth. The GaAs buffer layer was grown 1000Å to improve surface flatness. The RHEED observation showed 2×4 streak pattern during GaAs buffer layer growth. InAs layer was grown at 480°C. 100Å single crystal or amorphous GaAs cap layer was grown for TEM observation, while no cap layer was grown for AFM observation. Typical sample structure is illustrated in Fig.2-3 and typical growth condition is shown in Table 2-2.

The growth rate was calibrated by RHEED oscillation technique [16]. However, the intensity of specular spot becomes weak abruptly in the very early stage of InAs growth on GaAs, since InAs grows three-dimensionally. Therefore, the

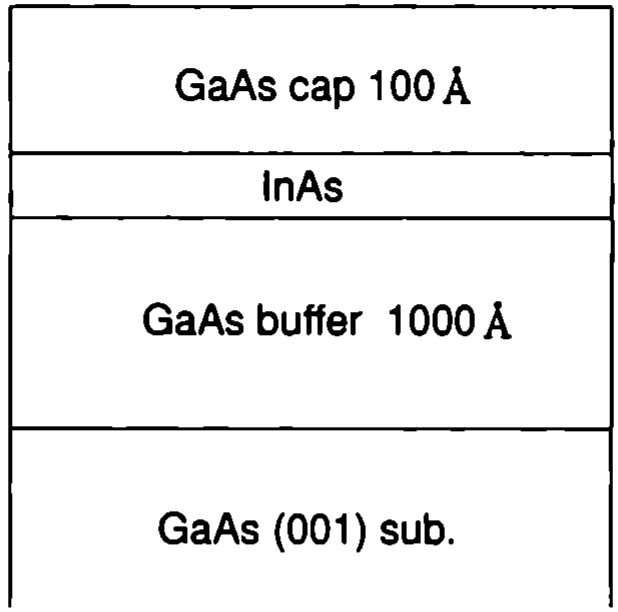

Fig.2-3 Typical structure of grown sample. 100Å single crystal or amorphous GaAs cap layer is grown for TEM observation while no cap layer is grown for AFM observation.

Table 2-2 Typical growth condition used in this study.

	growth temperature(°C)	growth rate(ML/s)	V/III
InAs	480	0.1~0.17	10~47
GaAs	580	0.69	3~5

growth rate of InAs on GaAs cannot be measured by this method. We estimated the growth rate of InAs by those of InGaAs and GaAs, because $In_xGa_{1-x}As$ where x is less than 0.2 grows two-dimensionally on GaAs for thick enough layers to measure RHEED oscillation period. One can estimate the growth rate of InAs knowing the growth rates of InGaAs and GaAs by following equation:

$$v_{InAs} = v_{InGaAs} - v_{GaAs} \tag{2-1}$$

where, v_{InAs}, v_{InGaAs}, and v_{GaAs} represent the growth rates of InAs, InGaAs and GaAs, respectively. Also because of three-dimensional growth, the layer thickness used in this thesis is defined as the product of growth rate and growth time, in other words, "we grow xML of InAs" means that "we supply xML amount of In and As atoms if the growth mode lasts two-dimensionally".

AFM observation was carried out by SPI3700(Seiko Instruments Inc.) system. The cantilever type of "contact" and scan type of "topography" were normally selected. TEM sample was formed by mechanical lapping followed by conventional Ar-ion milling. TEM images were observed by JEOL 2000EX system. The acceleration voltage was 200kV. For plan-view observation, bright field images under two-beam configuration were taken except for especially mentioned. The diffraction spot of (220) or (2$\bar{2}$0) was selected beside (000). Diffraction spots for cross-sectional observations were selected properly according to the purpose.

2.3 Reflection high energy electron diffraction observation

Observed RHEED patterns during InAs growth are shown in Fig.2-4. Two electron beam incidence directions, those are, [110] and [1$\bar{1}$0] directions were taken, since surface structures along [110] and [1$\bar{1}$0] directions are asymmetric in zincblende structured semiconductors. Surface structure just after GaAs buffer

layer growth at 580°C is 2×4. This means that the growth is performed under As-stabilized condition. However, surface structure of GaAs changed into 2×3 when the substrate temperature was lowered to 480°C for the InAs growth. When 1ML of InAs is grown, the RHEED pattern remains still streak. Thus, the initial layer of InAs grows two-dimensionally on GaAs. However, the diffraction spot observed from [1$\bar{1}$0] direction changes from streak to spotty drastically at 1.8ML. From this change, it is considered that the InAs island is formed around 1.8ML. One can see the spotty pattern with developed facet streak observed from [1$\bar{1}$0] direction at 2ML. On the other hand, diffraction spot observed from [110] direction indicates no facet pattern, though it is somewhat spotty. Further growth of InAs brought no particular change in RHEED pattern except for the fact that the diffraction spot observed from [110] direction became more spotty. The facet orientation can be estimated as (113)A by the angle between two facet streaks which start from the same diffraction spot. However, it should be reminded that orientation cannot be determined explicitly, because facet streak is broadened.

In order to examine whether island has facets of <10x> planes, RHEED patterns with incident electron beam along <100> directions are observed. Figs.2-5 show the RHEED patterns observed from [100] and [010] directions when the InAs layer is 4ML. No particular facet streak is not seen at least under 10ML. Therefore island has no facets without (113)A.

From the spacing of diffraction rods or spots, we can obtain the surface lattice spacing in the growing plane. Fig.2-6 shows the surface lattice spacing estimated from Figs.2-4 against InAs layer thickness. Both surface lattice spacings along [110] and [1$\bar{1}$0] directions are converted to that of <100> direction for the comparison with lattice constants of GaAs and InAs in Fig.2-6. When 1ML of InAs is grown, the surface lattice spacing is the same as lattice constant of GaAs for both [110] and [1$\bar{1}$0] directions. However, the lattice spacing becomes larger between 1 and 2ML. After 2ML, the lattice spacing approaches the lattice constant of InAs gradually. When InAs layer thickness is 10ML, the lattice spacing is almost the same as the lattice constant of InAs. These experimental results indicate

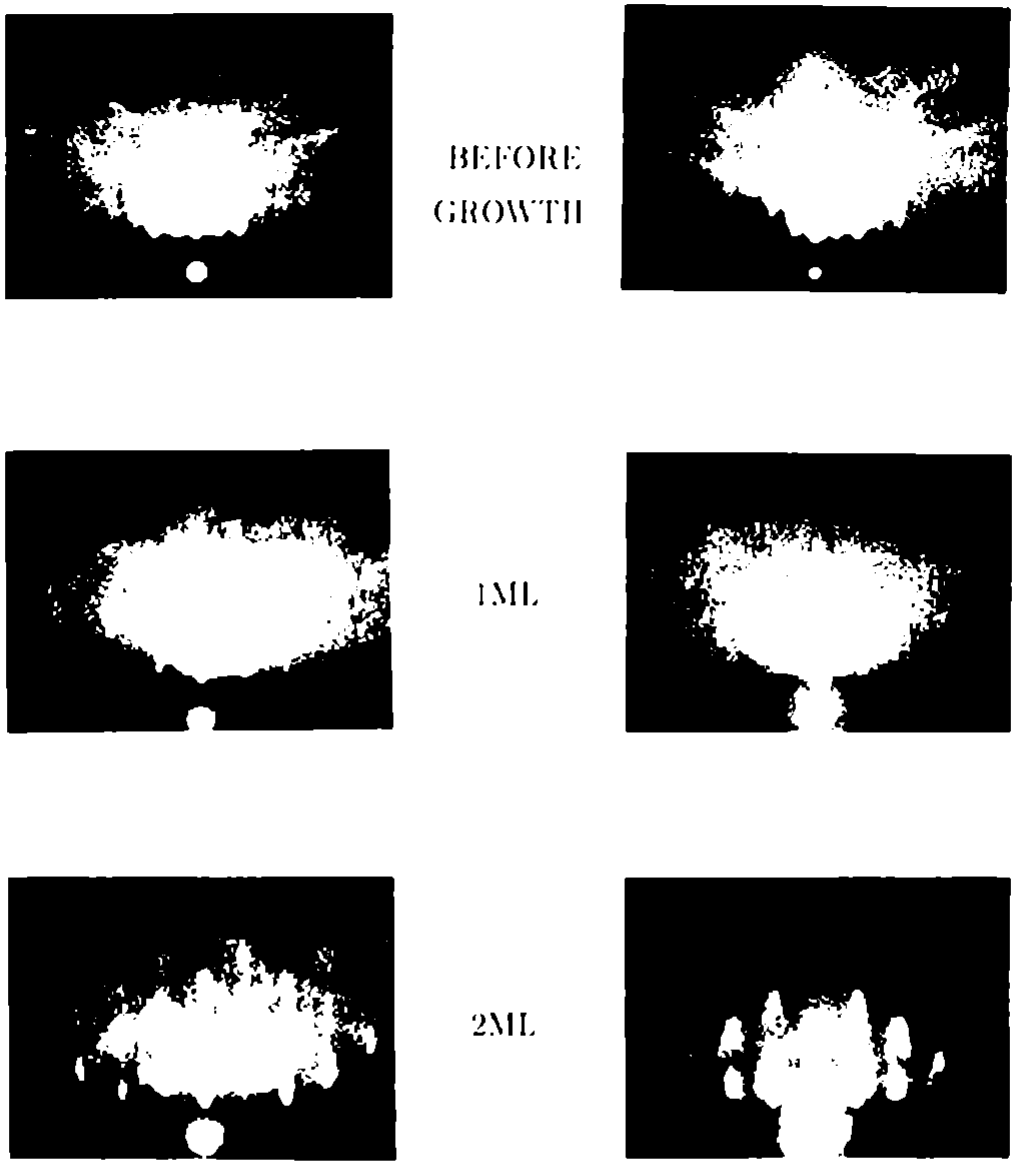
BEFORE
GROWTH
1ML
2ML
[110]
[1$\bar{1}$0]

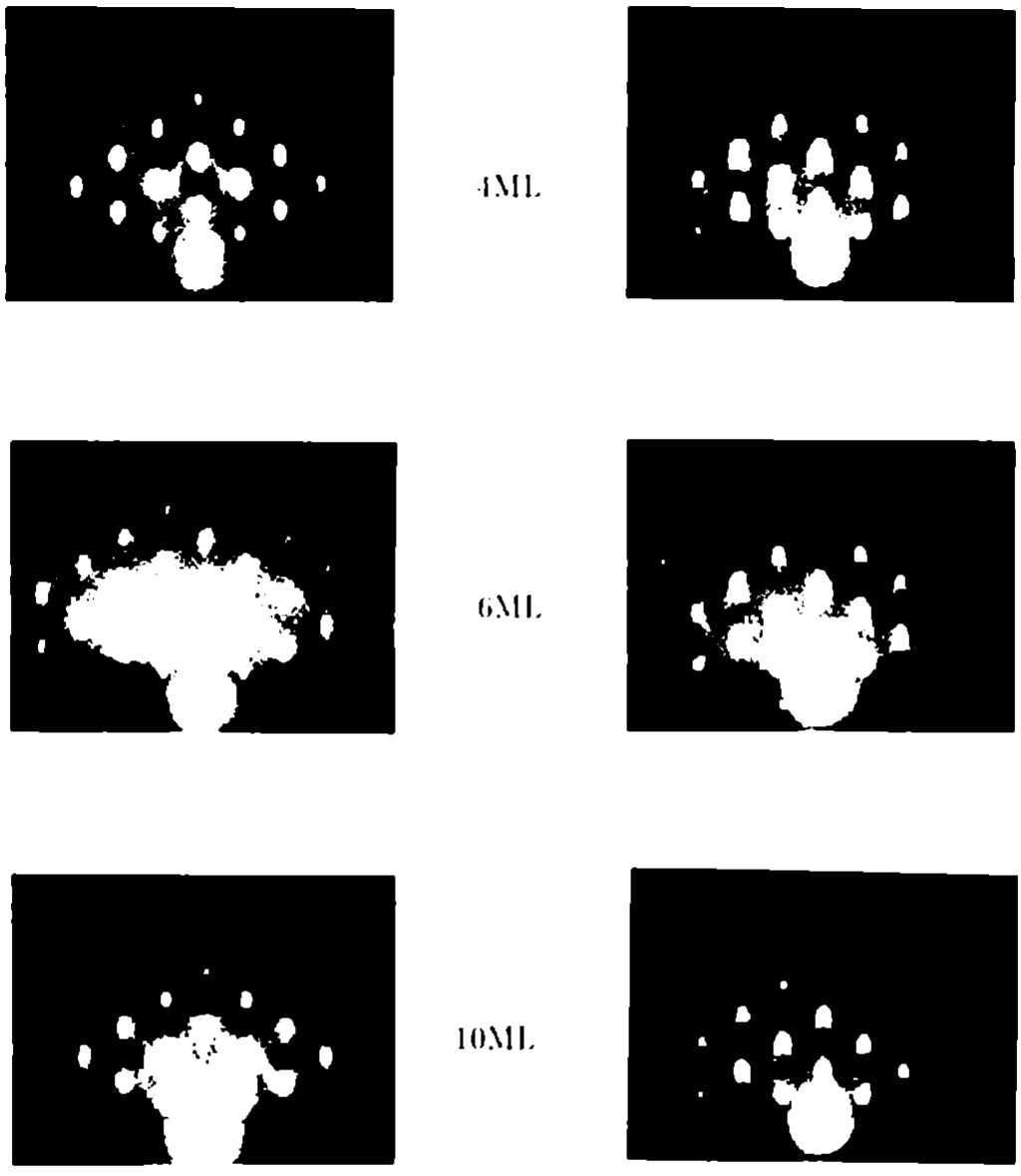

Fig.2-4 Observed RHEED patterns during InAs growth.

[100] [010]

Fig.2-5 RHEED patterns observed from [100] and [010] directions where InAs layer thickness is 4ML.

that the strain relaxation of InAs grown on GaAs is performed between 2 and 10ML. Asymmetry of strain relaxation between [110] and [1$\bar{1}$0] directions is not observed. Generally, there are two ways to release the strain in the epitaxial layer: 1) surface lattice strain relaxation by island growth and 2) strain relaxation by misfit dislocation generation. These two ways of strain relaxation are observed by RHEED as two steps of surface lattice spacing change, for example, in Ge layer growth on Si [17] where the lattice-mismatching is 4.2%. On the other hand, there is only one step of surface lattice spacing change in InAs/GaAs. Thus, it is considered that the island growth and misfit generation occur almost the same time. The difference of strain relaxation process between InAs/GaAs and Ge/Si can be attributed to the difference of lattice-mismatching.

2.4 Atomic force microscope observation

The observed AFM images are shown in Figs.2-7. One can see the density of InAs islands increases as the InAs layer thickness increases. When the 1.0ML of

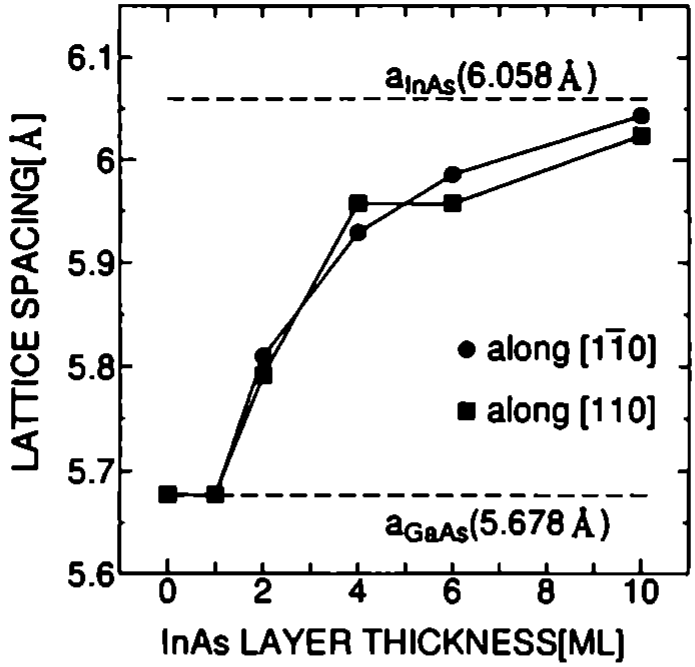

Fig.2-6 Surface lattice spacing of InAs calculated by diffraction rods or spots in RHEED patterns observed from [110] and [1$\bar{1}$0] directions. Surface lattice spacings are converted to that of <100> direction for the comparison with lattice constants of GaAs(a_{GaAs}) and InAs(a_{InAs}) at 480°C.

InAs is grown, the InAs islands are hardly seen and the grown layer surface is considerably flat. The surface singularity at 1ML agrees well with the streaky RHEED patterns. The situation does not change until 1.5ML. The density and the size of island increase slightly at 1.8ML. Then, the density at 2.0ML becomes drastically greater than that at 1.8ML. It is considered that the formation of InAs islands begins at about 1.8ML. The rapid island formation can be understood from the result of RHEED observation. When 2.0ML InAs is grown, two types of InAs islands appear as seen in Fig.2-7(e), i.e., the small(<250Å) and the large(>400Å) islands. The small islands are the hemispherical shape with height of 30Å and also seen in Figs.2-7(a)~(d). The size and shape of these islands seem

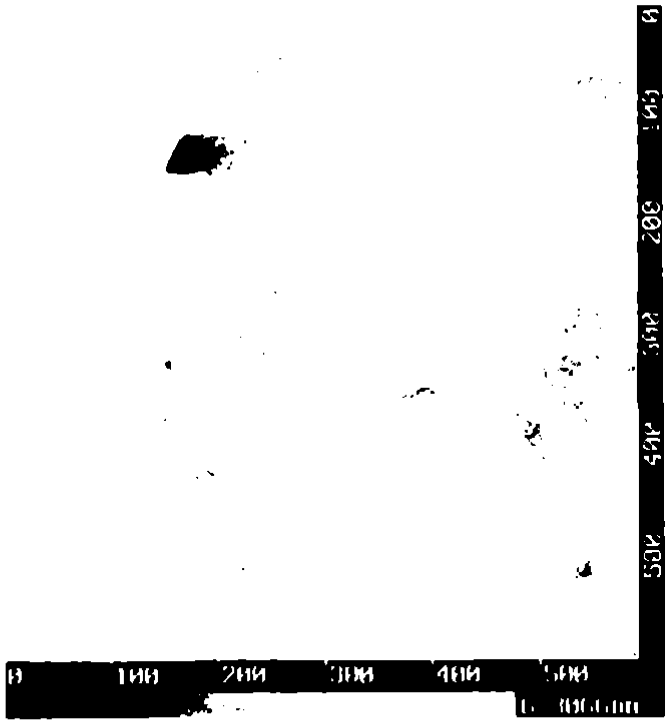

(a)1.0ML

1000 Å

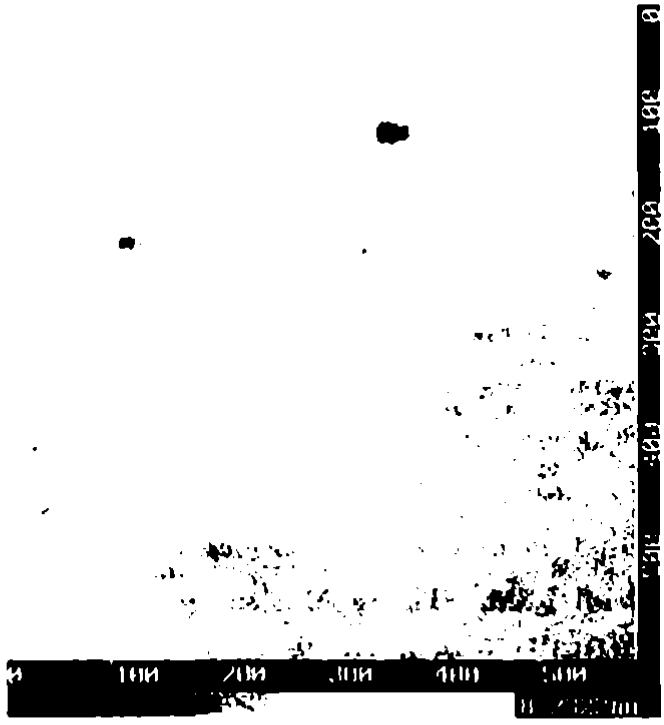

[110]

[001] [1$\bar{1}$0]

(b)1.3ML

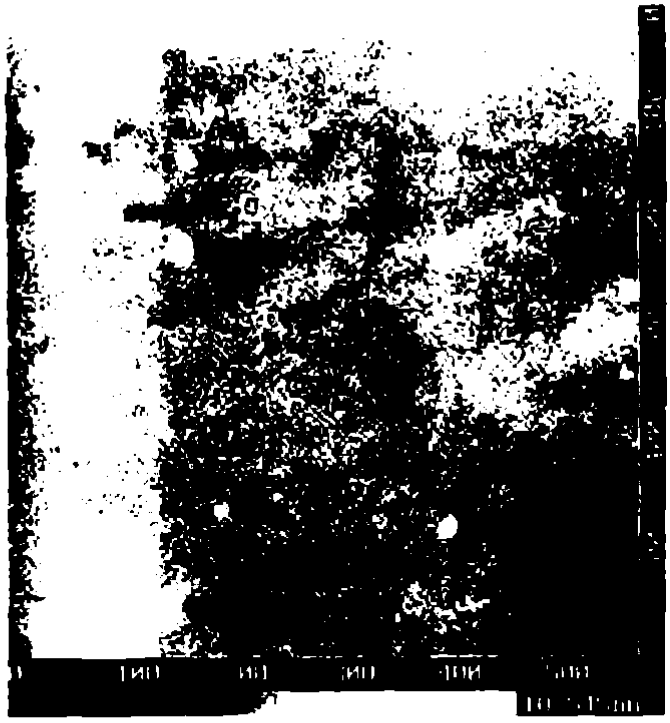

(c)1.5ML

1000 Å

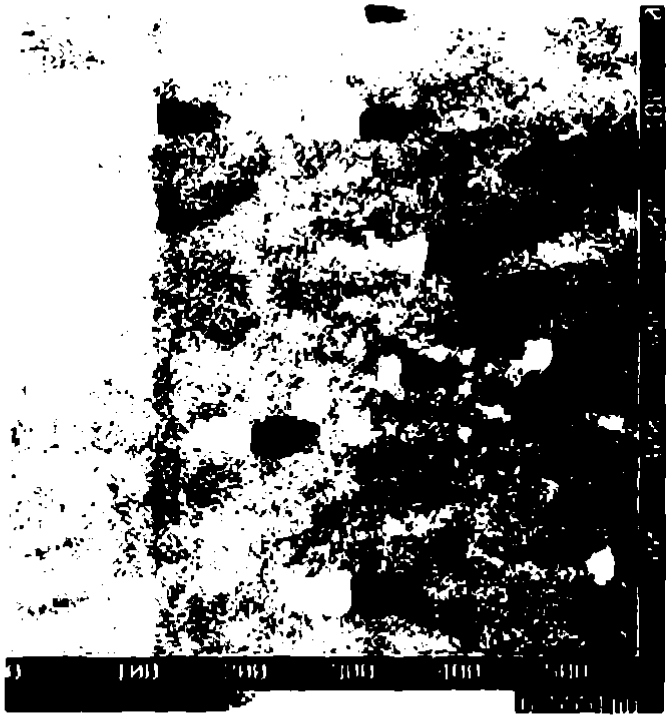

[110]

[001] [1$\bar{1}$0]

(d)1.8ML

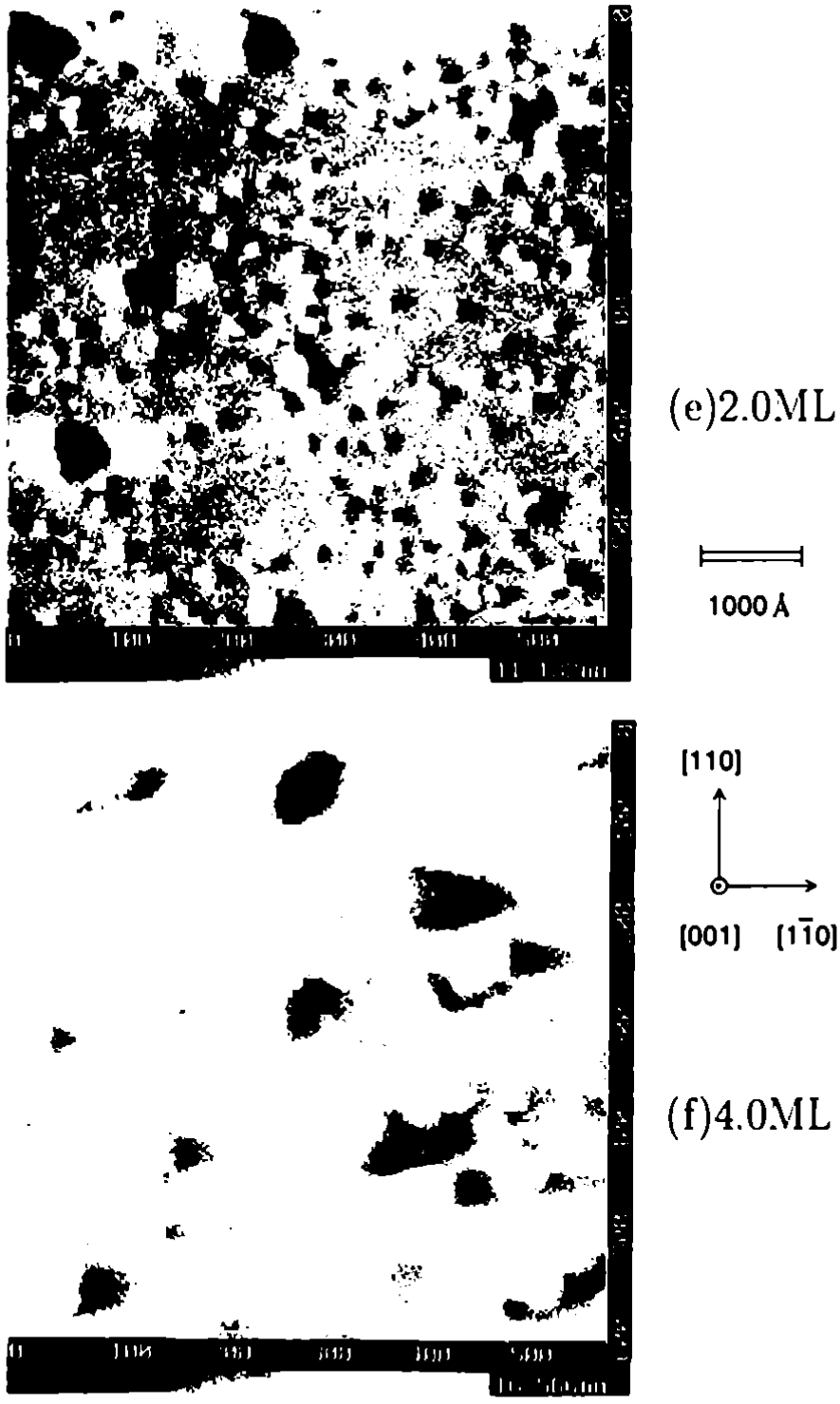

Fig.2-7 AFM images of InAs grown on GaAs where InAs layer thickness is variously changed. Thickness of InAs is (a)1.0ML, (b)1.3ML, (c)1.5ML, (d)1.8ML, (e)2.0ML and (f)4.0ML.

to be similar each other.

The large islands are about three~four times in size greater than the small ones, and the shapes are not similar each other. Density of the large islands is about 1/40 compared with that of the small ones at 2ML, but increases remarkably when the InAs layer thickness becomes 4.0ML, while the density of the small islands becomes somewhat less than that at 2.0ML. The sizes of the small islands remain almost the same with increasing the InAs thickness. On the contrary, the sizes of the large islands take various sizes and various shapes as InAs layer thickness changes from 2.0 to 4.0ML. Therefore the large islands are thought to be formed by coalescence of small islands.

In spite of the intensive observation, no specular facet were recognized for both small and large islands though the RHEED patterns indicate the existence of (113)A planes. The reason is not clear, however, it is considered that relation among island size, island-to-island distance and size of cantilever tip may be concerned.

2.5 Transmission electron microscope observation

The plan-view TEM observation results show almost the same results as those of AFM. The InAs islands are hardly observed at 1.0~1.5ML and the density of InAs island increases drastically at 1.8ML. The relation of the small island density and InAs layer thickness is shown in Fig.2-8. There is a discrepancy of island density between TEM and AFM measurements at 1.8ML. It would be attributed to the difference in layer thickness. Since islands are formed abruptly, small difference in the InAs layer thickness results in large discrepancy in island density around 1.8ML. Figures 2-9 show the plan-view TEM images at 1, 2 and 4ML. When the InAs layer thickness is 1ML, TEM image shows no particular contrast, which means that the lattice spacing in the growth plane is uniform

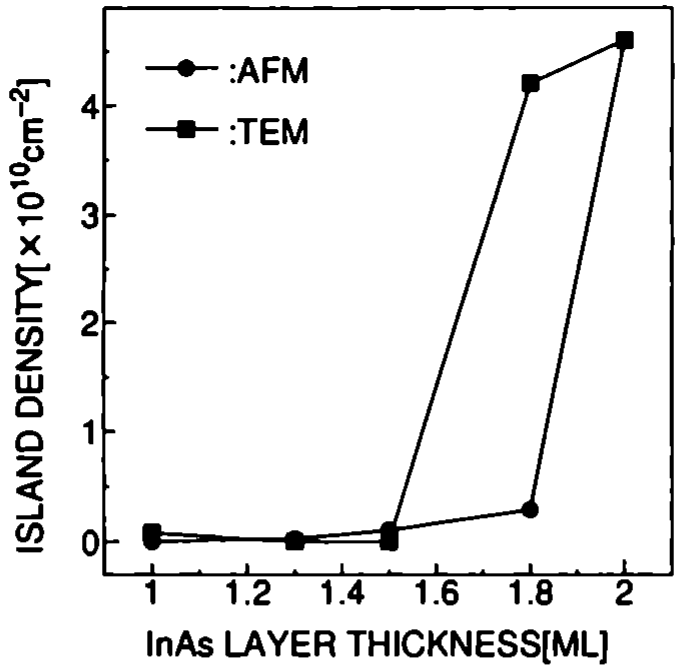

Fig.2-8 The density of small island measured from AFM and plan-view TEM images as a function of InAs layer thickness.

through the path of transmitted electron and that the strain in the epitaxial layer is uniformly distributed within observed area. The accordance of the lattice spacings of InAs layers and GaAs cap and buffer layers are also indicated by the RHEED observation as described before. Since electron diffraction is sensitive to the lattice spacing, TEM image well reflects the strain distribution. On the contrary, there are many dotted images which indicate the InAs islands in Fig.2-9(b). This contrast well agrees with the AFM image of Fig.2-7(e). Because no misfit dislocations are observed in Fig.2-9(b), strain relaxation in InAs islands is not enough and islands are still compressively strained. However, when 4ML-thick InAs is grown, many fringes are seen in Fig.2-9(c). These fringes are considered to be moiré patterns caused by the misfit dislocations [7,18,19]. The fringes run along both [110] and [1$\bar{1}$0] directions. From the fact that the misfit dislocations

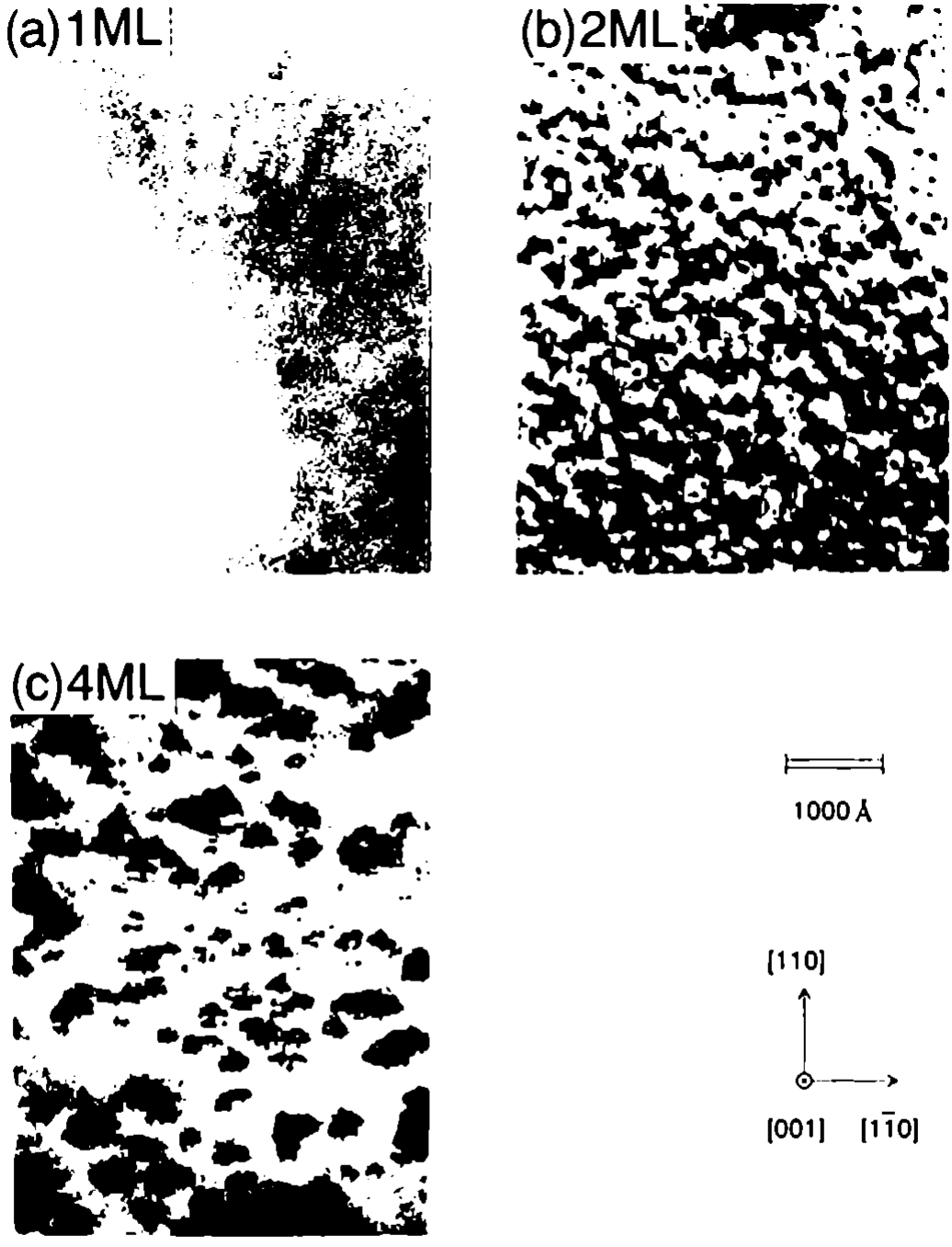

Fig.2-9 Plan-view TEM images of InAs. Thickness of InAs is (a)1ML, (b)2ML and (c)4ML. 100Å single crystal GaAs cap layer was grown for 1ML-thick sample while 100Å amorphous GaAs cap layers were grown for 2 and 4ML-thick samples.

Fig.2-10 Bright field cross-sectional TEM image of 2ML-thick InAs.

are generated between 2 and 4ML, the critical thickness of InAs grown on GaAs is between 2 and 4ML. Comparing AFM image of Fig.2-7(f) and TEM image of Fig.2-9(c), one can see that the size of large InAs island is similar to that of the moiré pattern. Thus, the misfit dislocations are generated in the large InAs islands. Figure 2-10 is the decisive TEM image which indicates that the dislocation is generated in the large island. Two threading dislocations which extend from the island to surface are clearly seen. Although the small island image is not clearly seen in Fig.2-9(c), it is considered that the lattice strain may veil the small islands.

Figures 2-11 show the dark field cross sectional TEM images at 1, 2, and 4ML. As guessed from plan-view observation, the InAs layer grows two-dimensionally and the strain distribution is uniform at 1ML. However, when the InAs layer thickness is 2ML, some black and white contrast images are seen along with the

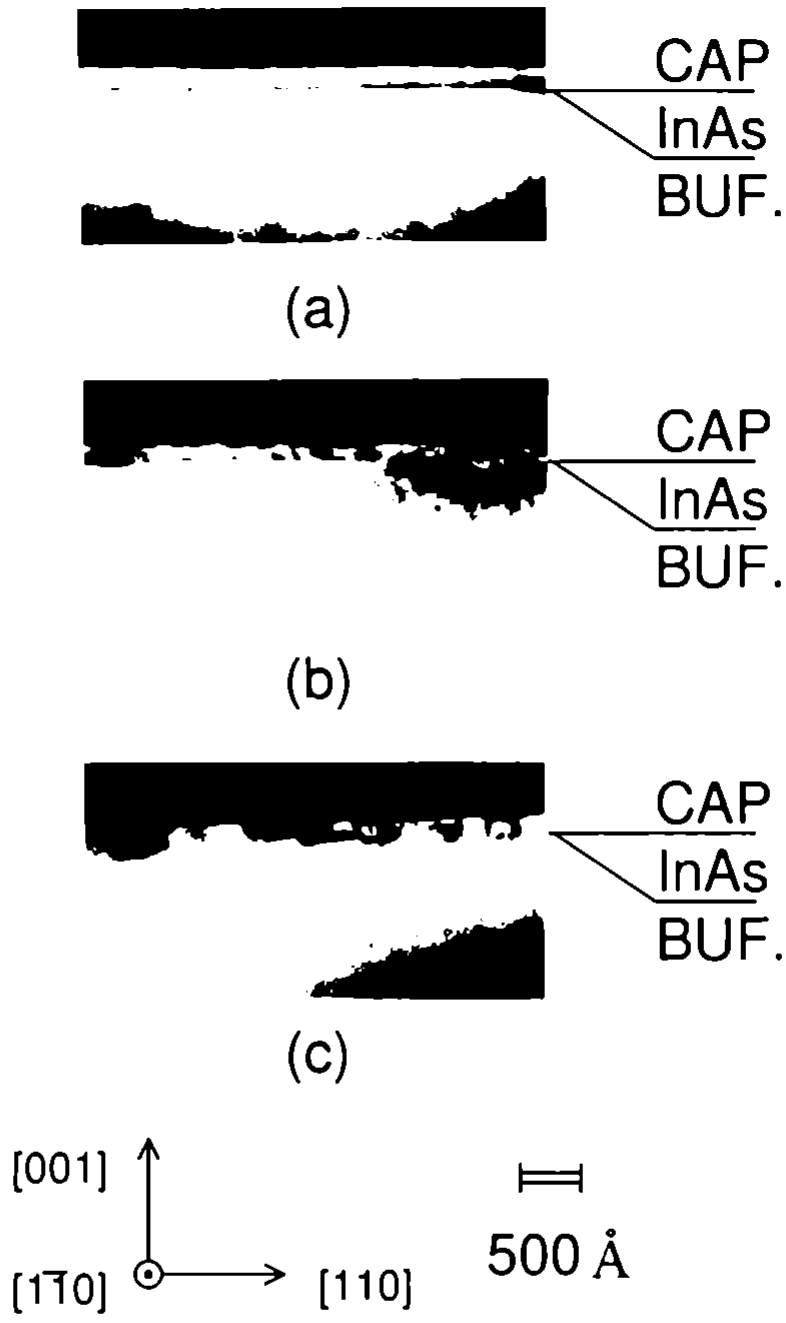

Fig.2-11 Dark field cross-sectional TEM images of 1, 2, and 4ML-thick InAs with 100Å - thick GaAs single crystal layer is grown. (111) diffraction spot was chosen for images. Thickness of InAs is (a)1ML, (b)2ML and (c)4ML.

InAs layer. These images reflects the strain nonuniformity which is caused by the islands. It is noteworthy that the strain is distributed not only in the InAs layer but also in the GaAs buffer and cap layers. Since the lattice spacing of InAs in the island is not the same as that of GaAs, the GaAs which surrounds InAs island suffers the tensile strain [22,23]. The strain in GaAs layer is much remarkably seen in Fig.2-11(c) where the InAs layer thickness is 4ML. Furthermore, another phenomenon is observed. Once the dislocations are generated and the lattice spacing of InAs returns to unstrained value, GaAs is energetically hard to grow on islands during cap layer growth while inter-islands area is stable growth site. The depression of GaAs layer on InAs islands is seen in Fig.2-11(c) and also observed by other groups [12,24]

The island size at 2ML is measured from plan-view TEM image. Histograms of the island size are shown in Figs.2-12. The average size of island is 150.2Å and 132.9Å along [110] and [1$\bar{1}$0] directions, respectively. The island height is estimated as 30Å from the island size in [1$\bar{1}$0] direction and the fact that the island has (113)A facet. This estimated height agrees very well as that measured by AFM. However, the island size in the growth plane measured from plan-view TEM is smaller than that measured by AFM. The island is slightly elongated in [1$\bar{1}$0] direction. The density of island is $1.1\times10^{11}cm^{-2}$ in the growth plane, though AFM observation indicates the density is $4.5\times10^{10}cm^{-2}$. The disagreements of the island size and island density may be attributed to the existence of GaAs cap layer. H. Kitabayashi et al. observed island agglomeration even after In flux is stopped [20]. In the case of TEM observation, GaAs cap layer was grown successively after InAs growth, on the other hand, InAs layer was exposed to As flux during lowering substrate temperature for about 10min for AFM observation. Thus, the GaAs cap layer suppresses the island agglomeration in TEM samples and leads to small size and high density islands.

The island elongation becomes more notable at 4ML. The structural anisotropy in the growth plane is considered to be caused by the structural difference in two orthogonal surface steps. It is known that the atom and dangling bond

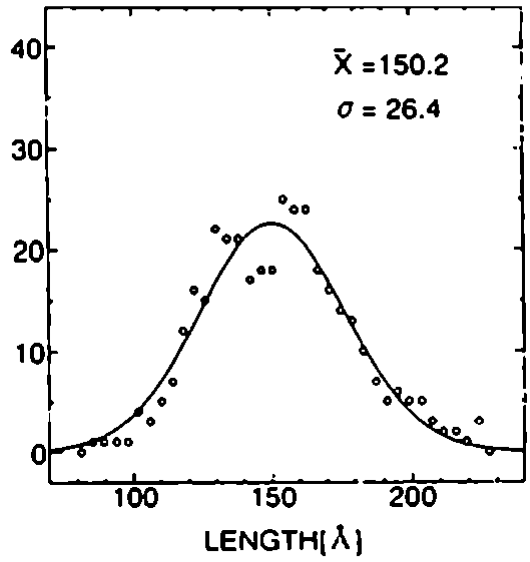

(a)

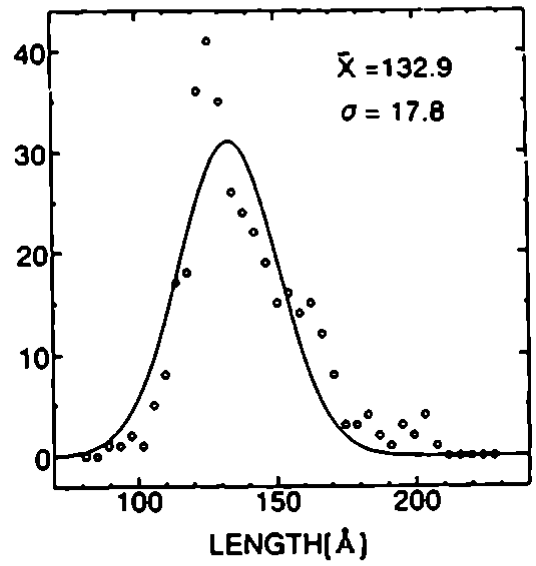

(b)

Fig.2-12 Histograms of the island size measured from TEM images, where InAs layer thickness is 2ML. Island size is along [1$\bar{1}$0] direction in (a) and along [110] direction in (b).

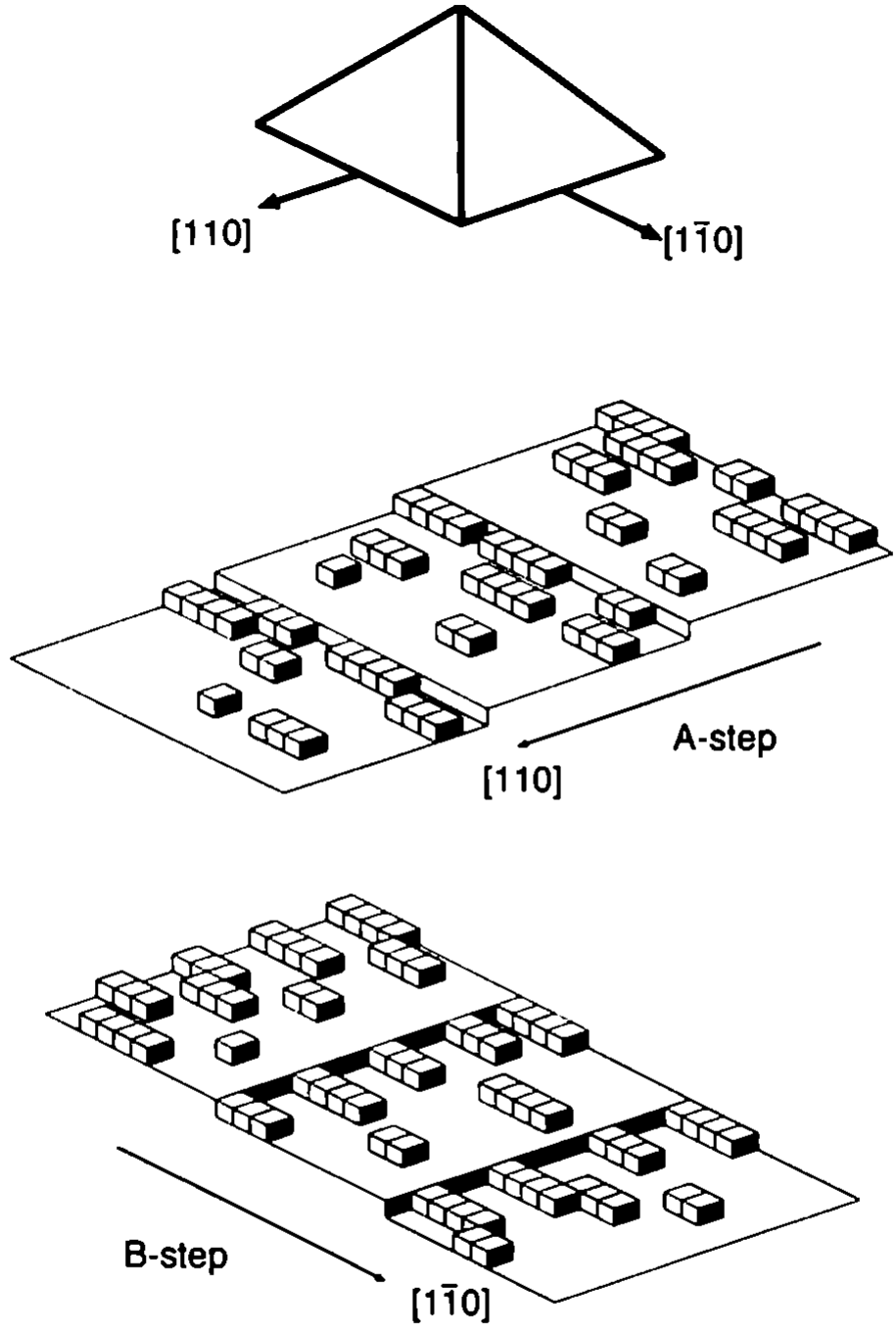

Fig.2-13 Schematic illustrations of anisotropic island evolution due to the anisotropy in growth rate of orthogonal surface steps.

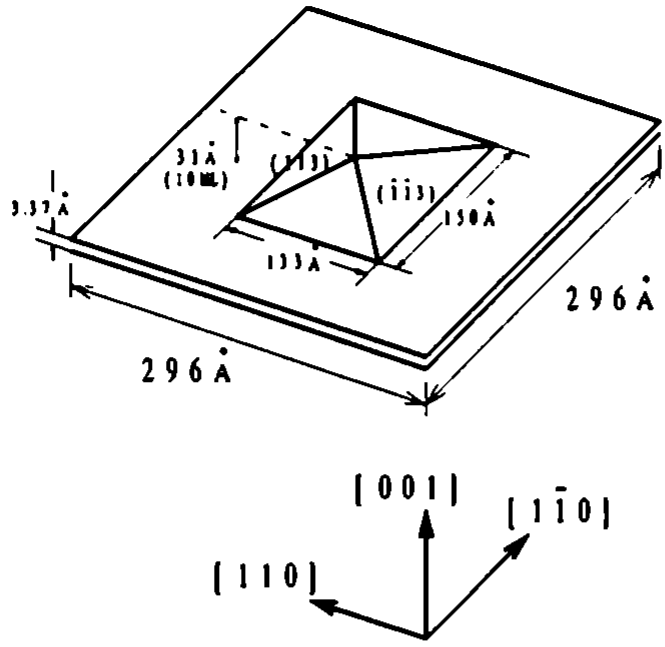

Fig.2-14 Schematic structure of 2ML grown InAs suggested from RHEED and TEM observations.

arrangements of step toward [110] direction, A-step, differ from those of step toward [1$\bar{1}$0] direction, B-step in zincblende structured crystal. If the growth is performed under As-stabilized condition, growth rate at B-step is faster than that at A-step [21]. This anisotropy in growth rate results in elongation of island along [1$\bar{1}$0] direction as shown in Fig.2-13.

Knowing island size, height and density, the thickness of InAs two-dimensional layer which is underlying island can be calculated by subtracting the volume of island from that of 2ML amount of InAs. The calculated thickness is 3.37Å . Because the thickness of 1ML of InAs coherently strained on GaAs is 3.25Å, the thickness of two-dimensional layer is about 1ML. The structure of 2ML grown InAs suggested by RHEED and TEM observations is illustrated in Fig.2-14.

In order to study the dislocation type in large island, the dark field images with diffraction spots of (220) and (2$\bar{2}$0) were taken. Figures 2-15 show the dark

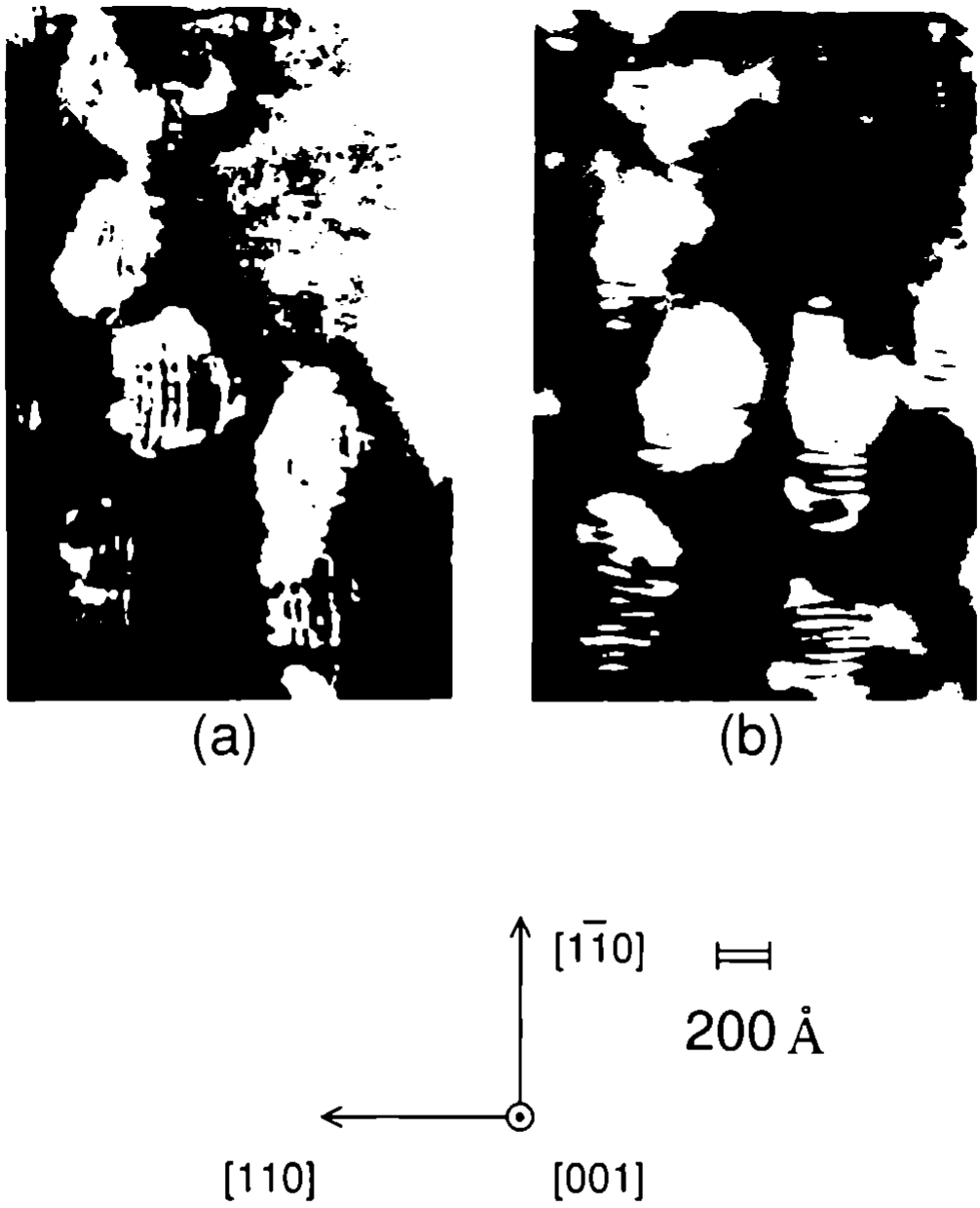

Fig.2-15 Dark field plan-view TEM images of the same dislocation with orthogonal diffraction spots. Diffraction spot is (a) $\mathbf{g}$=(220) and (b) $\mathbf{g}$ = (220).

field dislocation images taken with orthogonal **g** vectors. In Figs.2-15, one can find that the moiré fringes run both [110] and [1$\bar{1}$0] directions and the fringes disappeared when the **g** vectors which are vertical to the fringes are selected. Considering the fact that dislocation in zincblende structured crystal mostly runs along <110> direction in (001) plane and that the dislocation relieves strain in transverse direction, the dislocation direction can be assigned as parallel to the fringe. Representing **b** as a Burgers vector of dislocation, the dislocation image disappeared when **g**·**b**=0. Thus, the these dislocations are identified as edge dislocations. The edge dislocation can relax the strain effectively because the Burgers vector lies in the growth plane. However, it is difficult to generate edge dislocation directly in the zincblende structured crystal, since the shortest lattice vector in each sublattice is along <111> direction which makes 60° angle with <110> direction. The observed edge dislocation is composed of a pair of 60° dislocations which run the same direction and have different Burgers vectors as shown in Fig.2-16(Lomer-lock type) [19]. Relation of the Burgers vectors of two 60° dislocations and that of 90° dislocation(edge dislocation) is represented by next equation:

$$\frac{a}{2}[110] = \frac{a}{2}[101] + \frac{a}{2}[01\bar{1}] \qquad (2\text{-}2)$$

where a denotes the lattice constant of InAs and [1$\bar{1}$0] dislocation direction is supposed. Composed edge dislocation is sessile because the Burgers vector does not lie in <111> plane. Dislocation generation mechanism is considered that two 60° dislocations are generated at the edge of island successively and then form one edge dislocation.

From the interval of each fringe in moiré pattern, one can estimate the lattice spacing of InAs island by following equation:

$$a_m = \frac{a_{InAs} \times a_{GaAs}}{| a_{InAs} - a_{GaAs} |} \qquad (2\text{-}3)$$

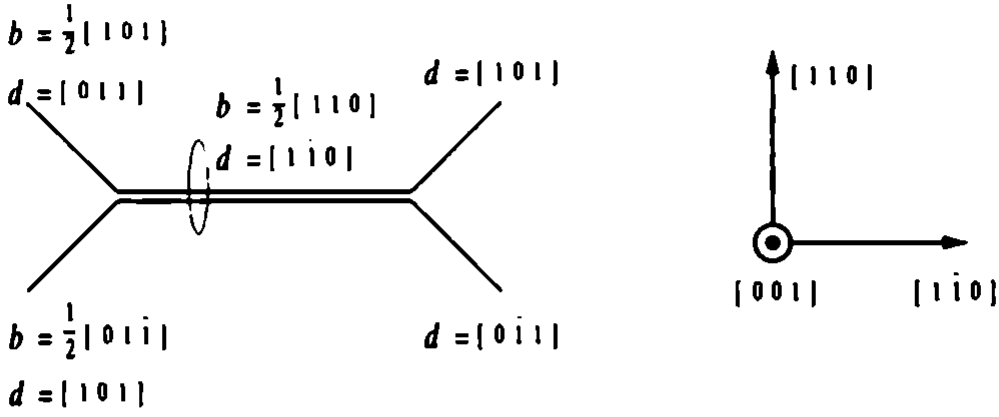

Fig.2-16 An edge dislocation consisted of a pair of 60° dislocations. Dislocation is assumed to run along [1$\bar{1}$0] direction.

where a_{InAs} and a_{GaAs} represent the lattice spacings of InAs and GaAs, respectively, and a_m represents the interval of each fringe. Although GaAs buffer layer suffers tensile strain, substituting 4.00Å , which is 1ML-length along <110> direction of unstrained GaAs, into a_{GaAs}, and measured interval of each fringe into a_m, the lattice spacing of InAs along <110> direction can be calculated as 4.21Å when the InAs layer thickness is 4ML. This value is almost the same as the 1ML-length of unstrained InAs, 4.28Å , thus, the dislocation in the island works effectively for the strain relaxation.

2.6 Discussion

From the experimental results, it was found that there are three stages in the InAs growth on GaAs:

1. InAs grows two-dimensionally on GaAs until 1.5ML.

2. InAs grows three-dimensionally and begins to nucleate small islands around 1.8ML.

3. InAs grows three-dimensionally and begins to nucleate large islands at 2.0ML.

The growth mechanism of InAs on GaAs is considered as follows. InAs grows two-dimensionally at the beginning. Although the InAs suffers compressive strain when two-dimensional growth, the surface energy is minimized by covering the GaAs surface by InAs, because the surface energy of InAs is less than that of GaAs [25]. Thus the total energy is minimized. Once the surface is covered by InAs, the surface energy does not change while the strain energy increases as growing InAs. In this case, the strain energy is dominant. However, as the strain becomes large, InAs grows three-dimensionally to minimize the total energy by expanding in the interface plane. This change of the growth mode is the beginning of the abrupt small island formation. Because the island density changes suddenly, it is considered that not only the newly supplied atoms but also already sited atoms form the islands. In this case, at least the 1ML-thick InAs remains on the GaAs two-dimensionally to minimize the surface energy as shown in Fig.2-14. As described above, the size and the shape of the InAs small island does not concerned with the InAs thickness, it seems there exists certain island size which is the most stable. In fact, growing by increasing the number of certain scale islands is more reasonable than growing by enlarging the islands size in view of the strain energy. When the density of the small islands becomes large so that islands coalesce each other, the large islands are formed by coalescence of several small islands. At this time, the elastic strain accommodated in the islands is so

large that the misfit dislocations are generated. Once the misfit dislocations are generated in the InAs islands, it is energetically desirable to grow by enlarging large islands rather than increasing small islands in which no misfit dislocations exist. For these reasons, the size and shape of large InAs islands is not similar each other. Theoretical approach of island formation is intensively described in chapter 3.

For the utilization of InAs island to quantum dot, the suitable InAs layer thickness is 1.8~2ML, because the island size are similar to each other and there are no misfit dislocations.

2.7 Summary

In this chapter, the MBE growth and structural characterization of InAs on GaAs is investigated. *In-situ* RHEED observation revealed that the InAs grows two-dimensionally until 1.8ML, then the growth mode changes into three-dimensional abruptly. The InAs island has (113)A facet. Surface lattice spacing gradually reaches to InAs lattice constant after islands are formed.

Very few islands were seen by AFM observation when InAs layer thickness was less than 2.0ML, however, many islands were observed when 2ML-thick InAs was grown. The island size is 250Å in diameter and 30Å in height. This island seemed to be similar each other. Beside this small islands, large islands greater than 400Å in diameter were seen. The density of large island increases with InAs layer thickness while that of small island decreased.

From plan-view TEM observation, it was found that small island is coherently grown, on the other hand, many dislocations were generated in large island and the strain in the island is almost relaxed. Observed dislocation is Lomer-lock type which relaxes the strain effectively. Not only InAs island but also GaAs buffer and cap layer which surrounds island are strained. The size of coherently grown island observed by plan-view TEM was slightly smaller than that observed by AFM since the GaAs cap layer suppresses agglomeration of InAs islands.

When device application of InAs island is considered, the fluctuation in island size becomes serious problem. The fluctuation in island size investigated in this study is about 10~20%. In order to make island size uniform, the growth condition such as substrate temperature, V/III ratio and growth rate should be optimized.

References

1) As for GaAsP/GaAs, for example, J.W. Matthews, A.E. Blakeslee, J. Cryst. Growth **27**, 118 (1974).

2) As for InGaAs/GaAs, for example, S. Fujita, Y. Nakaoka, T. Uemura, M. Tabuchi, S. Noda, Y. Takeda, and A. Sasaki, J. Cryst. Growth **95**, 224 (1989).

3) H. Munekata, L.L. Chang, S.C. Woronick, and Y.H. Kao, J. Cryst. Growth **81**, 237 (1987).

4) H. Nakao and T. Yao, Jpn. J. Appl. Phys. **28**, L352 (1989).

5) Landolt-Börnstein Numerical Data and Fundamental Relationshis in Science and Technology. Vol.17a Editted by O. Madelung(Springer-Verlag, Berlin, 1982).

6) L. Goldstein, F. Glas, J.Y. Marzin, M.N. Charasse, and G. Le Roux, App. Phys. Lett. **47**, 1099 (1985).

7) M. Tabuchi, S. Noda, and A. Sasaki, in *Science and Technology of Mesoscopic Structures*, edited by S. Namba, C. Hamaguchi, and T. Ando (Springer, Tokyo 1992), p.379, paper presented at 1st Int. Symp. Sci. and Technol. of Mesoscopic Structures (Nov.6-8, 1991, Nara, Japan) p.18.

8) C.W. Snyder, J.F. Mansfield, and B.G. Orr, Phys. Rev. B**46**, 9551 (1992).

9) D. Leonard, M. Krishnamurthy, C.M. Reaves, S.P. Denbaars, and P.M. Petroff, Appl. Phys. Lett. **63**, 3203 (1993).

10) J.M. Moison, F. Houzay, F. Barthe, L. Leprince, E. Andre, and O. Vatel, Appl. Phys. Lett. **64**, 196 (1994).

11) A. Madhukar, Q. Xie, P. Chen, and A. Konkar, Appl. Phys. Lett. **64**, 2727 (1994).

12) Q. Xie, P. Chen, and A. Madhukar, Appl. Phys. Lett. **65**, 2051 (1994).

13) M. Tabuchi, S. Noda, and A. Sasaki, J. Cryst. Growth, in press.

14) Y. Nabetani, T. Ishikawa, S. Noda, and A. Sasaki, J. Appl. Phys. **76**, 347 (1994).

15) Y. Nabetani, N. Yamamoto, T. Tokuda, and A. Sasaki, J. Cryst. Growth **146**, 363 (1995).

16) J.H. Neave, P.J. Dobson, and B.A. Joyce, Appl. Phys. Lett. **47**, 100 (1985).

17) M. Ichimura, A. Usami, A. wakahara, and A. Sasaki, J. Appl. Phys. **77**, 5144 (1995).

18) F. Houzay, C.Guille, J.M. Moison, P. Henoc, and F. Barthe, J. Cryst. Growth **81**, 67 (1987).

19) M. Lentzen, D. Gerthsen, A. Forster, and K. Urban, Appl. Phys. Lett. **60**, 74 (1992).

20) H. Kitabayashi and T. Waho, J. Cryst. Growth **150**, 152 (1995).

21) H. Asai, J. Cryst. Growth **80**, 425 (1987).

22) D.J. Eaglesham and M. cerullo, Phys. Rev. Lett. **64**, 1943 (1990).

23) S. Guha, A. Madukar, and K.C. Rajkumar, Appl. Phys. Lett. **57**, 2110 (1990).

24) X.W. Lin, J. Washburn, Z. Liliental-Weber, E.R. Weber, A. Sasaki, A. Wakahara, and Y. Nabetani, Appl. Phys. Lett. **65**, 1677 (1994).

25) M. Yano, H. Yokose, Y. Iwai, and M. Inoue, J. Cryst. Growth **111**, 609 (1991).

Chapter 3

Theoretical approach of island formation and strain distribution in island

3.1 Introduction

There are two important layer thicknesses in lattice-mismatched heteroepitaxy. One is so-called critical layer thickness under which dislocation is not generated. Another is a transition layer thickness at which the growth mode of epitaxial layer changes from two-dimensional to three-dimensional. Thus far, the prediction of critical layer thickness for dislocation generation have been investigated by several groups [1,2]. Estimation of critical layer thickness is required to design semiconductor devices composed of lattice-mismatched system and also described in chapter 5 in this thesis. On the contrary, very few works on the prediction of transition layer thickness have been reported [3,4]. In order to fabricate QDs by strain induced island growth, it is important to predict the transition thickness. This problem is meaningful especially the islands are grown by OMPVE, since no *in-situ* surface characterization technique has been established yet.

Beside transition thickness, the strain distribution in island is an interesting

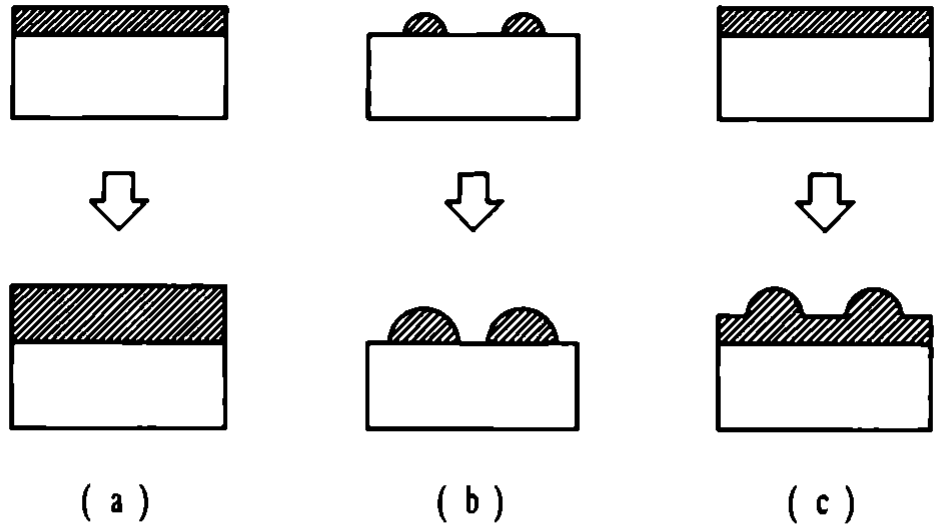

Fig.3-1 Schematic illustrations of growth modes in heteroepitaxy. (a)Frank-van der Merwe(FM), (b)Volmer-Weber(VW) and (c)Stranski-Krastanov(SK) mode.

subject. Because island grows coherently on the substrate, certain strain is distributed in islands. Strain in island changes the band structure such as band gap which results in optical and electrical properties of islands. Thus, the calculation of strain distribution in island is important.

In this chapter, the transition thickness is theoretically estimated by taking surface and strain energies into account. The estimated transition thickness is compared to experimental results. This theoretical approach will be a guide for QD formation by island growth lattice-mismatched systems. The strain distribution in the island is also calculated by assuming appropriate island.

3.2 Calculation process

3.2.1 Transition thickness

There are three kinds of growth mode in heteroepitaxy as shown in Fig.3-1 [5].

1. two-dimensional layer growth(Frank-van der Merwe mode, FM)
2. three-dimensional island growth(Volmer-Weber mode, VW)
3. two-dimensional layer growth followed by three-dimensional island growth (Stranski-Krastanov mode, SK)

As revealed by previous section, the growth mode of InAs on GaAs is classified as SK. We can predict the growth mode for a given combination of epitaxial layer and substrate by Wulff's theorem taking interface into account [6]. Figure 3-2(a) shows the equilibrium shape of a single crystal. From Fig.3-2(a), relation between surface energies of each plane and distance from Wulff point to each surface is derived as follows:

$$\frac{\sigma_1}{h_1} = \frac{\sigma_2}{h_2} = \cdots = \frac{\sigma_i}{h_i} = \cdots = \frac{\Delta\mu}{2v} \tag{3-1}$$

where σ_1, σ_2, and σ_i denote the surface energies of surface 1, 2, and i, respectively, h_1, h_2, and h_i distances from Wulff point O to surface 1, 2, and i, respectively, $\Delta\mu$ the change of chemical potential per atom when atom is incorporated into crystal from vapor phase, and v the volume of one atom. Eq.3-1 is a well-known Wulff's theorem. Similarly the equilibrium shape of heteroepitaxially grown crystal is shown in Fig.3-2(b), and similar equation as Eqs.3-1 is derived:

$$\frac{\sigma_1}{h_1} = \frac{\sigma_2}{h_2} = \cdots = \frac{\sigma_i}{h_i} = \cdots = \frac{\sigma_{epi}}{h_{epi}} = \frac{\sigma_{int} - \sigma_{sub}}{h_{int}} = \frac{\Delta\mu}{2v} \tag{3-2a}$$

$$\sigma_{int} = \sigma_{epi} + \sigma_{sub} - \gamma + \epsilon \tag{3-2b}$$

where σ_{epi}, σ_{sub} denote the surface energies of epitaxial layer and substrate, respectively, σ_{int} the interface energy between substrate and epitaxial layer. Similarly, h_{epi} and h_{int} denote distances from Wulff point to epitaxial layer surface and to interface, respectively. Interface energy σ_{int} is represented by Eq.3-2b. γ

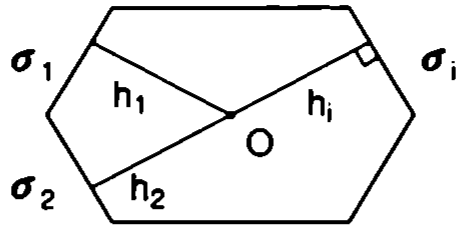

(a)

O : Wulff point

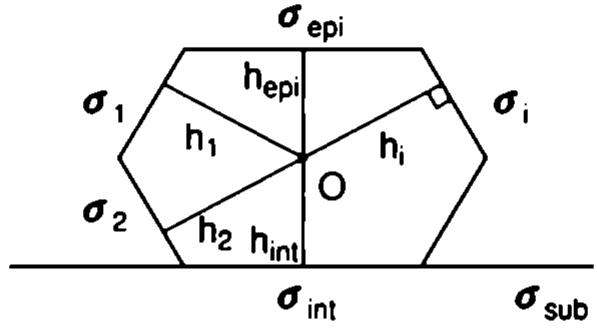

(b)

σ_i	**surface energy**	σ_{epi}	**surface energy of epitaxial layer**
σ_{sub}	**surface energy of substrate**	σ_{int}	**interface energy**
γ	**adhesion energy**	ϵ	**strain energy**
$\Delta\mu$	**change in chemical energy**	v	**volume of one atom**

Fig.3-2 Schematic illustrations for explanation of Wulff's theorem. (a)Equilibrium shape of single crystal. (b)Equilibrium shape in heteroepitaxy.

is called adhesion energy. This term is equivalent to the sum of σ_{epi} and σ_{sub} for homoepitaxy. Strain energy ϵ plays an important role to the interface energy in lattice-mismatched heteroepitaxy, because strain energy is generated as a result that the lattice spacing of coherently grown epitaxial layer is adjusted to the lattice constant of substrate at the interface. In Eq.3-2a, h_{int} becomes 0 when $\sigma_{int} = \sigma_{sub}$. This situation can be interpreted that the lower part of epitaxial crystal does not exist. Furthermore epitaxial crystal disappears when $\sigma_{int} - \sigma_{sub} = -\sigma_{epi}$ or $h_{int} = -h_{epi}$. This means that the epitaxial layer does not grow three-dimensionally. Then, two-dimensional growth and three-dimensional growth can be distinguished by next equations:

$$\sigma_{int} - \sigma_{sub} < -\sigma_{epi} \quad \cdots \quad \text{two} - \text{dimensional growth} \tag{3-3a}$$

$$\sigma_{int} - \sigma_{sub} > -\sigma_{epi} \quad \cdots \quad \text{three} - \text{dimensional growth} \tag{3-3b}$$

Considering that there are no dangling bonds at heterointerface, the contribution of chemical energy to interface energy can be neglected. Then, Eqs.3-3 can be written as follows by using term of strain energy ϵ.

$$\sigma_{sub} - \sigma_{epi} > \epsilon \quad \cdots \quad \text{two} - \text{dimensional growth} \tag{3-4a}$$

$$\sigma_{sub} - \sigma_{epi} < \epsilon \quad \cdots \quad \text{three} - \text{dimensional growth} \tag{3-4b}$$

Note that the strain energy ϵ increases as epitaxial layer grows while the surface energies σ_{sub}, σ_{epi} remain the same. In other words, the energy relation changes from Eq.3-4a to 3-4b as growth proceeds. This change does indicate the kinetic process of SK growth mode in the lattice-mismatched heteroepitaxy.

From Eqs.3-4, the transition thickness can be estimated quantitatively. The strain energy was calculated by valence-force field(VFF) model [7,8]. In VFF model, the strain energy is calculated by bond stretching and angle wagging between two bonds as shown in Fig.3-3. VFF model is applicable to microscopic structure, because strain energy is calculated from the position of each atom.

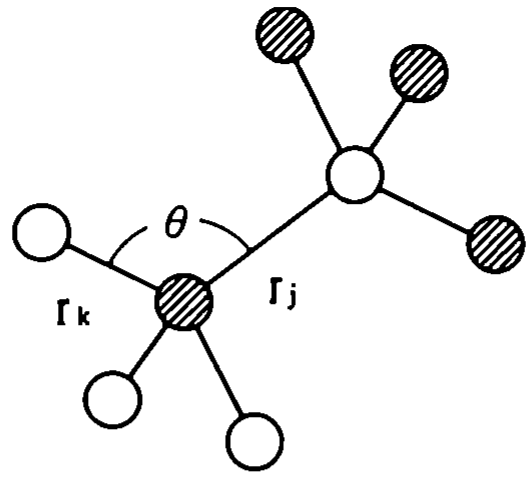

Fig.3-3 Atom arrangement for VFF model.

Concretely, stain energy ϵ of each atom in zincblende structured crystal is represented by following equation:

$$\epsilon = \frac{1}{2}\sum_{j=1}^{4}\frac{3}{4}\alpha_j\frac{[\Delta(\mathbf{r}_j^1\cdot\mathbf{r}_j^1)]^2}{r_j^{0\,2}} + \frac{1}{2}\sum_{s=1}^{2}\sum_{\substack{j,k=1\\ j\neq k}}^{4}\frac{3}{4}\beta_{jk}^s\frac{[\Delta(\mathbf{r}_j^s\cdot\mathbf{r}_k^s)]^2}{\mathbf{r}_j^0\cdot\mathbf{r}_k^0} \qquad (3\text{-}5)$$

where s denotes group III and group V atoms. The bonds around each atom are denoted by j,k=1~4, and $\mathbf{r}_j^s$ and $\mathbf{r}_k^s$ are the bond vectors around s atom. r_j^0 is the equilibrium bond length j. α and β represent the elastic constants for bond stretching and angle wagging between two bonds, respectively. Bond lengths r and elastic constants α, β of P-related and As-related III-V compound semiconductors are summarized in Table 3-1.

In order to calculate the strain energy in two-dimensionally grown layer, the strain energy should be summed up with respect to one atom row along growth direction as illustrated in Fig.3-4. The strain energy is minimized by moving atom positions so that the derivative of Eq.3-5 becomes 0.

For estimation of surface energy, the binding energy, i.e., cohesive energy per bond, was used [9,10]. To simplify surface energy estimation, surface reconstruction

Table 3-1 Bond length and elastic constants for VFF model [8].

	r	α	β
	[a.u]	10^3dyn/cm	
AlP	4.470	*47.17	*9.07
GaP	4.460	47.32	10.44
InP	4.802	43.04	6.24
AlAs	4.631	*42.89	*9.86
GaAs	4.626	41.19	8.95
InAs	4.957	35.18	5.50

*These values were calculated under the assumption that the relations of α and β in AlSb, GaSb, and InSb are applicable in P-related and As-related compounds.

Table 3-2 Binding energy per bond [9,10].

	S[eV]
AlP	*1.904
GaP	1.656
InP	1.500
AlAs	1.777
GaAs	1.522
InAs	1.400

*This value was calculated under the assumption that the relation of binding energy in AlAs, GaAs, and InAs is applicable in P-related compounds.

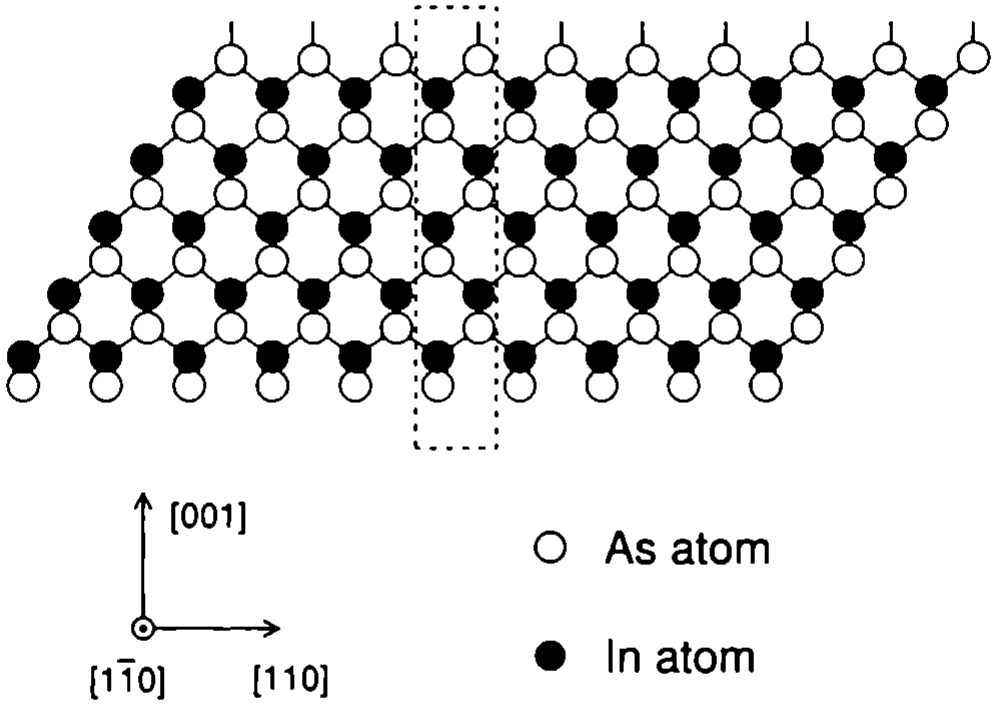

Fig.3-4 Example of atom row along growth direction for summation of strain energy.

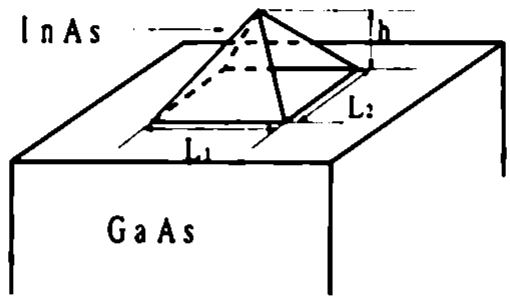

(a)

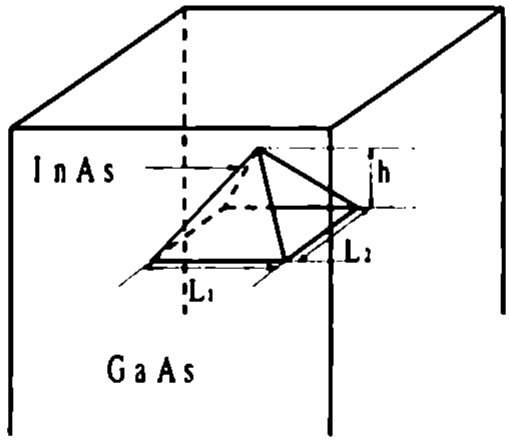

(b)

Fig.3-5 Island configurations for strain distribution calculation. (a)InAs island surface is free. (b)InAs island is embedded in GaAs. Island height h, and size in growth plane L_1, L_2 are 16ML for both cases.

is neglected and surface structure of 1×1 is assumed here. Then, each surface atom has two dangling bonds in the growth plane, that is, (001) plane. Since two surfaces are produced by dividing crystal, surface energy per bond becomes a half of binding energy. The binding energy per bond, S, of P-related and As-related III-V compound semiconductor are summarized in Table 3-2.

3.2.2 Strain distribution in island

Strain energy distribution in island was calculated also by VFF model. Two island configurations were considered as shown in Figs.3-5. In Fig.3-5(a), InAs island surface is not covered so that the atoms on island surface can move freely. On the contrary, InAs island is embedded in GaAs Fig.3-5(b). 1ML-thick InAs two-dimensional layer is inserted between GaAs and InAs island. Island size and shape are same for both configurations. Island size is 16ML in growth plane and also 16ML in height. Lateral surface of island is composed of four {111} planes. Although the assumed island size and shape are different from observed structure, island size were taken as large as possible in the restriction of hard ware. Difference of island shape would not cause serious problem when qualitative analysis is discussed. In the calculating process, periodical boundary condition was applied, that is, crystals illustrated in Figs.3-5 lie side by side in growth plane. Under the island, the lattice spacing was fixed to the lattice constant of GaAs, however, only 1ML of GaAs was allowed to move. Dislocation was not introduced in the island.

3.3 Results and discussion

3.3.1 Transition thickness

Calculated strain energy in InAs two-dimensionally grown layer on GaAs as a function of layer thickness is shown in Fig.3-6. In Fig.3-6, the strain energy is summed up with respect to one atom row along [001] direction as mentioned

above. The abscissa denotes InAs layer thickness in the unit of atomic layer. The surface energies per bond of InAs and GaAs are also shown. From Eqs.3-1, island growth starts when the strain energy exceeds the difference in surface energies between substrate and epitaxial layer.

The difference of surface energy is twice of the difference in surface energy and is calculated as 0.122eV. Then, the transition thickness at which the growth mode changes from two-dimensional to three-dimensional is estimated as 1.1 in unit of atomic layer, i.e., 0.55ML. The calculated thickness is thinner than the experimental result of 1.8ML.

Figure 3-7 shows calculated transition thickness of $In_xGa_{1-x}As$ grown on GaAs based on our model. Experimental results are also shown for comparison [3.11]. One can see that the difference becomes remarkably at low In composition region. To investigate the origin of disagreement, we have calculated the strain energy which corresponds to the difference of transition thickness between our model and experimental results. The result is shown in Fig.3-8. Considering that N. Grandjean et al. measured the transition thickness by the spacing of diffraction rods or spots in RHEED while P.M. Petroff et al. observed only the change in RHEED pattern(from streak to spotty), the transition thickness measured by former group is more reliable, especially at low In composition region. Then, the difference of strain energy between those at calculated and experimental transition thicknesses becomes almost 0.27eV and slightly decreases as In composition increases.

There are two origins which cause the underestimation of transition thickness. One is that the energy accommodated in island. Our model deals with only total energy, which is sum of surface and strain energy, of two-dimensional layer and does not take energy of island into account. Three-dimensional growth begins when the total energy of two-dimensional layer becomes larger than that of island, similar to the energy balance model of dislocation generation prediction [2]. However, it is impractical to calculate the total energy of island because island size and shape is unknown. If we assume appropriate island and calculate total

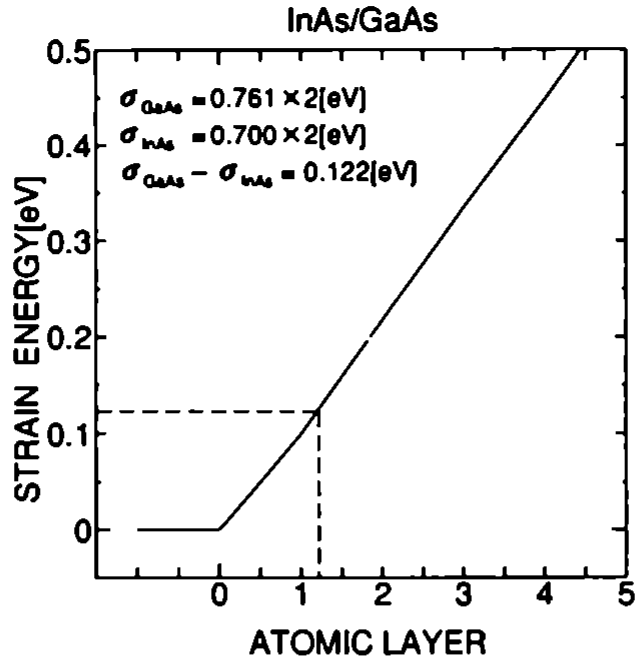

Fig.3-6 Sum of strain energy in InAs atom row. Surface energies of GaAs(σ_{GaAs}) and InAs(σ_{InAs}) are shown. Dotted line indicates strain energy and InAs layer thickness at which the growth mode changes form two-dimensional to three-dimensional.

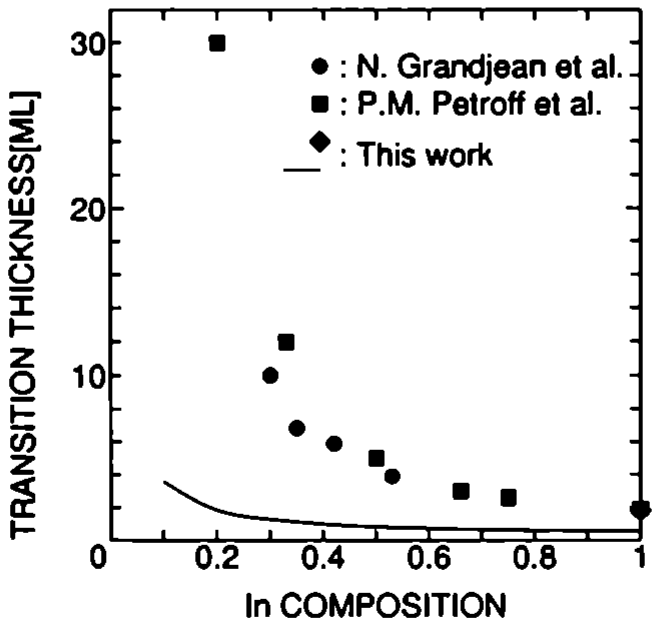

Fig.3-7 Calculated transition thickness for $In_xGa_{1-x}As/GaAs$. Experimental data by other groups are also shown for comparison.

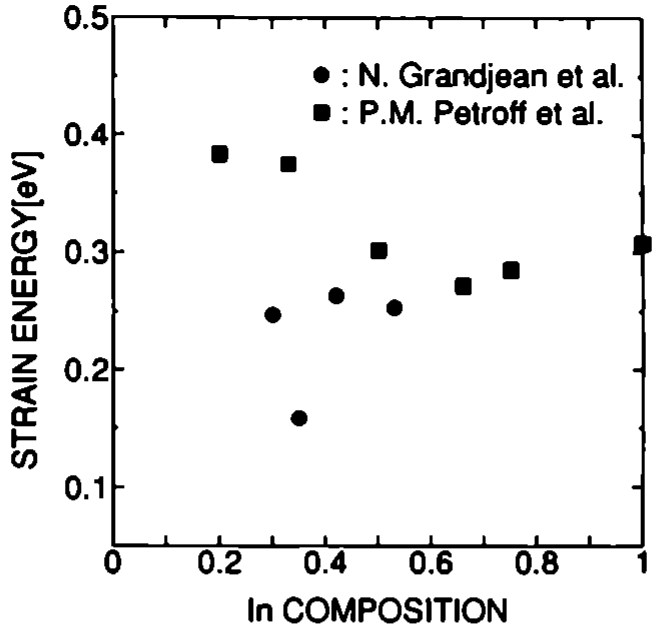

Fig.3-8 Strain energy corresponds to the difference of transition thickness between our model and experimental results.

energy, the transition thickness would be estimated. Conversely, the transition thickness which agrees the experimental result may be obtained by choosing certain island. This sequence is, however, nonsense.

Another reason is the fact that the growth is performed under non-equilibrium condition. Wulff's theorem is valid at equilibrium condition where the crystal does not grow nor desorb, on the other hand, the situation in MBE growth is non-equilibrium generally. In other word, the substrate temperature during MBE growth is lowered to prevent desorption of group V atoms in insufficient group V overpressure. In such a condition, total energy in epitaxial layer, which is the driving force for three-dimensional growth, needs more strain energy to start three-dimensional growth.

S. Ohkouchi et al. have observed STM images of GaAs grown on InAs (001) substrate by MBE [12,13] This combination of InAs substrate and GaAs epitaxial layer can be classified as VW growth mode and is expected to grow three-

dimensionally from the beginning of growth. However, they reported that GaAs grows two-dimensionally until 0.75ML and then three-dimensional growth occurs. Moreover, atoms which has already grown two-dimensionally is stripped off from InAs surface and taken into islands when the three-dimensional growth occurs. The strain energy summed up for one atom row along [001] direction for 0.75ML-thick GaAs grown on InAs was calculated as 0.27eV. This experiment also indicates that certain extra energy is required to form island.

3.3.2 Strain distribution in island

Calculated strain distribution in several (001) planes is shown in Figs.3-9 and 3-10. When island surface is free, one can see that the strain energy is smaller in upper part of island than in lower part. Furthermore, the strain distribution is different between lower and upper parts. The strain distribution seems concave in lower part while convex shape strain distribution is seen in upper part. Since atoms on island surface can move freely, strain energy at island surface becomes smaller than that in island center, thus, the strain distribution in upper part of island becomes convex shape. On the other hand, the atoms at periphery of island foot are bonded with under GaAs layer which leads compressive strain and also bonded with upper InAs which moves to outer island. As a result, two kinds of bonding cause unnatural bond configuration and large strain is induced. C. Priester et al. has obtained similar results by assuming several facet planes [14]. It is noteworthy that strain extends even to GaAs layer under island. This result agrees with the cross sectional TEM observation.

Compared to the surface free island, the strain energy in embedded island is greater. This trend seems more remarkable in upper part of island. Furthermore the strain distribution is concave regardless of height. Because island surface contacts with GaAs, atoms at island surface are strained while atoms at inner island are bonded with only InAs. This situation does not change with respect to height. Therefore, the strain distribution becomes concave shape and the strain

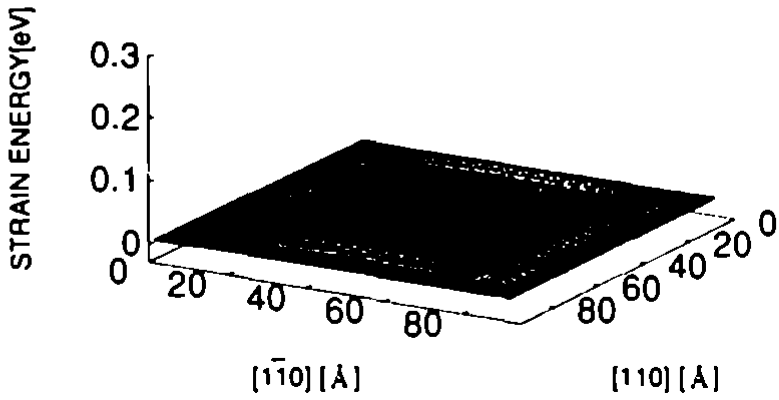
STRAIN ENERGY[eV]
0.3
0.2
0.1
0
0
20
40
60
80
[1$\bar{1}$0] [Å]
0
20
40
60
80
[110] [Å]

(a)

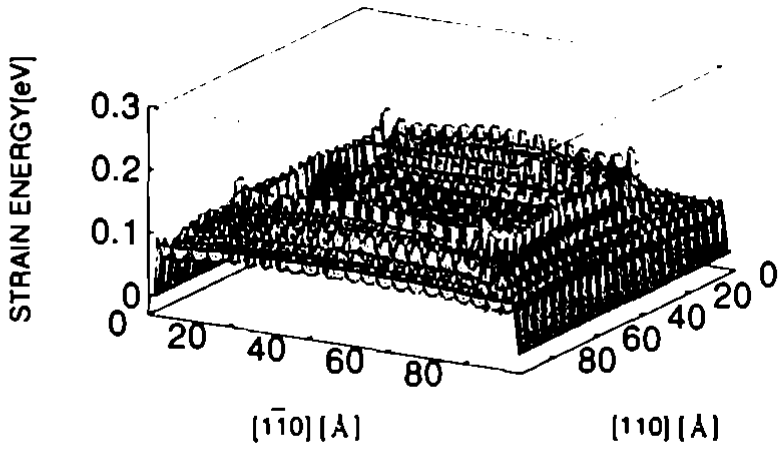
STRAIN ENERGY[eV]
0.3
0.2
0.1
0
0
20
40
60
80
[1$\bar{1}$0] [Å]
0
20
40
60
80
[110] [Å]

(b)

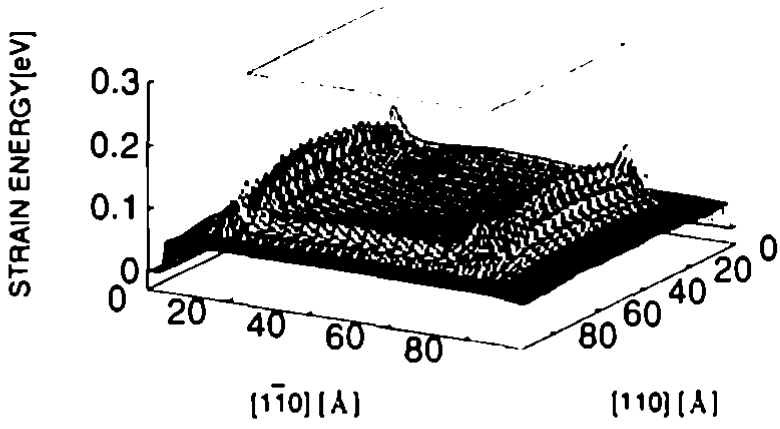
STRAIN ENERGY[eV]
0.3
0.2
0.1
0
0
20
40
60
80
[1$\bar{1}$0] [Å]
0
20
40
60
80
[110] [Å]

(c)

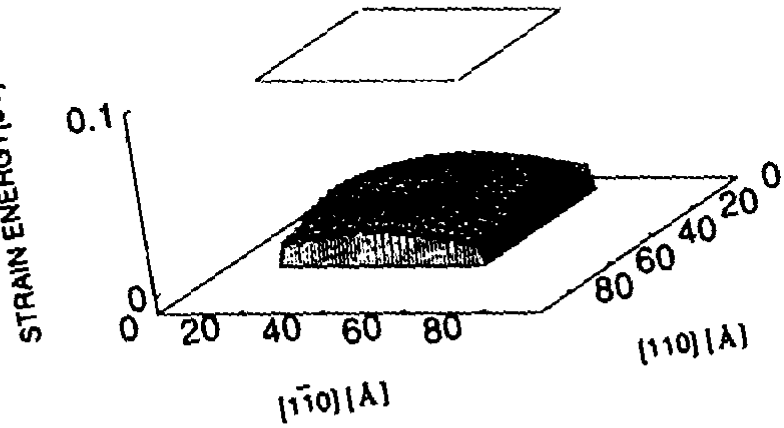
STRAIN ENERGY[eV]
0.1
0
0
20
40
60
80
[1$\bar{1}$0] [Å]
0
20
40
60
80
[110] [Å]

(d)

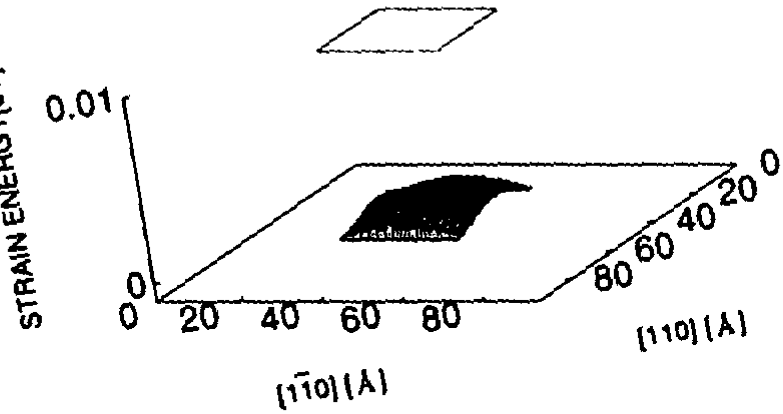
STRAIN ENERGY[eV]
0.01
0
0
20
40
60
80
[1$\bar{1}$0] [Å]
0
20
40
60
80
[110] [Å]

(e)

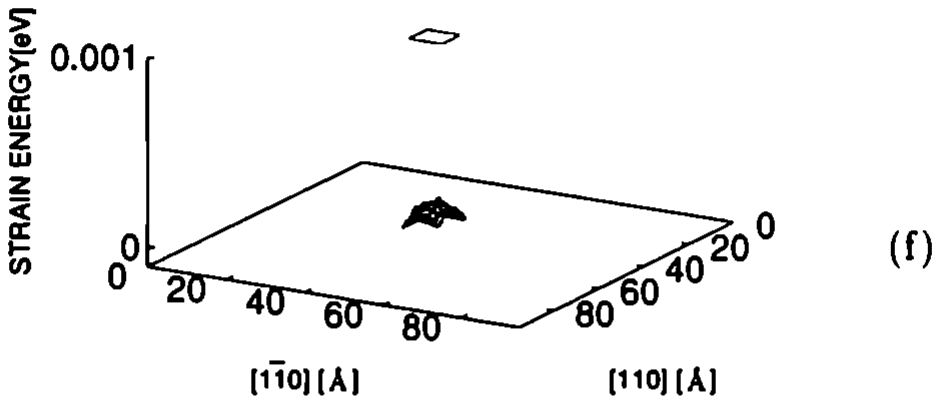

Fig.3-9 Strain distribution in several (001) planes in surface free island. The lateral size along [110] and [1$\bar{1}$0] is in unit of Å. Squares above each graph indicate the interface between InAs and GaAs, and enclosed parts correspond to InAs. (a)GaAs layer just under island, (b)1st InAs layer from interface, (c)2nd InAs layer from interface, (d)5th InAs layer from interface, (e)10th InAs layer from interface and (f)15th InAs layer from interface.

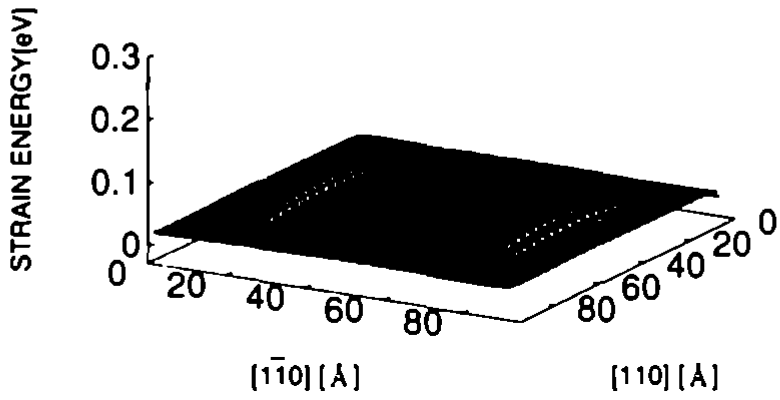
STRAIN ENERGY[eV]
0.3
0.2
0.1
0
0
20
40
60
80
[1$\bar{1}$0] [Å]
0
20
40
60
80
[110] [Å]

(a)

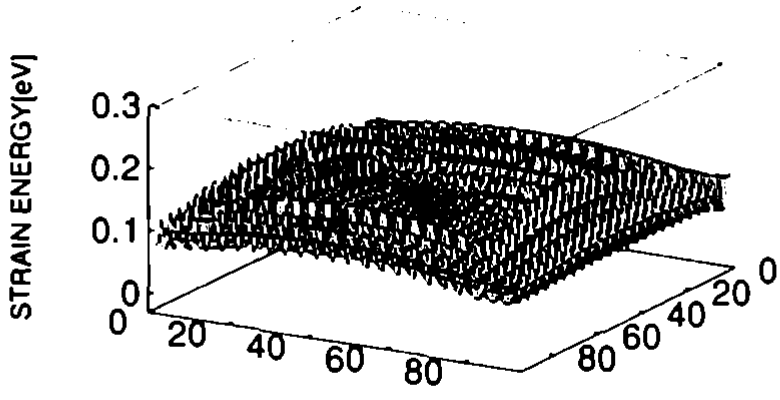
STRAIN ENERGY[eV]
0.3
0.2
0.1
0
0
20
40
60
80
[1$\bar{1}$0] [Å]
0
20
40
60
80
[110] [Å]

(b)

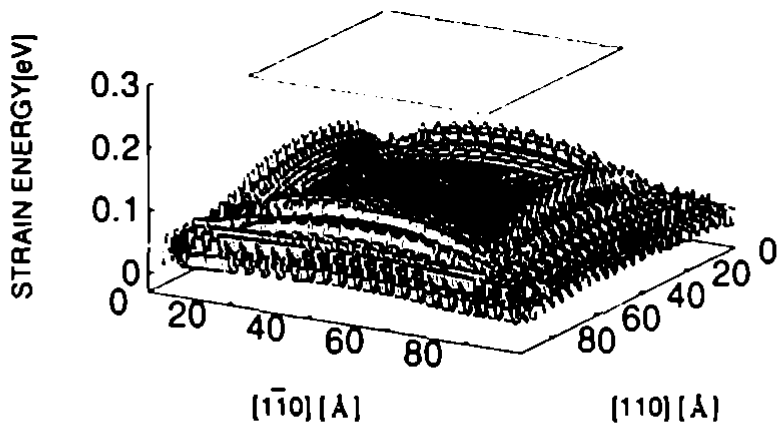
STRAIN ENERGY[eV]
0.3
0.2
0.1
0
0
20
40
60
80
[1$\bar{1}$0] [Å]
0
20
40
60
80
[110] [Å]

(c)

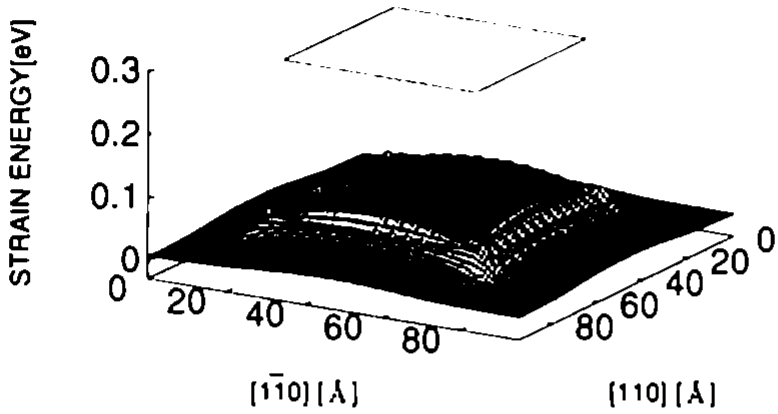
STRAIN ENERGY[eV]
0.3
0.2
0.1
0
0
20
40
60
80
[1$\bar{1}$0] [Å]
0
20
40
60
80
[110] [Å]

(d)

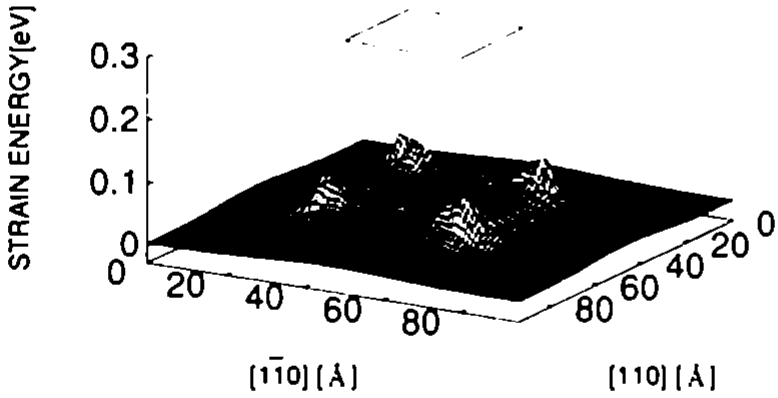
STRAIN ENERGY[eV]
0.3
0.2
0.1
0
0
20
40
60
80
[1$\bar{1}$0] [Å]
0
20
40
60
80
[110] [Å]

(e)

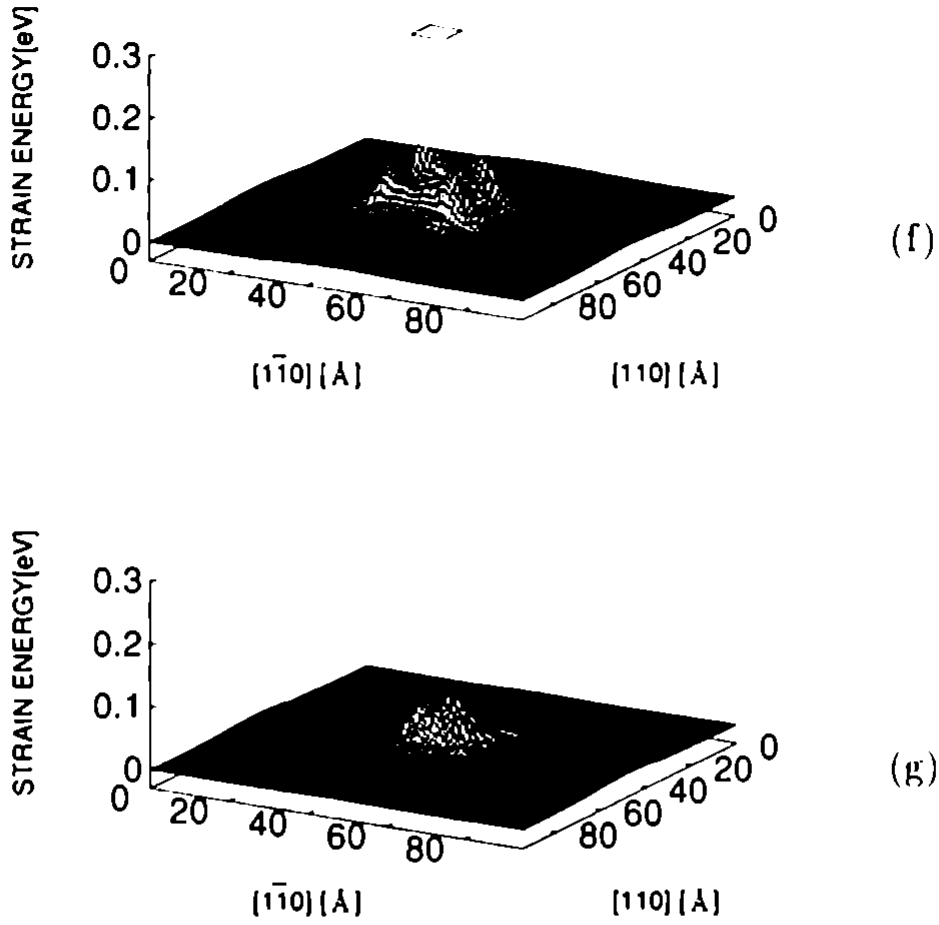

Fig.3-10 Strain distribution in several (001) planes in island. Island is embedded in GaAs. The lateral size along [110] and [1$\bar{1}$0] is in unit of Å. Squares above each graph indicate the interface between InAs and GaAs, and enclosed parts correspond to InAs. (a)GaAs layer just under island, (b)1st InAs layer from interface, (c)2nd InAs layer from interface, (d)5th InAs layer from interface, (e)10th InAs layer from interface, (f)15th InAs layer from interface and (g)18th InAs layer from interface.

energy does not decrease drastically with respect to height. It is important to notice that the strain distributes not only in InAs island but also in surrounding GaAs.

From calculated strain distribution in InAs and surrounding GaAs, it is considered that the band structure such as potential height is changed. Although VFF model cannot classify the strain into each coordinate compositions such as ϵ_{xx}, ϵ_{yy} and ϵ_{zz}, position of each atom is obtained. In this case, band gap would be estimated using deformation potential by calculating strain in growth plane and growth direction from each atom position. However, band gap calculated such method is defined within very local space and hence suspicious to apply further calculation. Band structure should be calculated by tight binding method since all the atom positions are known, though it takes enormous time to calculate.

3.4 Summary

In this chapter, the transition thickness of island growth and strain distribution in island were calculated. The transition thickness at which the growth mode changes from two-dimensionally to three-dimensionally was estimated in terms of strain and surface energies based on Wulff's theorem. Strain energy was calculated by VFF model and binding energy was used as surface energy. As results, calculated transition thickness for InGaAs/GaAs was thinner than experimental results. Disagreement was attributed to the neglect of total energy of island and non-equilibrium growth condition in MBE. However, precise transition thickness may be predicted by adding certain energy to strain energy.

Calculated strain distribution in island was different between surface free island and embedded island. Strain energy decreases in upper and outer parts of island in case of free surface. On the contrary, strain energy does not change along growth direction and is larger at InAs/GaAs boundary than at island center in case of embedded island. It is desired to calculate the band structures from calculated atom positions.

References

1) J.W. Matthews and A.E.Blakeslee, J. Cryst. Growth **115**, 118 (1974).

2) R. People and J.C. Bean, Appl. Phys. Lett. **47**, 322 (1985).

3) N. Grandjean, J. Massies, and F. Raymond, Jpn. J. Appl. Phys. **33**, L1427 (1994).

4) M. Biagini and A. Catellani, J. Appl. Phys. **76**, 3516 (1994).

5) A.A. Chernov, *Modern Crystallography III* (Springer-Verlag, Berlin, 1984).

6) R. Kern, G. Le Lay, and J.J. Metois, *Current Topics in Materials Science*, vol.3 Editted by E. Kaldis(North-Holland, 1979).

7) P.N. Keating, Phys. Rev. **13**, 637 (1966).

8) R.M. Martin, Phys. Rev. **B15**, 4005 (1970).

9) M. Yano, H. Yokose, Y. Iwai, and M. Inoue, J. Cryst. Growth **111**, 609 (1991).

10) J.C. Phillips, *Bond and Bands in Semiconductors* (Academic Press, New York, 1973).

11) P.M. Petroff and S.P. DenBaars, Superlattices Microstruct. **15**, 15 (1994).

12) S. Ohkouchi, I. Tanaka and N. Ikoma, Jpn. J. Appl. Phys. **33**, 1489 (1994).

13) S. Ohkouchi and N. Ikoma, Jpn. J. Appl. Phys. **33**, 3710 (1994).

14) C. Priester, I. Lefebvre, G. Allan, and M. Lannoo, Mechanisms of This Film Evolution. Symposium, 131 (1994).

Chapter 4

Optical property of InAs on GaAs

4.1 Introduction

The band structures of GaAs and InAs are both direct and the band lineup at heterointerface of InAs and GaAs is type-I which means that both electrons and holes are confined in the same space. The band gaps of GaAs and InAs are 1.424 and 0.354eV at room temperature, respectively [1]. These electronic properties are advantageous for light-emitting device, especially for infrared optical communication. Further, the discontinuities of conduction and valence bands at heterointerface are quite large, strong quantum effect brought by suitable quantum structure is expected. In spite of such attractive material properties, the heterostructure of InAs/GaAs with no defects is difficult to fabricate due to the large lattice-mismatching of 7.2%. However, small InAs island which has no defects was formed on GaAs at very early stage in MBE growth as revealed in chapter 2. The island size is about 150~250Å in diameter and 30Å in height. The density is as high as $1.1\times10^{11}cm^{-2}$ in the growth plane. Since the island size is considerably small, it is expected that this self-assembled island can be utilized as a QD.

Luminescence from ideal QD is known as ultra narrow peak due to δ function like DOS. Sharp DOS improves threshold current and its temperature dependence of LD [2-5]. Fluctuation of lasing wavelength due to temperature is also stabilized. Another important feature of QD is the low optical phonon scattering. Energy state of carrier in ideal QD is perfectly quantized and the intervals between quantum energy states become larger when QD size is reduced. If the intervals of energy states become larger than the energy of optical phonon, absorption of optical phonon is forbidden. On the contrary, phonon emission is prohibited when the interval of energy states is smaller than phonon energy. Then, carrier relaxation from higher energy states by phonon scattering is suppressed. This property can be used for inter-subband LD in which realization of population inversion is extremely difficult because of short carrier relaxation time.

In order to confirm the possibility of application of InAs island for QD, it is necessary to investigate electrical and optical properties. Thus far, several groups including us have characterized the optical property of InAs grown on GaAs [6-10]. However, most of the previous works have not related the optical property to the InAs structure. Since InAs epitaxial structure drastically changes especially at the beginning of growth as shown in chapter 2, investigation of optical property of InAs with respect to the layer thickness is extremely important and stimulating.

In this chapter, the optical properties of InAs grown on GaAs is investigated where InAs layer thickness is variously changed. Photoluminescence(PL), PL polarization, electroluminescence(EL) and photocurrent(PC) spectroscopies were measured. As results, strong luminescence dependence on InAs structure is shown. High luminescence efficiency of island and polarization are revealed.

4.2 Experimental setup

PL was performed with a 5145Å Ar-ion laser. Samples were cooled by closed type He flow cryostat(>10K) or liquid nitrogen(77K). Luminescence was monochromated by 0.75m-long monochromator and detected by Ge pin diode cooled by

liquid nitrogen. The spatial resolution of monochromator is 4Å . Lock-in detection technique was used to gain S/N ratio. Samples for PL measurement have 100Å-thick single crystal GaAs cap layer so that InAs becomes QW or QDs in GaAs.

Polarization of PL was measured with the system illustrated in Fig.4-1. One can see the polarizer in front of the monochromator. Polarization property of gratings in monochromator was calibrated by halogen lamp which emits no polarized luminescence. To measure the polarization of luminescence, two configurations were adopted, i.e., polarizer was rotated while sample was fixed, and sample was rotated while polarizer was fixed.

EL and PC were measured at room temperature(RT). EL was also performed with the same measurement system as PL except for the fact that carriers were injected by direct current. PC was measured under reverse bias condition without additional load. GaAs/InAs/GaAs pin photo diode structures were fabricated for EL and PC measurement. The 4000Å-thick Si-doped GaAs cladding layer was grown on an n-GaAs substrate at 580°C at first. Then, an undope InAs active layer with various thickness was grown at 480°C. The 4000Å-thick Be-doped p-GaAs cladding layer was grown on the active layer. Since growth temperature of 480°C is low for ideal GaAs growth, growth temperature was increased gradually from 480°C to 580°C to improve the crystalline quality of p-GaAs cladding layer. Finally, the 1000Å-thick Be-doped p^+-GaAs contact layer was grown. Au/Cr mesh and Au/Ge/Ni flat electrodes were formed by photo lithography and evaporation for p^+- and n-GaAs layers, respectively. Ohmic contacts were formed by alloying at 380°C for 60sec in H_2 ambient. The finished sample structure is shown in Fig.4-2.

4.3 Photoluminescence spectroscopy

Figure 4-3 shows the PL spectra of 1.0~2.0ML-thick InAs at 10K. One can see the sharp peaks at 1.0, 1.3 and 1.5ML. Peak wavelengths are 842, 865 and

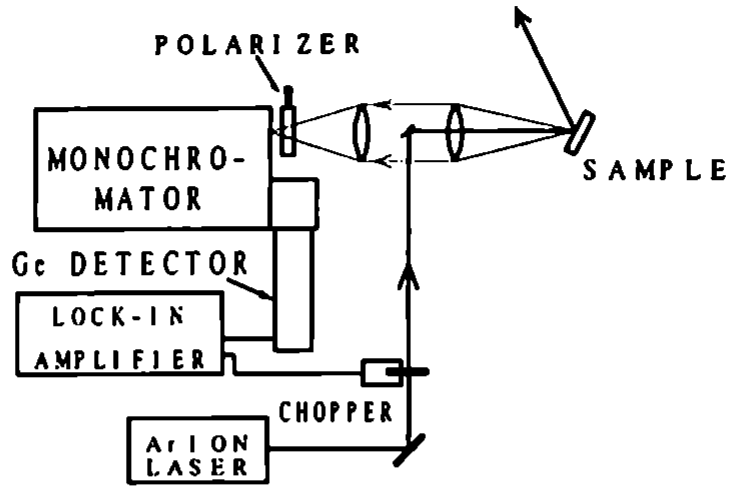

Fig.4-1 Schematic illustration of measurement system for polarization of PL. The polarizer in front of monochromator was removed when conventional PL was measured.

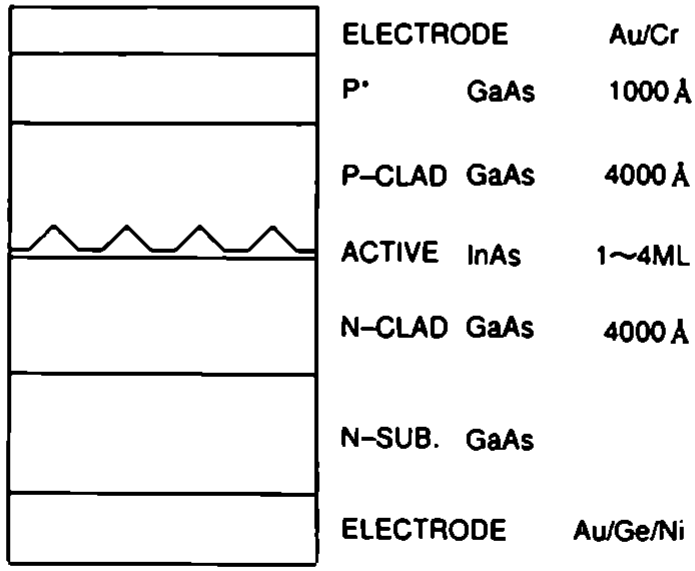

Fig.4-2 Schematic illustration of sample structure for EL and PC. A pin photo diode was composed by p-GaAs, undoped InAs and n-GaAs layers.

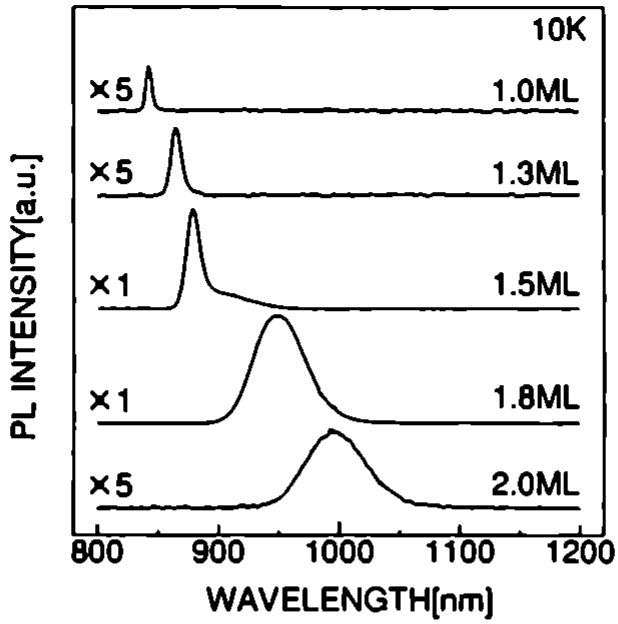

Fig.4-3 PL spectra observed from 1.0 to 2.0ML-thick InAs grown on GaAs. 100Å-thick single crystal GaAs cap layer was grown to make up SQW structure. Transition of sharp to broad peak is shown which corresponds to the island formation.

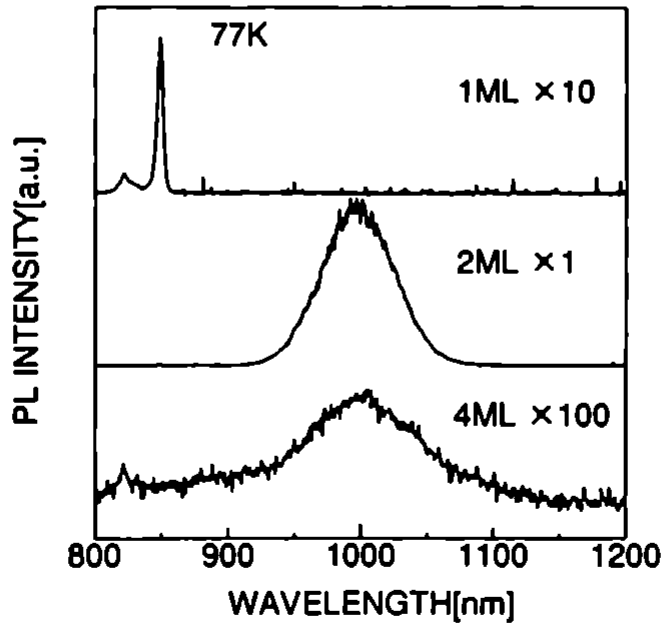

Fig.4-4 PL spectra from 1, 2 and 4ML-thick InAs grown on GaAs. The luminescence peak wavelength at 4ML is the same as that at 2ML, though the intensity is weaker.

878nm, respectively. Since RHEED, AFM and TEM observations indicate that InAs grows two-dimensionally at these thicknesses, the luminescence is emitted from GaAs/InAs/GaAs single quantum well. The narrow full width at half maximum(FWHM) as 10meV means the uniformity of the InAs layer thicknesses. It is generally recognized that luminescence from QW in which well width is not integer ML has multiple peaks due to inhomogeneity of layer thickness in growth plane [11]. However, as seen in Fig.4-3, there is only one peak in luminescence spectra when InAs layer thickness is thinner than 1.5ML. Furthermore, the peak wavelength shift to longer as layer thickness increases. Therefore, it is considered that the terrace width in InAs layer is shorter than exciton diameter and the exciton feels averaged potential. Another peak appears at the longer wavelength side at 1.5ML. This peak implies the occurrence of island growth, though significant InAs islands were not observed by AFM and TEM at 1.5ML. The optical property of the InAs layer is sensitive to its structure. At 1.8ML, the FWHM becomes drastically broad as 60meV. The luminescence spectrum does not greatly change between 1.8 and 2.0ML, though the peak wavelength shifts to longer. Thus, not only the island density increases but the island size becomes slightly larger with increasing InAs layer thickness. If the luminescence is emitted from QDs, the FWHM is expected to be narrow. However, the diameter of excited light is 0.1mm in our experiment and there are 10^7 islands in the excited area. The broad FWHM can be attributed to the fluctuation in island size as revealed in chapter 2. Recently, J.Y. Marzin et al. has performed micro PL measurement which can measure PL from area as small as 2.0μm in diameter [10]. They observed many peaks with ultra narrow FWHM at the same wavelength region as conventional PL spectra.

The PL spectra from 1, 2 and 4ML measured at 77K are shown in Fig.4-4. One can see a weak peak in shorter wavelength beside main peak at 1ML. This weak luminescence is emitted from GaAs layer and indicates that the carriers are spilled over from 1ML-thick QW. On the contrary, no luminescence related to GaAs is seen at 2ML. It is interesting that the luminescence wavelengths of 2ML-

and 4ML-thick InAs QWs are almost the same but the intensity is weaker in 4ML. This result is interpreted that the large island in which misfit dislocations are generated does not concern with luminescence because dislocation works as non-radiative center [12]. Low density of coherently grown small island and high density of strain relaxed large island resulted weak luminescence intensity in 4ML-thick sample. The growth mode interpreted from PL results is the same as that of AFM and TEM observations.

4.4 Photoluminescence polarization spectroscopy

It is generally known that luminescence from a quantum structure which has structural anisotropy exhibits polarization property, because the wave function becomes anisotropic and direction of dipole moment is spatially quantized [13-16]. As shown in chapter 2, InAs island grown on GaAs is elongated in [1$\bar{1}$0] direction rather than [110] direction. It is considered that PL from island is polarized due to the structural anisotropy.

Before measurement of PL polarization, the polarization property of monochromator should be clarified. In order to clarify the polarization property of monochromator, PL of Si-doped GaAs substrate was measured at first. Figures 4-5(a) and (b) show the PL peak intensities of Si-doped GaAs substrate where substrate was set so that the substrate orientations become orthogonal each other. The peak wavelength was 840nm. Although the PL of GaAs substrate is not polarized, the results indicate strong polarization. Since the PL intensities are strongest when the gratings and polarization direction of polarizer is parallel regardless of the substrate orientation, this polarization property is caused by gratings. Knowing polarization property of gratings, we measured the PL polarization of 1 and 2ML-thick InAs samples as shown in Figs.4-5(c)~(f). Peak wavelengths of 1 and 2ML-thick InAs samples are 850 and 1000nm, respectively. Almost the same results as Si-doped GaAs substrate were seen for 1ML-thick InAs sample, that is, the polarization directions are different between two sample set configurations.

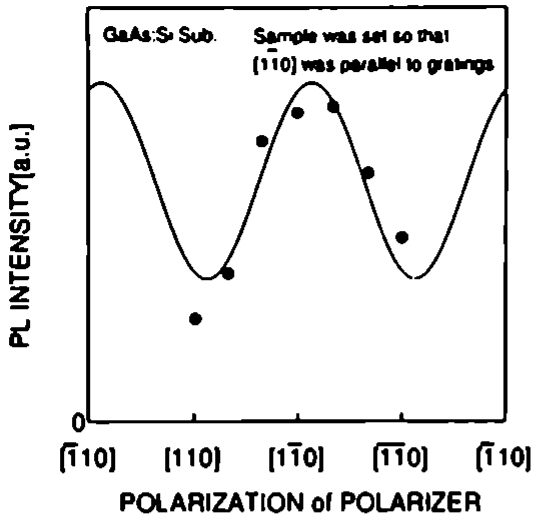
GaAs:Si Sub.
Sample was set so that
[1$\bar{1}$0] was parallel to gratings
PL INTENSITY[a.u.]
0
[$\bar{1}$10] [110] [1$\bar{1}$0] [$\bar{1}\bar{1}$0] [$\bar{1}$10]
POLARIZATION of POLARIZER

(a)

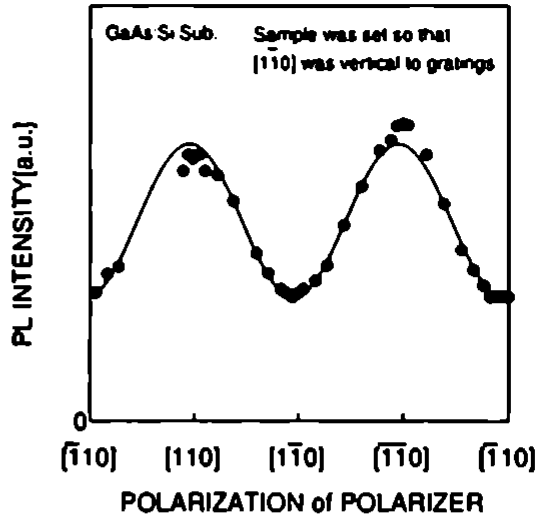
GaAs:Si Sub.
Sample was set so that
[1$\bar{1}$0] was vertical to gratings
PL INTENSITY[a.u.]
0
[$\bar{1}$10] [110] [1$\bar{1}$0] [$\bar{1}\bar{1}$0] [$\bar{1}$10]
POLARIZATION of POLARIZER

(b)

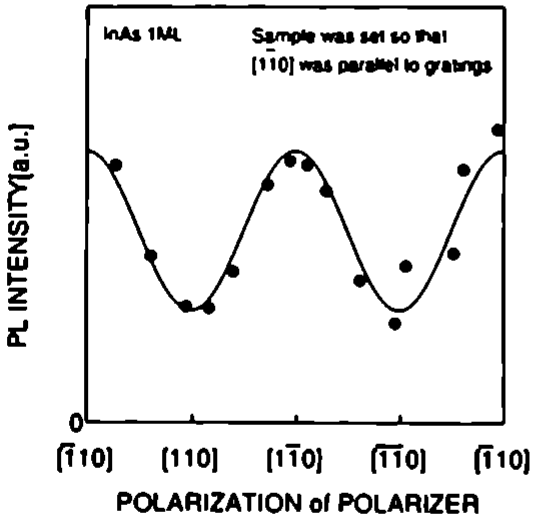
InAs 1ML
Sample was set so that
[1$\bar{1}$0] was parallel to gratings
PL INTENSITY[a.u.]
0
[$\bar{1}$10] [110] [1$\bar{1}$0] [$\bar{1}\bar{1}$0] [$\bar{1}$10]
POLARIZATION of POLARIZER

(c)

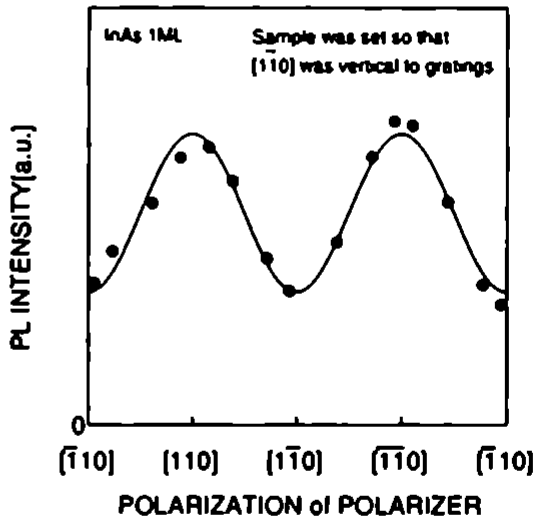
InAs 1ML
Sample was set so that
[1$\bar{1}$0] was vertical to gratings
PL INTENSITY[a.u.]
0
[$\bar{1}$10] [110] [1$\bar{1}$0] [$\bar{1}\bar{1}$0] [$\bar{1}$10]
POLARIZATION of POLARIZER

(d)

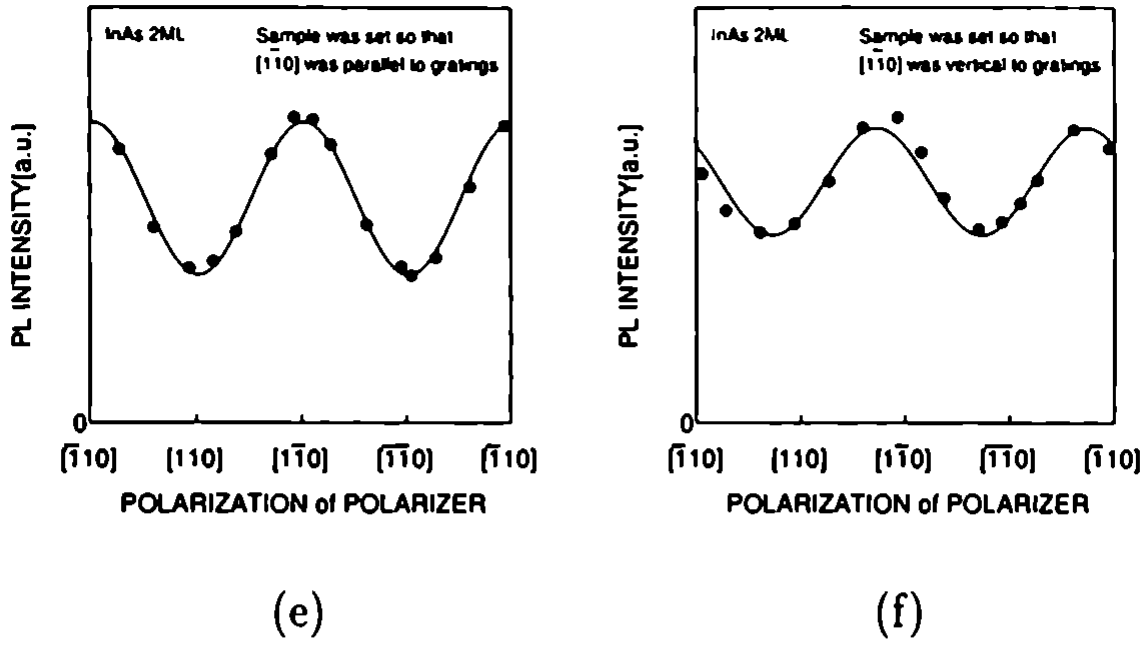

Fig.4-5 Polarization properties of PL from Si-doped GaAs substrate(a),(b), 1ML-thick InAs(c),(d) and 2ML-thick InAs (e),(f). Solid circles represent the PL peak intensities and solid lines are fitted curve by assuming sinusoidal function. Abscissa indicates the polarization direction of polarizer. [1$\bar{1}$0] direction of sample was set parallel to the polarization direction of gratings in the monochromator in (a), (c) and (e), while sample set angle was rotated 90° in (b),(d) and (f).

Therefore the PL from 1ML-thick InAs, in other words, GaAs/InAs/GaAs single quantum well is not polarized. On the other hand, PL intensities are the strongest when the polarization direction of polarizer is parallel to [1$\bar{1}$0] direction regardless of sample set configuration for 2ML-thick sample as seen in Figs.4-5(e) and (f). From these methodical experiments, one can deduce that the PL from 2ML-thick InAs or InAs island is polarized along [1$\bar{1}$0] direction. The polarization along [1$\bar{1}$0] agrees with theoretical prediction as discussed later.

Figures 4-6 show the PL polarization spectra calibrated by polarization property of gratings using halogen lamp. PL spectra of two orthogonal polarization

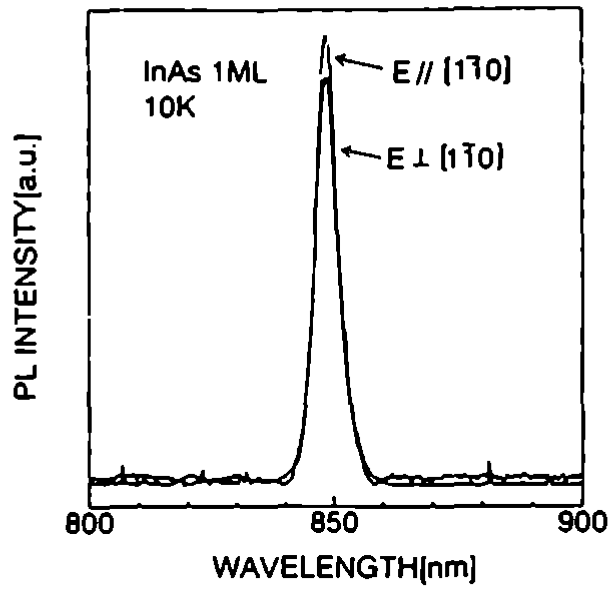

(a)

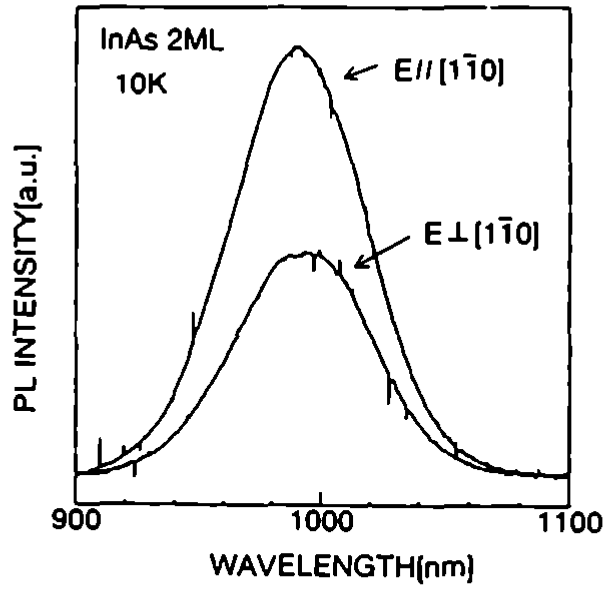

(b)

Fig.4-6 Polarized PL spectra parallel and vertical to [1$\bar{1}$0] direction. Thickness of InAs is (a)1ML and (b)2ML. The polarization property of the gratings in monochromator was calibrated by halogen lamp.

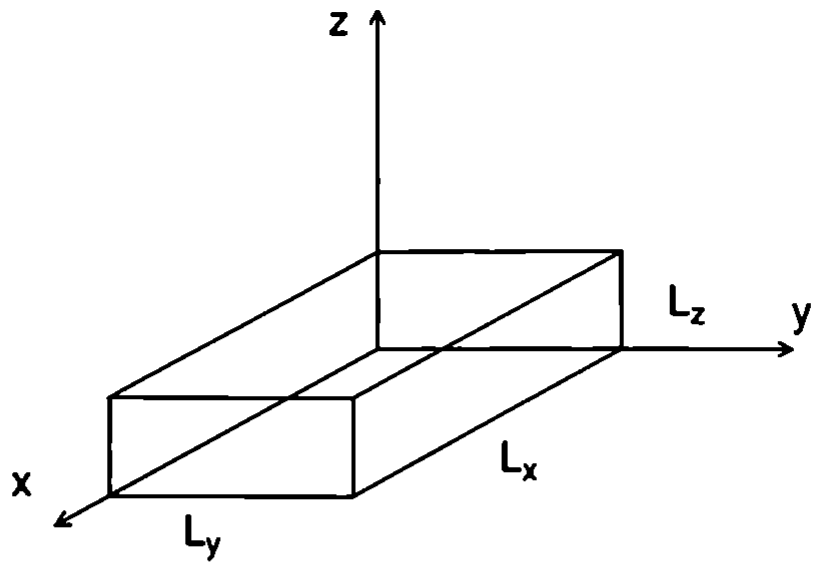

Fig.4-7 Schematic illustration of QD for the explanation of polarization.

directions have almost the same properties when the InAs layer thickness is 1ML. On the contrary, PL from InAs island shows strong polarization along [1$\bar{1}$0] direction. The peak intensity ratio between [1$\bar{1}$0] and [110] direction polarizations is about 60% while that at 1ML is 92%. In spite of intensive measurement, significant wavelength dependence on polarization direction was not observed

Polarization of luminescence can be related to the difference of dipole moments along two orthogonal directions. In case of quantum dot illustrated in Fig.4-7, luminescence polarization in x-y plane is calculated by following equation [17].

$$P = \frac{k_x^2 + k_z^2}{k_y^2 + k_z^2} \tag{4-1}$$

where P denotes the ratio of dipole moment along x and y directions, k_x, k_y and k_z the wave numbers along x, y and z directions, respectively. Assuming that k_x, k_y and k_z are in reciprocally proportion to the island size of 150Å , 133Å , and 30Å , the polarization P can be estimated as 98.7%. There is a large discrepancy

between experimental and calculated results. Some reasons for the discrepancy are considered. At first, precise polarization was not measured due to imperfect measurement system. As seen in Fig.4-6(a), peak intensities of two polarizations are different for 1ML-thick InAs in which polarization is not expected. Second, some islands are electrically connected in [110] direction and QWW like structure is formed by QDs. Even on nominally just-oriented substrate, there must be monolayer steps. As mentioned in chapter 2, two kinds of step exist on (001) plane of zincblende structured crystal and the atom sticking coefficient at step, in other words, the growth rate, is higher in B-step, which runs along [110] direction, than A-step. This anisotropy of growth rate improves the linearity of A-step and degrades that of B-step. Some works on STM observations of GaAs homoepitaxy on misoriented substrates have been carried out and difference of step linearity between A- and B-steps has been shown [18,19]. On A-step, the step edge is straight, however, on B-step, the step edge is very rough with many kink sites. N. Ikoma et al. observed scanning tunneling microscope(STM) of 2ML grown InAs on GaAs substrates 1.0 ° misoriented toward [110] direction and found that the InAs small islands are preferentially formed at steps [20]. They said that the step on the lower terrace is the favorable nucleation sites for InAs islands. Considering the anisotropy of step linearity and that InAs island formation at step edge, InAs islands are likely to assemble along [110] direction. Figure 4-8 shows plan-view TEM image of 2ML-thick InAs grown on GaAs (001) just-oriented substrate. One can see the line of islands along [1$\bar{1}$0] direction. Similar result has been obtained by AFM observation. The polarization of PL from such QWW becomes larger than that of QD since wave number along QWW, k_x which appears in the numerator of Eq.4-1 becomes 0. However, the calculated polarization of QWW is 95% and still larger than experimental result.

Third, strain distribution in island affects the dipole moment. From theoretical work by H. Shen et al., dipole moment is enhanced by compressive strain parallel to the dipole moment [21]. InAs island coherently grown on GaAs is elongated along [110] direction and compressively strained as calculated in previous chap-

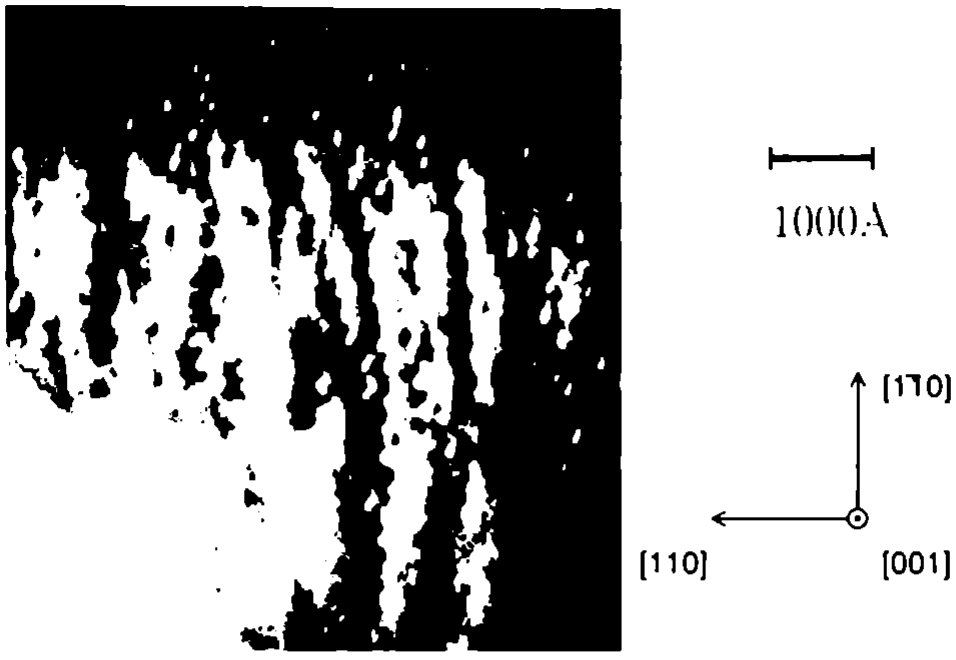

Fig.4-8 Plan-view TEM image of 2ML-thick InAs on GaAs just-oriented substrate. InAs islands connected in [110] direction is seen.

ter. The anisotropy of strain distribution enhances the dipole moment along [110] direction. Difference in anisotropy of island facet may also enhance the polarization. In order to clarify the precise origin of large polarization, further study is required.

4.5 Electroluminescence spectroscopy

Figure 4-9 shows the EL spectra where InAs thickness is varied from 1.0 to 2.0ML. One can see a peak at 880nm(1.41eV) from all samples. This peak is considered due to GaAs cladding layer, since the InAs active layer is so thin that some carriers overflow from the active layer to the cladding layer as observed in PL. The peak at 930nm(1.33eV) is seen when the InAs layer thickness is 1.0, 1.3, and 1.5ML. This peak is 90meV lower than GaAs band gap. Impurities such as Si or Be do not form such deep level. This peak can be assigned as the emission

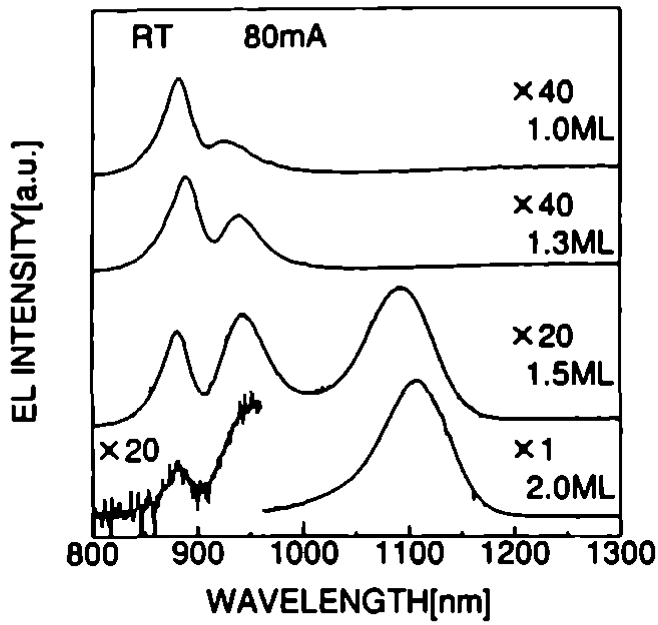

Fig.4-9 EL spectra of various InAs layer thickness. Injected current was 80mA and measurement temperature was RT.

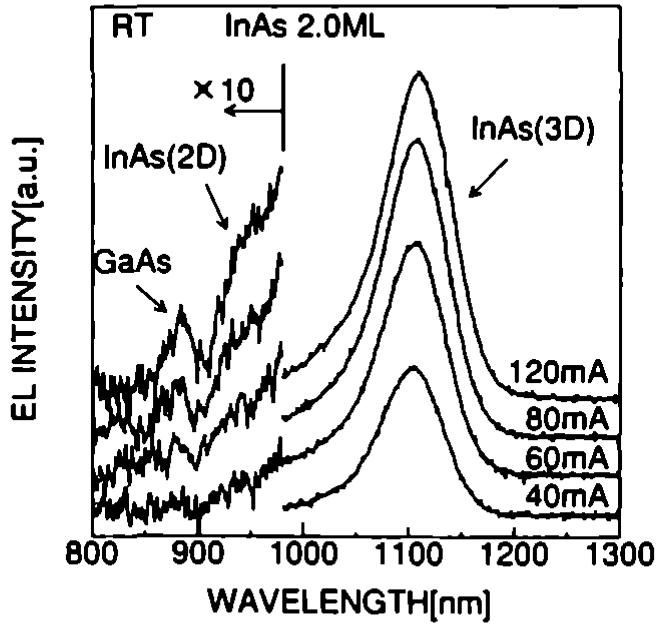

Fig.4-10 EL spectra of 2ML-thick InAs with various injection current.

from the two-dimensional InAs layer. Discrepancy of wavelength between PL and EL can be attributed to the difference in measurement temperature; PL was measured at 10K while EL was at RT. Another peak at 1090nm(1.14eV) is seen when the InAs layer thickness becomes 1.5ML and the FWHM is as wide as 80meV. This peak becomes dominant and other peaks are suppressed when the InAs layer thickness becomes 2.0ML. The peak is assigned to the InAs island from the comparison with PL. The wide FWHM reflects the fluctuation in the island size. The luminescence from GaAs cladding layer was hardly seen. The better emission capability of islands is understood from the fact that the relatively large peak is seen at 1090nm from 1.5ML sample, although the RHEED, AFM and TEM observations revealed very few islands at 1.5ML. The strong emission from QDs in spite of such low density indicates that the carrier collection and luminescence efficiencies of the island is very high. EL spectrum at 2.0ML is almost the same as that at 1.5ML, but the peak intensity is 20 times larger.

Figure 4-10 shows the EL spectra of 2.0ML sample with various injection current. The intensity of broad peak increases with increasing injection current. Besides emission from islands, two weak peaks appear in the shorter wavelength region. These peaks are identical to those observed when the InAs layer thickness is less than 1.5ML. Thus the peaks are assigned to GaAs cladding and two-dimensionally grown InAs layer, respectively. It is noteworthy that the luminescence from InAs two-dimensionally grown layer was observed. This is the proof that the InAs two-dimensionally grown layer still remains even when three-dimensional growth occurs. However, in previous section of PL, we could not observe the luminescence from two-dimensional layer. This PL result supports the considerable incorporation of two-dimensionally grown atoms into the islands. There are two important differences in the carrier excitation between EL and PL. First, the total excited carrier concentration of the EL is about three times larger than that of PL in our experiments. Another is the difference in carrier excitation process. In PL, the incident photon is absorbed to excite carriers, then carriers diffuse to lower potential space and recombine. Since the incident photon num-

ber decreases exponentially from the surface, it is considered that carriers are not sufficiently supplied to InAs active layer. On the other hand, carriers are directly injected and recombine preferentially around active layer in EL, because of the double hetero structure. Thus, the effective carrier concentration around InAs active layer of EL becomes much higher than that of PL. As a result, luminescence from two-dimensionally grown layer was observed by EL while it could not be observed by PL. Taking result of EL into account, it is thought that certain amount of two-dimensionally grown In and As atoms still remain even when the atom incorporation occurs at growth temperature of 480°C. This growth mode differs from ordinary Stranski-Krastanov mode in which the thickness of two-dimensional layer remains the same when the island formation occurs.

The existence of InAs two-dimensional layer, in other words, wetting layer, indicates that it is energetically stabler to cover GaAs surface by InAs instead of growing larger InAs island even when the island formation starts. This behavior is explained by the fact that the surface energy of InAs is lower than that of GaAs as discussed in previous chapter.

It is reported that significant amount of the atoms in the two-dimensionally grown layer are incorporated into the islands during their formation [8,22]. However, the precise thickness of the rest two-dimensional layer has not been clarified. Q. Xie et al. and X.W. Lin et al. observed the cross-sectional TEM images of InAs/GaAs grown by MBE and showed the existence of two-dimensional layer [23,24]. In the case of TEM, the precise thickness of two-dimensional layer can not be estimated because the image contrast is considerably smeared by strain. J.Y. Marzin et al. estimated the size of island by PL and calculated the thickness of two-dimensional layer by subtracting the volume of islands from that of supplied amount of InAs [10]. However, good agreement was not observed between estimated two-dimensional layer thickness and luminescence wavelength which is observed by photoluminescence excitation(PLE). In our case, the InAs layer thickness was varied systematically from 1.0 to 2.0ML. The optical properties of InAs grown layer is very sensitive to the layer thickness because the density

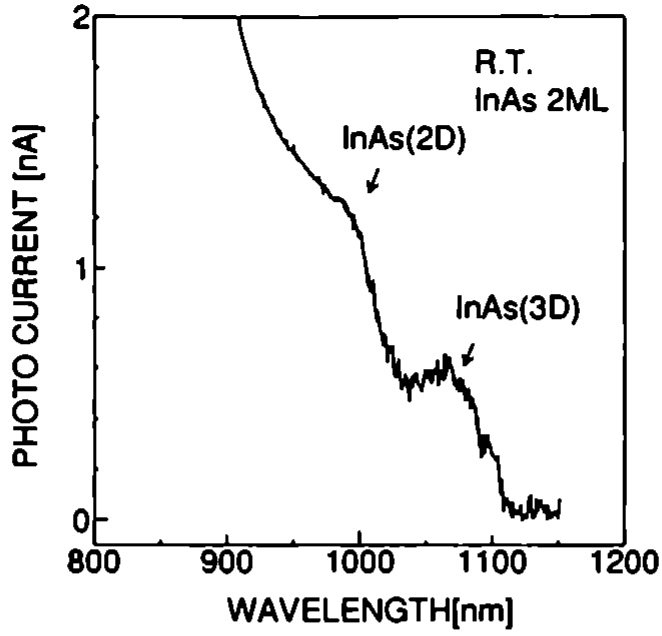

Fig.4-11 PC spectrum of 2ML-thick InAs. Two absorption peaks of two-dimensionally and three-dimensionally grown InAs are observed.

of InAs island can be changed from 0 to $10^{11}cm^{-2}$ in this region. As results of EL, luminescence from two-dimensional layer besides that from InAs QDs was observed when the InAs layer thickness was 2.0ML and the peak wavelength was the same as those which were observed when the InAs layer thickness was 1.0 ~1.5ML. Thus, we can deduce the thickness of two-dimensional layer of 2.0ML grown InAs to be almost 1.0ML.

4.6 Photocurrent spectroscopy

Photocurrent spectrum is shown in Fig.4-11. One can see that photocurrent decreases as the wavelength of the input light increases because the absorption edge of GaAs in this region. However, it is apparent that there are two more absorption peaks at 1000 and 1080nm. These peaks are considered to be related to InAs flat layer and InAs QDs, respectively as those observed by EL.

4.7 Discussion

From optical measurements, the behavior of luminescence spectra from InAs strongly depends on InAs layer thickness. Here, the peak wavelength is discussed.

Figure 4-12 compares the peak wavelengths or photon energies of PL, EL and band gaps of electron and heavy hole in GaAs/InAs/GaAs SQW calculated by effective mass approximation. Strain induced band gap and band offset for InAs were taken into account by model of C.G. Van de Walle [25]. Electronic parameters used in calculation are summarized in Table 4-1 [1,25].

One can see the photon energies of PL and EL from two-dimensional layer are slightly higher than calculated energies. Although EL photon energy agrees better than PL, current flow in EL chip may increase the temperature higher than RT. It is suspicious whether effective mass approximation is valid for such thin layer, however, if we assume it is valid, another reason for the discrepancies must be considered. One reason is the surface segregation of In. It is generally known that In atoms in InAs layer segregate into upper GaAs during cap layer growth [26-28]. Replacement factor R, which indicates that R fraction of In atoms in one layer are replaced with Ga atoms in upper layer, is estimated as high as 80% at growth temperature higher than 500°C in MBE. Thus, it is considered that certain amount of In atoms not more than 80% segregate at 480° which is the growth temperature in this study. Band structure of GaAs/InAs/GaAs SQW is modified by segregation as illustrated in Figs.4-13 and energy states in modified band gap becomes larger than that without segregation.

In case of two-dimensionally layer, layer thickness is less than 2ML, thus, InAs layer is likely to disappear when segregation occurs. However in case of island, In atoms which are far from surface are not concerned with segregation. Furthermore, strain which is one of the driving force of segregation is lower at island surface than in two-dimensional layer as calculated in chapter 3. In this case, segregation at island surface is suppressed. From these considerations, In segregation becomes less important for island than that for two-dimensional layer.

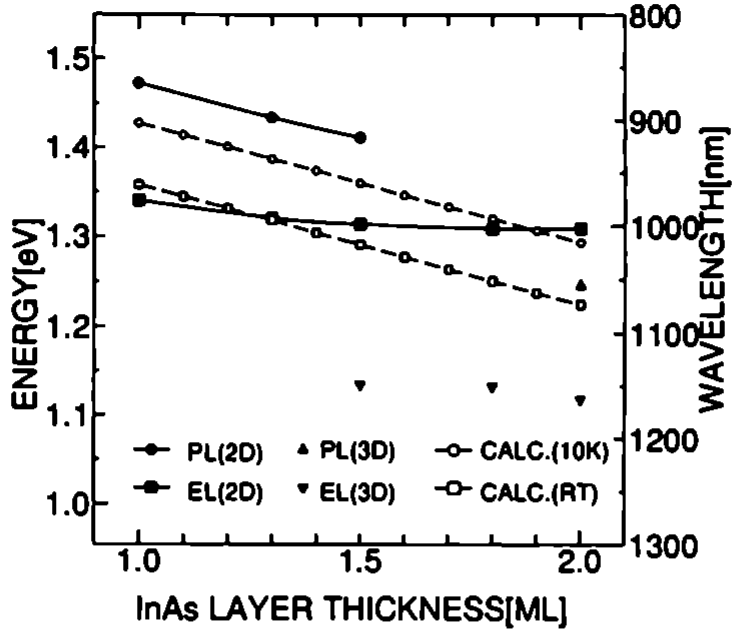

Fig.4-12 Peak wavelengths of PL and EL. Theoretical calculations based on effective mass approximation taking strain into account are also plotted for comparison.

Table 4-1 Electronic parameters used for quantum energy calculation [1,25]. E_g band gap energy, Δ_0 spin-orbit splitting energy, a_v deformation potential of valence band, a deformation potential of band gap, b shear deformation potential, m_e effective mass of electron, m_{hh} effective mass of heavy hole.

	E_g[eV]	Δ_0[eV]	a_v[eV]	a[eV]	b[eV]	$m_e[m_0]$	$m_{hh}[m_0]$
InAs	0.418(10K)	0.38	1.00	-6.08	-1.8	0.022	0.35
	0.354(RT)						
GaAs	1.517(10K)	0.34	1.16	-8.33	-1.7	0.063	0.50
	1.424(RT)						

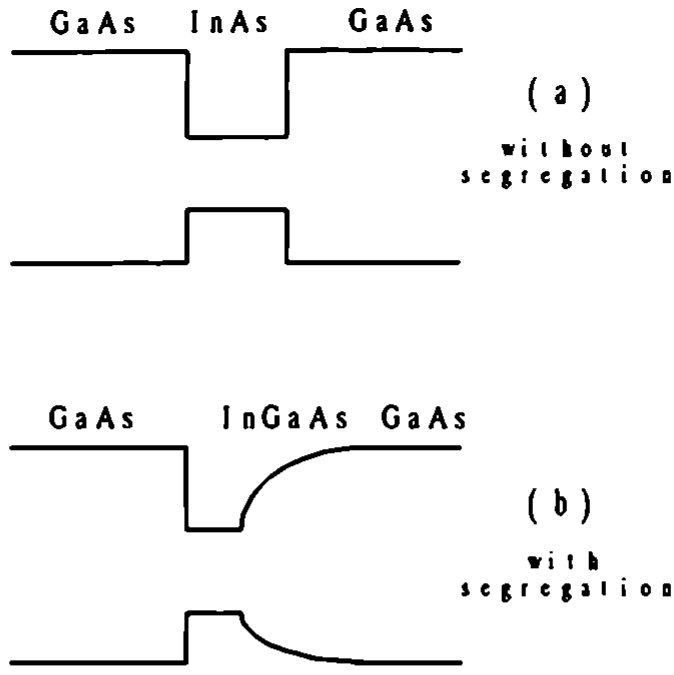

Fig.4-13 Band structures of GaAs/InAs/GaAs SQW without(a) and with(b) In segregation.

The photon energy of PL and EL from island is much lower, in other words, the wavelength is much longer, than calculated one for two-dimensional layer. Naturally, this discrepancy has its origin in the difference of quantum structure shape between three-dimensional island and SQW. As revealed in chapter 2, island hight is about 30Å . Calculated photon energy from 30Å -thick InAs SQW is 0.80 and 0.74eV for 10K and RT, respectively. Even one takes segregation effect into account, the observed photon energy is much higher than calculated value. This disagreement does indicate the existence of lateral carrier confinement ability of InAs island. Therefore it can be deduced that self-assembled InAs island has a nature of QD.

4.8 Summary

The optical properties of coherently grown InAs on GaAs was investigated by various spectroscopies.

PL showed that luminescence spectrum strongly reflects the structure of InAs. Sharp peak with FWHM of 10meV was observed while two-dimensionally growth occurs(<1.5ML), on the contrary, broad peak was seen when the layer thickness is larger than 1.5ML where InAs islands were formed. The PL intensity becomes weak while the peak wavelength remains the same when the misfit dislocations were generated. Although the precise origin is not clarified, the PL from InAs islands has polarization property along [1$\bar{1}$0] direction which is the longest direction of island.

Almost the same results were obtained by EL spectroscopies of pin photo diode with InAs active layer. The high luminescence capability of InAs island was shown. By increasing injection current, luminescence from 1ML-thick two-dimensionally grown layer beside that from island was observed when InAs layer thickness was 2ML. Therefore the fact that island incorporates the atoms already grown two-dimensionally was revealed. PC spectroscopy result supports this modified SK growth modes of InAs on GaAs.

The segregation of In into GaAs cap layer was indicated by comparison of peak wavelength of experiment and calculation based on effective mass approximation.

Since the wavelength of luminescence from islands was much shorter than that calculated for SQW assuming the well width is equal to island height, InAs islands have nature of QD.

References

1) Landolt-Börnstein Numerical Data and Fundamental Relationshis in Science and Technology. Vol.17a Editted by O. Madelung(Springer-Verlag, Berlin, 1982).

2) W.T. Tsang and R.L. Hartman, Appl. Phys. Lett. **38**, 502 (1981).

3) W.T. Tsang, Appl. Phys. Lett. **39**, 785 (1981).

4) Y. Arakawa and H. Sakaki, Appl. Phys. Lett. **40**, 939 (1982).

5) Y. Arakawa, K. Vahara, and A. Yariv, Appl. Phys. Lett. **45**, 950 (1984).

6) L. Goldstein, F. Glas, J.Y. Marzin, M.N. Charasse, and G. Le Roux, App. Phys. Lett. **47**, 1099 (1985).

7) M. Tabuchi, S. Noda, and A. Sasaki, in *Science and Technology of Mesoscopic Structures,* edited by S. Namba, C. Hamaguchi, and T. Ando (Springer, Tokyo 1992), p.379, paper presented at 1st Int. Symp. Sci. and Technol. of Mesoscopic Structures (Nov.6-8, 1991, Nara, Japan) p.18.

8) S.S. Dosanjh, P. Dawson, M.R. Fahy, B.A. Joyce, R. Murray, H. Toyoshima, X.M. Zhang, and R.A. Stradling, J. Appl. Phys. **71**, 1242 (1992).

9) D. Leonard, M. Krishnamurthy, C.M. Reaves, S.P. Denbaars, and P.M. Petroff, Appl. Phys. Lett. **63**, 3203 (1993).

10) J.Y. Marzin, J.M. Gerald, A. Izraël, and D. Bariier, Phys. Rev. Lett. **73**, 716 (1994).

11) W. Seifert, N. Carlsson, M.E. Pistol, and L. Samuelson, J. Cryst. Growth **145** 758 (1994).

12) J.I. Pankove, *Optical Processes in Semiconductors*(Dover, 1971).

13) S. Tsukamoto, Y. Nagamune, M. Nishioka, and Y. Arakawa, J. Appl. Phys. **71**, 533 (1992).

14) R. Notzel, N.N. Lendentsov, L. Daweritz, K. Ploog, and M. Hohenstein, Phys. Rev. B**45**, 3507 (1992).

15) M. Wassermeier, H. Weman, M.S. Miller, P.M. Petroff, and J.L. Merz, J. Appl. Phys. **71**, 2397 (1992).

16) M.S. Miller, H. Weman, C.E. Pryor, M Krishnamurthy, P.M. Petroff, H. Kroemer, and J.L. Merz, Phys. Rev.Lett. **68**, 3464 (1992).

17) M. Asada, Y. Miyamoto, and Y. Suematsu, J. Quantum Electron. **22**, 1915 (1986).

18) M.B. Pashley, K.W. Haberern, and J.M. Gaines, Appl. Phys. Lett. **58**, 406 (1991).

19) I. Tanaka, S. Ohkouchi, and A. Hashimoto, Jpn. J. Appl. Phys. **31**, 2216 (1992).

20) N. Ikoma and S. Ohkouchi, Jpn. J. Appl. Phys. **34**, L724 (1995).

21) H. Shen, M. Warback, J. Pamulapati, P.G. Newman and M. Dutta, Phys. Rev. B**47**, 13933 (1993).

22) C.W. Snyder, B.G. Orr, D. Kessler, and L.M. Sander, Phys. Rev. Lett. **66**, 3032 (1991).

23) Q. Xie, P. Chen, and A. Madhukar, Appl Phys. Lett. **65**, 2051 (1994).

24) X.W. Lin, J. Washburn, Z. Liliental-Weber, E.R. Weber, A. Sasaki, A. Wakahara, and Y. Nabetani, Appl. Phys. Lett. **65**, 1677 (1994).

25) C.G. Van de Walle, Phys. Rev. B**39**, 1871 (1989).

26) J.M. Moison, C. Guille, F. Houzay, F. Barthe, and M. Van Rompay, Phys. Rev. B**40**, 6149 (1989).

27) H. Yamaguchi and Y. Horikoshi, J. Appl. Phys. **68**, 1610 (1990).

28) M. Sato and Y. Horikoshi, J. Appl. Phys. **69**, 7697 (1991).

Chapter 5

Dislocation suppression in InAs grown on GaAs by using misoriented substrates

5.1 Introduction

In lattice-mismatched heteroepitaxial growth, misfit dislocation is inevitable problem to obtain optimal electrical and optical properties of material. Generation and behaviors of various dislocations are very important subjects to investigate heteroepitaxial growth mechanism [1-9]. On the other hand, the suppression of the dislocation generation enables material applications to extend the synthesis of devices employing stained layer. Thus far, several works on the dislocation characterization and the theoretical prediction of a critical layer thickness have been reported [10-12]. However, all of the theories for the critical thickness are based on the continuum calculation, i.e., the macroscopic approach. It would not be applicable to the system in which the layer thickness is very thin and/or steps exist on the substrate and interact with the dislocations.

As revealed in previous chapter, the optical property of QD using self-assembled InAs islands is drastically degraded by misfit dislocation. To suppress dislocation

generation in InAs island is one of the prerequisite works to utilize InAs island to QD devices.

In this chapter, we grow InAs layers on the misoriented GaAs substrates by MBE and investigate the misorientation effect on dislocation behavior and the critical thickness by PL and TEM.

To investigate the interaction between step and dislocation on misoriented substrate, the strain energy was calculated based on the VFF model taking account of the interaction of the dislocation and the step on the substrate surface. As results, we show that the step at heterointerface works to suppress the generation of dislocations.

5.2 Experimental setup

The samples were grown by a MBE system as referred in chapter 2. Five different semi-insulating GaAs substrates were used: (001) just-oriented, 3.5° misoriented toward [1$\bar{1}$0] direction, 3.5° misoriented toward [110] direction, 5.0° misoriented toward [1$\bar{1}$0] direction, and 5.0° misoriented toward [110] direction. All the substrates were mounted on the same molybdenum holder soldering with In and grown simultaneously to avoid influences caused by different growth conditions.

On these substrates, at first 1000Å-thick GaAs buffer layers were grown, then 1~6ML InAs layers, and 100Å-thick single crystal GaAs cap layers were grown successively. Growth rate was fixed at 0.7ML/s for GaAs and at 0.2ML/s for InAs. Throughout the growth, As pressure was fixed at 1.0×10^{-5} Torr. The V/III flux ratio was 3 for GaAs and 10 for InAs.

To investigate crystalline quality of the samples, we measured PL and performed plan-view TEM to observe dislocation images.

5.3 Experimental results and discussion

5.3.1 Photoluminescence spectroscopy

The results are shown in Figs.5-1. When the InAs layer thickness is 1ML, each spectrum has its peak at 850nm and the FWHM is very narrow as 8meV(Fig.5-1(a)). There is no significant difference among all spectra. Peaks shift to the lower energy and FWHMs become wider(~80meV) when the InAs layer thickness is 2ML, as seen in Fig.5-1(b). These PL properties were explained in chapter 4. Figure 5-1(c) shows the results when the InAs layer is 4ML. This thickness is thought to be beyond the critical thickness as for the sample using just-oriented substrate [9]. As can be seen, both emission peaks of samples using substrates 3.5° and 5.0° misoriented toward [1$\bar{1}$0] direction appear on the higher energy side than those of samples using substrates just-oriented or misoriented toward [110] direction. The island size may be smaller in those samples. The FWHMs are almost the same as those of 2MLs. When the InAs layer thickness becomes 5ML, the PL was observed only from samples using the substrates misoriented toward [1$\bar{1}$0] direction. No luminescence was observed from all 6ML InAs samples.

5.3.2 Transmission electron microscope observation

Figures 5-2 show the plan-view TEM images of 5ML-thick InAs layer. In Figs.5-2(a), (c), and (e), many moiré patterns are seen. The dislocation length is finite as seen in Figs.5-2. Contrast to the Figs. 5-2(a), (c), and (e), very few moiré patterns can be seen in Figs.5-2(b) and (d). Instead of moiré fringes, many dotted images are seen in Figs.5-2(b) and (d). These are InAs islands [7,8] coherently grown with the lattice constant of GaAs substrate. Although these samples were grown simultaneously, there is a great difference in misfit dislocation density among five samples. The dislocation profiles are listed in Table 5-1. The number of the misfit dislocation of the sample using GaAs substrates 3.5° or 5.0° misoriented toward [110] direction are almost the same as that of sample us-

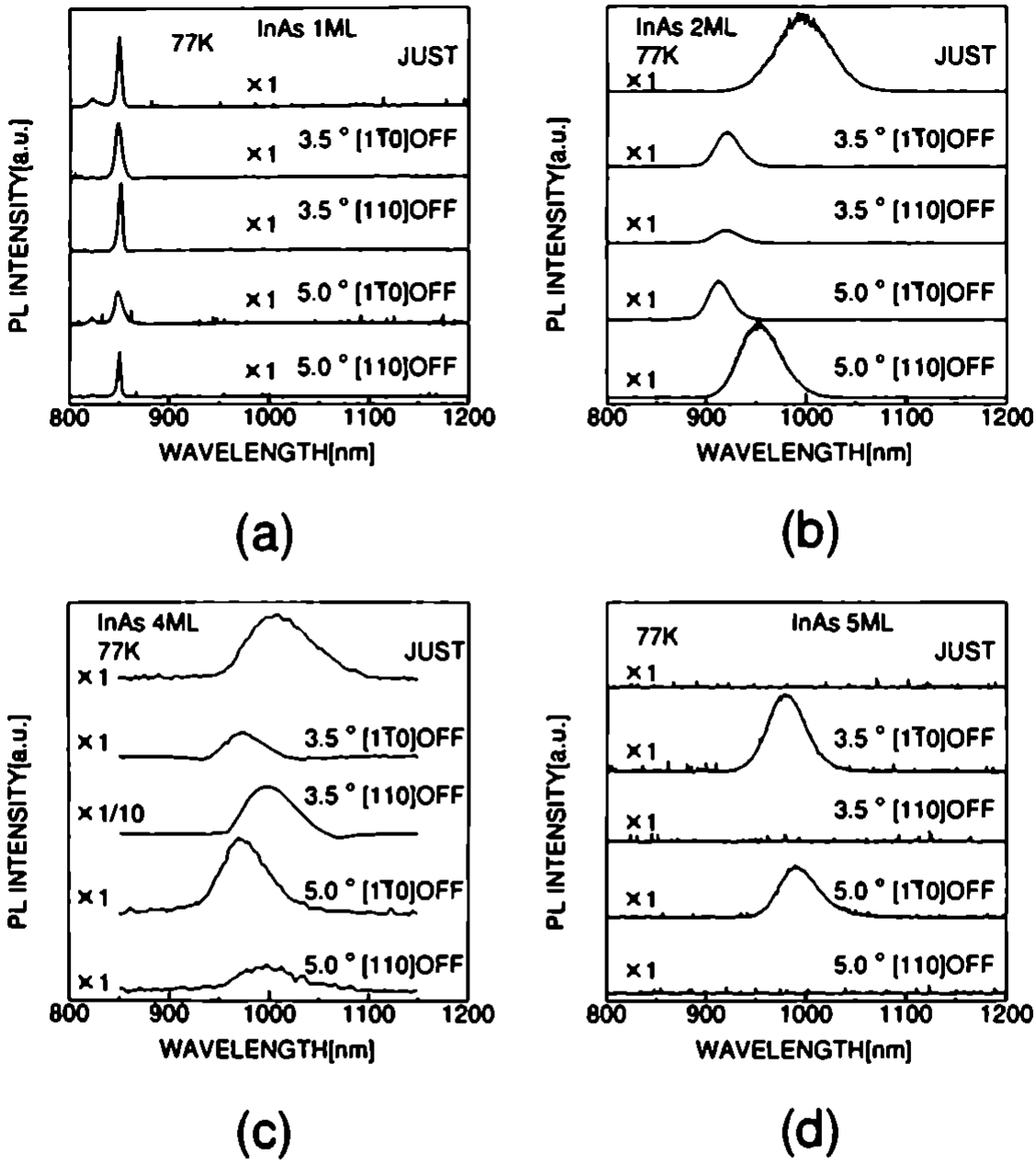

Fig.5-1 Observed PL spectra. Thickness of InAs is (a)1ML, (b)2ML, (c)4ML and (d)5ML.

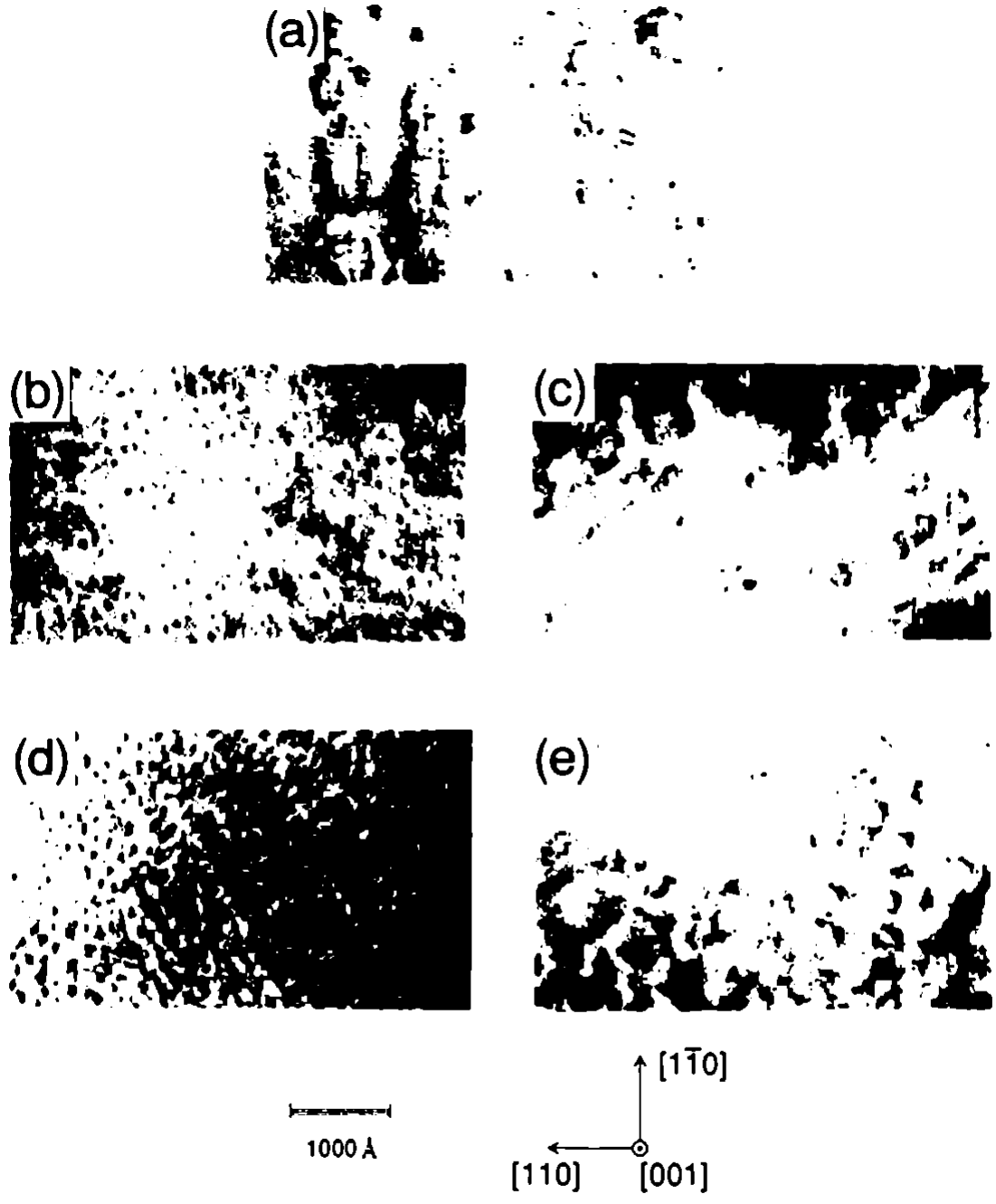

Fig.5-2 Plan-view TEM images of 5ML-thick InAs layer. (a)substrate just-oriented. (b)substrate 3.5° misoriented toward [1$\bar{1}$0] direction. (c)substrate 3.5° misoriented toward [110] direction. (d)substrate 5.0° misoriented toward [1$\bar{1}$0] direction. (e)substrate 5.0° misoriented toward [110] direction.

Table 5-1 Dislocation density at InAs 5ML measured in Figs.5-2.

	SUBSTRATE				
	JUST-ORIENTED	3.5°[1$\bar{1}$0]OFF	3.5°[110]OFF	5.0°[1$\bar{1}$0]OFF	5.0°[110]OFF
DENSITY $[10^{12}cm^{-2}]$*	160	8	202	12	220

* Observed area is 11500Å×8900Å

ing just-oriented substrate, while the samples using GaAs substrates 3.5° or 5.0° misoriented toward [1$\bar{1}$0] direction are much less in the number of the misfit dislocation than the sample using just-oriented substrate. In other words, the critical thickness of the InAs layer grown on the GaAs substrate 3.5° or 5.0° misoriented toward [110] direction is not different from that of the InAs layer grown on the GaAs just-oriented substrate, while the critical thickness of the InAs layer grown on the GaAs substrate 3.5° or 5.0° misoriented toward [1$\bar{1}$0] direction becomes thicker than that of the InAs layer grown on the GaAs just-oriented substrate. The ratio of dislocation density between the samples misoriented toward [110] and [1$\bar{1}$0] directions is about 20:1. Although there is a large difference of dislocation density with respect to the substrate misorientation direction, significant difference of dislocation density with respect to the substrate misorientation angle cannot be recognized.

We observed the plan-view TEM images of 2ML and 6ML-thick InAs samples using each substrate. In 2ML samples, many InAs islands were seen. On the contrary, there exist many misfit dislocations in all the 6ML InAs samples.

5.3.3 Discussion

It is considered that the misfit dislocation is generated during the InAs layer growth, i.e., before the cap layer growth and thus the GaAs cap layer is not

concerned with the generation of the misfit dislocation. The result that the PL was not observed from all 6ML InAs samples agrees well with the plan-view TEM result, i.e., there exist many misfit dislocations in the grown layer which act as non-radiative centers. The PL peak intensity of the 4ML-thick InAs grown on the GaAs substrate 3.5° misoriented toward [110] direction is 10 times larger than those of other 4ML-thick samples. However, the reason is not certain. Thus, some farther investigation would be required to see influences by the [110] misorientation by 3.5°, although they are considered less relative to those by the [1$\bar{1}$0] misorientation.

In practical, it is considered that the precise value of critical thickness can not be measured in ML order, since the onset of the dislocation generation does not occur uniformly in the growth plane and there is some fluctuation. Thus, if we assume that the dislocation density represents the rate of dislocation generation, the critical thickness of the InAs layer is 3ML on GaAs substrates just-oriented and 3.5° and 5.0° misoriented toward [110] direction, whereas that on GaAs substrates 3.5° and 5.0° misoriented toward [1$\bar{1}$0] direction is ~5ML from PL measurements and TEM observations.

From investigation of AFM in chapter 2, dislocations were found in large islands rather than small island. Thus, the difference of dislocation density in Figs.5-2 can be attributed to the difference of large island density, i.e., the large islands are more in samples grown on substrates just-oriented and 3.5° or 5.0° misoriented toward [110] direction than in samples grown on substrates 3.5° or 5.0° misoriented toward [1$\bar{1}$0] direction. As described above, small islands are more in samples grown on substrates 3.5° or 5.0° misoriented toward [1$\bar{1}$0] direction. From these observations, it is considered that the InAs small islands are hard to coalesce each other to form large islands on substrate misoriented toward [1$\bar{1}$0] direction. The shorter PL peak wavelength of samples using substrate misoriented toward [1$\bar{1}$0] direction at 4ML shown in Fig.5-1(c) can be explained by isolation of the small island rather than coalescence growth. However, since in-situ RHEED observation showed that the onsets of small island formation are around 1.8~2.0ML for

all samples, the thickness at which small islands are formed is not affected by the substrate misorientation.

The discrepancy of critical thickness on differently misoriented substrates can be explained by growth kinetics, qualitatively. Considering that A-step appears preferentially on substrate misoriented toward [110] direction while B-step on substrate misoriented toward [1$\bar{1}$0] direction and that the step front linearity is higher in A-step [13,14], it is thought that favorable sites for InAs small islands are much greater on substrate misoriented toward [110] direction because the numbers of the step and kink sites are greater than those on substrate just-oriented and misoriented toward [1$\bar{1}$0] direction. Therefore InAs growth on GaAs substrate misoriented toward [110] direction is considered to proceed by increasing the density of small island not by coalescence to form large island in which dislocations generated. The small island density at 5ML-thick InAs grown on substrate 5.0° misoriented toward [110] direction is $3.2\times10^{11}cm^{-2}$. This value is about three times larger than that at 2ML($1.1\times10^{11}cm^{-2}$). Suppose that certain amount of InAs two-dimensional layer, in other words, wetting layer covers the GaAs surface, and then almost all atoms which are supplied during three-dimensional growth contribute to formation of small island. When the island density becomes so large that the island coalesce each other, the large island are formed and the dislocations are generated in it.

5.4 Calculation of strain energy and discussion

5.4.1 Calculation of strain energy on misoriented substrates

As shown in previous section, the growth mode is different among just-oriented and two kinds of misoriented substrates and then the critical thickness on substrate misoriented toward [1$\bar{1}$0] direction is thicker. However, it is considered that the generation and behavior of dislocation on misoriented substrate are not the same as that on just-oriented substrate. Here, we show the calculation of

the strain energy by VFF model [15-19] as a function of the dislocation length by taking the step-crossing on the substrate surface into account. Basic concept of VFF method has been described in chapter 3.

In the calculating process, periodic boundary condition was taken with assuming that the unit crystals (26ML-width × 64ML-length × 6ML-height) lie side by side in the growth plane. The unit crystal is illustrated in Fig.5-3. Although the experimental results show that the InAs grows three-dimensionally about after 1.8ML, we took the unit crystal to be two-dimensionally to focus the discussion on the interaction between step and dislocation. The periodicity of 26ML is selected for the consideration of the lattice-mismatching between InAs and GaAs, in other words, dislocation should be generated at certain periodicity which corresponds to the least common multiple of the lattice constants of InAs and GaAs. On the other hand, 64ML-length is limited by hard ware, though the larger the periodicity, the longer dislocation we can calculate. The crystal size in the calculation was fixed regardless of the substrate misorientation. The InAs layer thickness is 5ML and below the InAs layer there exists 1ML-thick GaAs layer. The atoms of this layer can move to relax the strain, but the lower side of this layer was fixed at GaAs lattice constant. The surface of InAs is covered with As with consideration of the As-rich growth condition. To investigate the influence of substrate misorientation, we adopted 3.0° and 5.0° misorientation toward [110] direction and then the terrace width becomes 32Å(8ML) and 52Å(13ML), respectively. The misorientation angles have to be the same as experimental conditions, but the terrace width of 3.5° misorientation is 11.5ML which is not appropriate to the 64ML-length unit crystal. The step is considered to be one molecular layer height. The dislocation is supposed to be an edge dislocation consisting of a pair of 60° type dislocations as observed by TEM and is set along the [1$\bar{1}$0] direction so that the dislocation crosses steps. Both sides of edge dislocation become 60° or a screw type of dislocation and go out to the surface as illustrated in Fig.5-4. The term, *dislocation length*, used in this chapter means the length of the edge part of the dislocation. To set this type of dislocation in the unit crystal, we

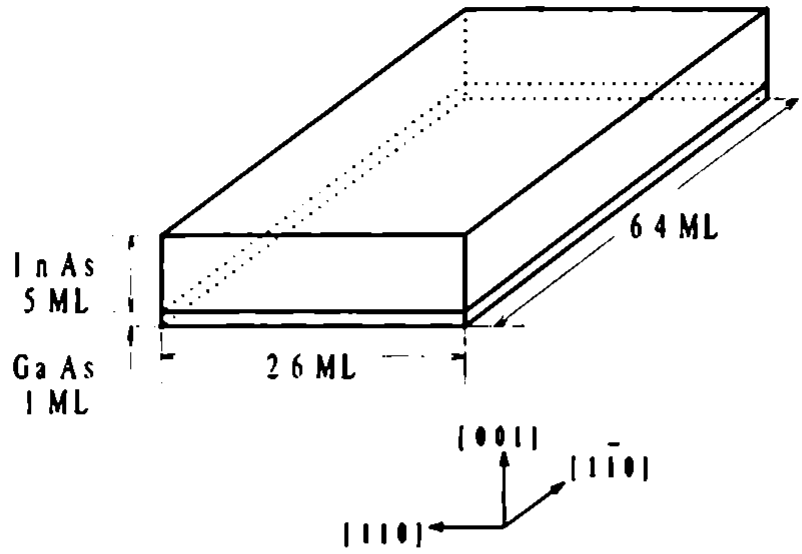

Fig.5-3 Unit crystal to calculate the strain energy with VFF model.

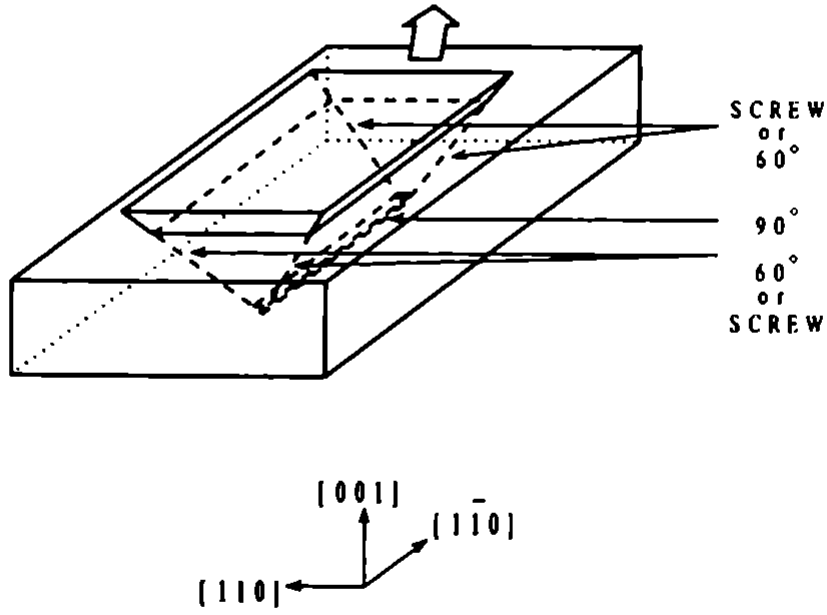

Fig.5-4 An edge dislocation consisted of a pair of 60° dislocations supposed for the calculation.

assumed the followings.

1. The center of the edge part of the dislocation is set at the center of the unit crystal as long as the cross point of dislocation and step is minimized.

2. The dislocation runs in the interface plane: it does not run through the GaAs or InAs but bends itself along the interface when the dislocation comes across the step.

The first assumption can be followed from the periodical structures being made up with the unit crystals. The second assumption is understood from the fact that the strain energy for the bent dislocation is far less than that for the non-bent dislocation.

Figure 5-5 shows the calculated strain energy averaged per one atom in the 5ML as a function of the dislocation length. First, we examine the results of the just-oriented substrate case. One can see that the strain energy with the finite long dislocation is larger than that without dislocation, when the dislocation length is relatively short. As the dislocation length increases, the strain energy decreases and then becomes lower than that without the dislocation. Finally, the strain energy is considered to asymptote 78.4meV which is the strain energy with the infinite long dislocation. This result indicates that the dislocation would not be generated while the dislocation length is short. In other words, the dislocation needs a certain minimum length to exist stably in a certain thickness of the grown layer. In the case of 5ML-thick InAs grown on GaAs, the minimum dislocation length is about 168Å, corresponding to 42 in unit of ML, from Fig.5-5.

Contrast to the just-oriented substrate, the strain energy increases with the dislocation length in the misoriented substrate. The strain energy increases every 8ML or 13ML which correspond to the terrace width of the misoriented substrate by 5.0° or 3.0°, respectively. It is seen in Fig.5-5 that the decreasing slopes are almost the same as that of just-oriented substrate during each stage. Then, it is considered that the extra strain energy is generated when the dislocation crosses the step on the substrate. Figure 5-6 shows the strain energy difference between

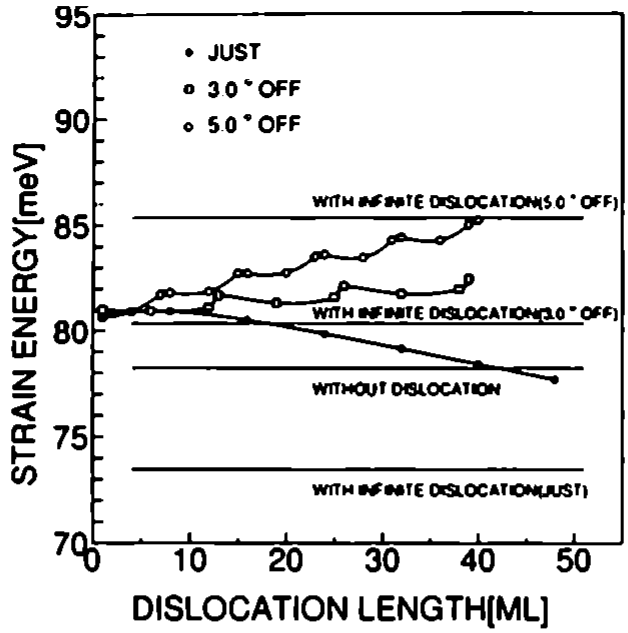

Fig.5-5 Calculation results of the strain energy averaged per atom in the 5ML-thick InAs against the dislocation length. Strain energy on just-oriented substrate monotonically decreases with the dislocation length, while those on misoriented substrates increase periodically.

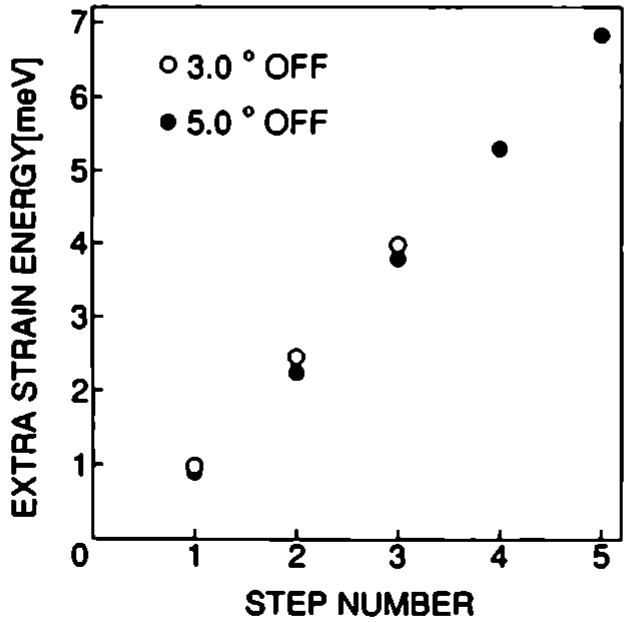

Fig.5-6 Strain energy difference between InAs layers grown on just and misoriented substrates.

InAs layers grown on just and misoriented substrates. From Fig.5-6, extra strain energy generated at each crossing is 1.5meV regardless of the misorientation angle. Thus, the steeper the misorientation angle is, the larger the strain energy becomes, because the step density increases with the misorientation angle. The strain energy with the infinite dislocation on the misoriented substrate is determined by a total of the extra strain energy at steps and the strain energy relaxed with the edge part of the dislocation.

The origin of the extra strain energy is explained in Fig.5-7 where the strain energy distributions in the grown layers of two samples using just-oriented and 5.0° misoriented substrates are shown. In Figs.5-7(b), the radi of individual circles represent the magnitude of the strain energy accommodated in corresponding each atom. The radi are normalized with a certain scale. Most of the strain is accommodated only in the atoms around the dislocation in case of just-oriented substrate. On the other hand, when the substrate is misoriented, the strain is accommodated in the atoms along one slip plane besides the atoms around the dislocation, and the total amount of the strain is greater than that of just-oriented case. Here, we consider the strain generation at the step with Fig.5-7(c) [20]. The edge dislocation 1 consisted of a pair of 60° dislocations runs along $[1\bar{1}0]$ direction at first. However, the dislocation 1 bends to [101] direction and becomes screw dislocation to cross the step on the substrate surface. Finally, the screw dislocation bends to [110] direction again and becomes the dislocation 2 to run along the growth plane. In this process, one of the two slip planes must change as depicted in Fig.5-7(c). This change of the slip plane is the origin of the extra strain energy on crossing the step. Although we assumed that the dislocation 1 bent to [101] direction which results in the change of the right hand side slip plane in Fig.5-7(c), there is no necessity for the dislocation 1 to bend to [101] direction. In the case of the dislocation 1 bent to $[0\bar{1}1]$ direction, the left hand side slip plane would change which produces the same extra strain energy.

Next, we calculated the strain energy in the grown layer as a function of InAs layer thickness. A pair of infinite 60° dislocations running along $[1\bar{1}0]$ direction

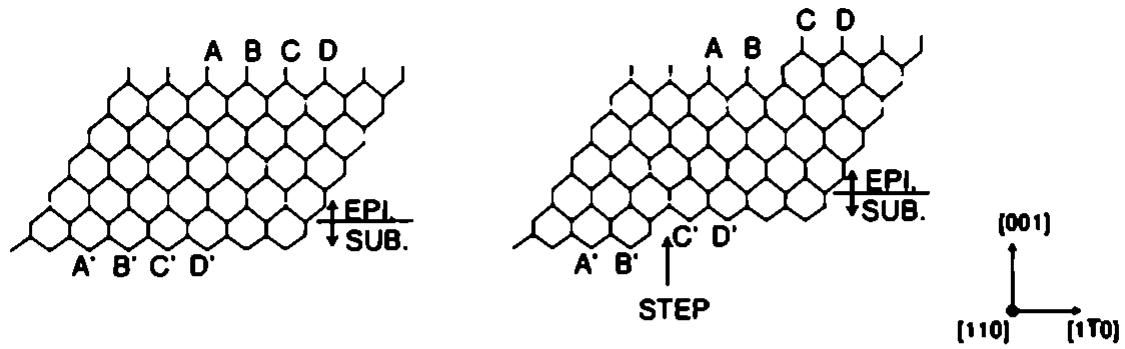

JUST-ORIENTED SUB. MISORIENTED SUB.

(a)

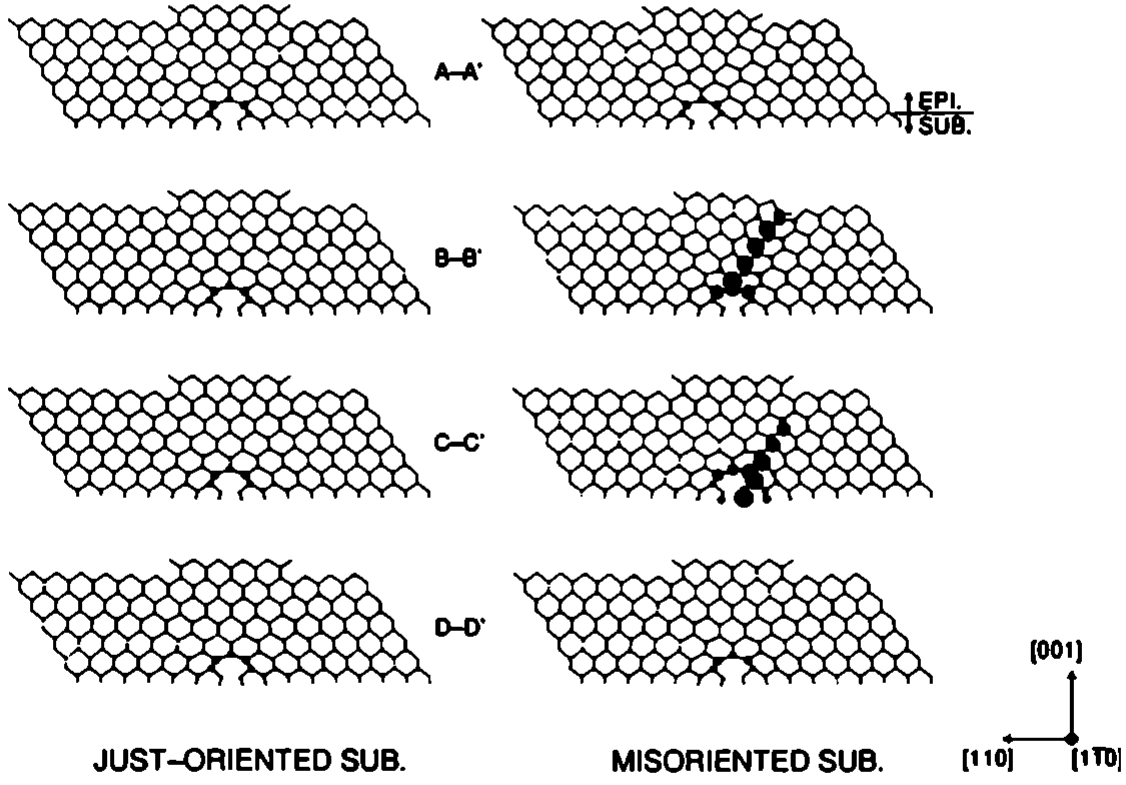

JUST-ORIENTED SUB. MISORIENTED SUB.

(b)

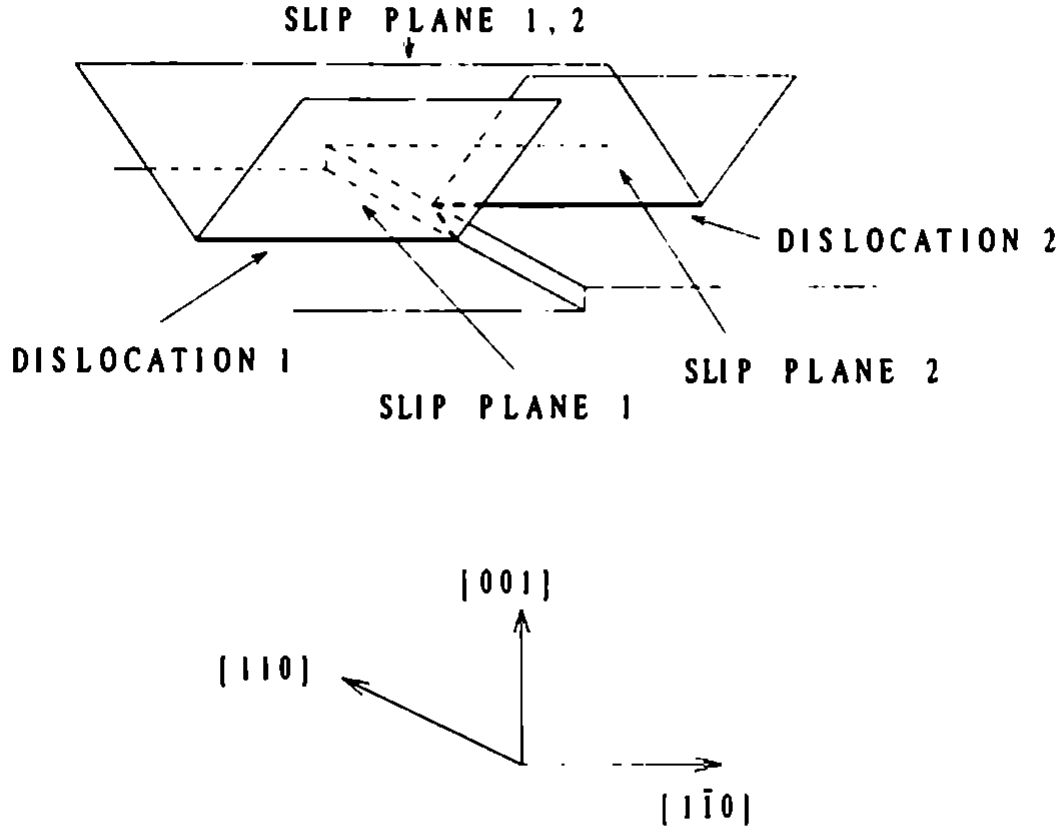

Fig.5-7 Atom arrangement and the strain energy distribution. (a) Atom arrangement viewed from [110] direction. (b) Strain energy distribution in the grown layer. Each plane is indicated in Fig.5-7(a). The radius of the individual circles represents the magnitude of the strain energy. (c) Dislocation bend and the change of the slip plane.

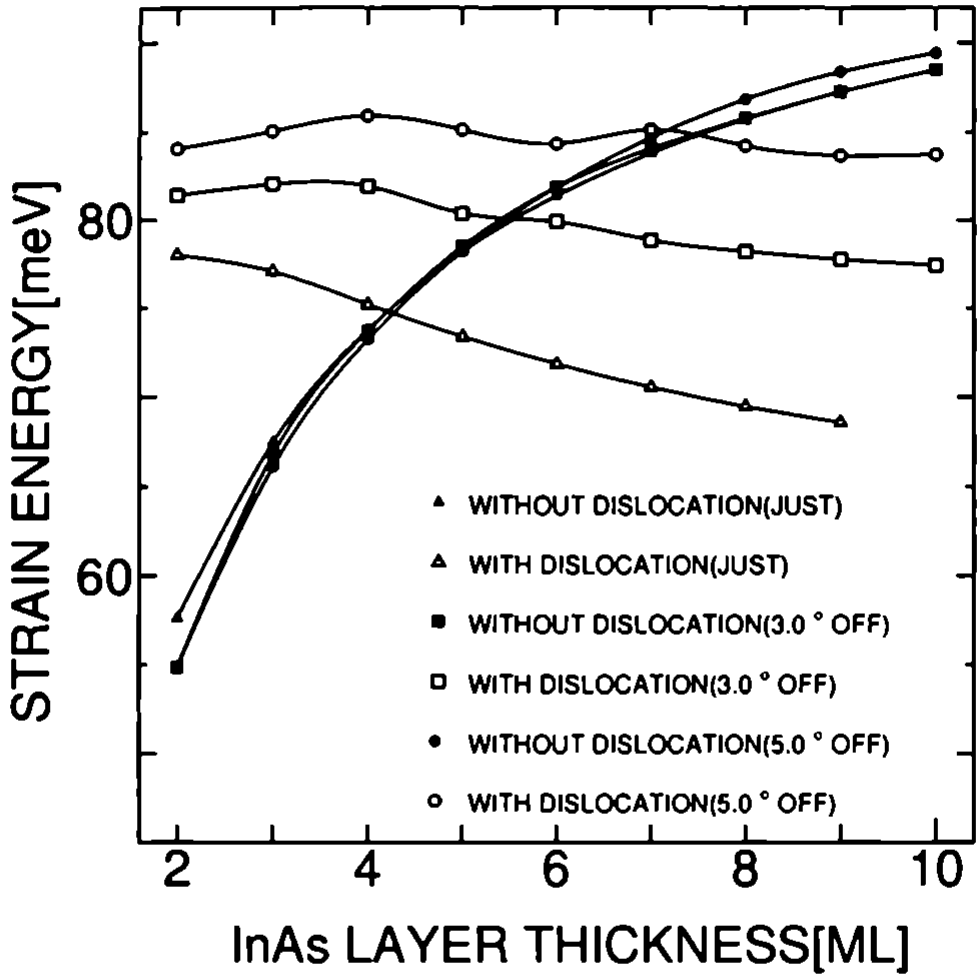

Fig.5-8 Calculation results of the strain energy per atom against the InAs layer thickness. The cross points of the strain energies with and without dislocation are the critical thickness.

and $[1\bar{1}0]$ direction substrate misorientation was supposed. Figure 5-8 shows the calculated results. In the figure, strain energies with dislocation are larger than that without dislocation while the InAs layer is thin in both cases. However, the situation changes with dislocation as the InAs layer thickness increases. The cross points of strain energies with and without dislocation are the critical thickness deduced from our model. From Fig.5-8, the critical thickness of InAs grown on just-oriented GaAs substrate is 4ML, and that on GaAs substrate misoriented by 5.0° or 3.0° is 7ML or 5ML, respectively. One can see that the strain energies without dislocation are not different with respect to the substrate misorientation angle, but the strain energies with dislocation largely depend. This difference is caused by the step density difference between two misorientation angles. The strain energy with dislocation of InAs on steeply misoriented substrate is larger than that on gently misoriented one. Thus, the critical thickness on misoriented substrate becomes thicker by the generation of the extra strain energy at step.

5.4.2 Discussion

From the calculation of the strain energy, it was found that the critical thickness with infinite dislocation on misoriented substrate is thicker than that on just-oriented substrate. Here, we consider the critical thickness of finite dislocation on misoriented substrate. As mentioned above, there is the minimum dislocation length under which dislocation cannot exist stably. If misorientation angle is small and the terrace width is larger than the minimum dislocation length, the situation is the same as the just-oriented substrate. Thus, the critical thickness is not increased. However, when the terrace width is less than the minimum dislocation length, the dislocation has to cross the step. As the calculated result indicates, the extra strain energy(about 1.5meV) is generated for the dislocation to cross one step. As the minimum dislocation has to cross five or three steps, 7.5 or 4.5meV extra strain energy is generated in case of 5.0° or 3.5° misorientation, respectively. The maximum strain relaxation by misfit dislocation, in other words,

the energy difference between without dislocation and with infinite dislocation is about 4.5(78.0-73.5)meV as seen in Fig.5-5. The strain relaxation is nearly equal or less than the extra strain energy. Thus, no strain is released by generation of misfit dislocation and dislocation would not be generated.

Comparing experimental results and computer simulation, however, the dislocations are generated regardless of the substrate misorientation once the large islands formed, though the extra strain energy plays important role when the substrate is misoriented. The two-dimensional unit crystal model we took does not fit to the experimental three-dimensional growth. In the two-dimensional growth, the strain energy increases monotonically with the layer thickness until the generation of dislocation. On the contrary, in three-dimensional growth, the strain energy increases drastically at the coalescence of the coherently grown islands because the volume of the coherently grown island increases and elastic strain relief in the lateral directions becomes less effective. If the drastic increase of the strain energy accumulated in the island, which works as the driving force of dislocation generation, may greater than the extra strain energy caused by the interaction between dislocation and step, the suppression effect of the dislocation by misoriented substrate may be concealed. Recently, A. Trampert et al. reported the two-dimensional growth of InAs on GaAs over 35MLs and they observed Lomer-lock type dislocations at the interface [21]. In this case, the substrate misorientation effect on suppression of dislocation generation by extra strain energy may be observed.

Another consideration about insufficiency of VFF model is the misorientation direction dependence of critical thickness increase. This problem may be attributed to the different properties of two orthogonal dislocations. It is well known that two types of like-sign dislocations in zincblende structured crystal, i.e., α and β dislocations are not chemically equivalent [22-27]. Since the VFF model can calculate only the strain energy, the chemical property of the dislocation, for example energy of dangling bond at dislocation core, cannot be taken into account. It is observed that the mobility of α dislocation is greater than that of β

dislocation, which results in the anisotropic dislocation density. K.L. Kavanagh et al. showed by TEM that 60° α dislocation forms first in one <110> direction in InGaAs/GaAs. T. Okada et al. observed anisotropic strain relaxation in InAsP/InP with 60° misfit dislocation predominantly along [110] direction rather than [110] direction. Because the dislocation core structures are not clear in our experiment, we cannot specify the dislocation type to be α or β. However, if the dislocation lies on the glide plane, the dislocation along $[1\bar{1}0]$ direction is specified to be α dislocation. In this case, the dislocation along $[1\bar{1}0]$ direction is likely to be generated primarily from the above discussion. Then VFF model can explain the anisotropic substrate misorientation effect on the critical thickness because dislocation along $[1\bar{1}0]$ crosses step only in the case of substrate misorientation toward $[1\bar{1}0]$ direction.

5.5 Summary

In summary, we have studied the critical thickness of the MBE grown InAs on GaAs substrates just-oriented, 3.5° and 5.0° misoriented toward [110] and [110] directions. PL measurements have shown that 1, 2ML-thick InAs layers grown on each substrate are almost the same properties. However, when the InAs layer thickness is 4ML, the peaks of samples using substrates misoriented toward $[1\bar{1}0]$ direction has been blue-shifted, and moreover when the InAs layer thickness is 5ML, luminescence have been observed only from samples using substrates misoriented toward $[1\bar{1}0]$ direction.

TEM observation of 5ML InAs has shown that there has been a large difference of dislocation density among the samples; the dislocation densities of the samples using substrates misoriented toward [110] direction are almost the same as that on the just-oriented substrate, while the dislocation densities of the samples using substrates misoriented toward [110] direction are much lower than that on the just-oriented substrate. The increase of critical thickness is the result of the suppression of the coalescence of coherently grown islands on the substrates

misoriented toward [110] direction.

To investigate the interaction between dislocation and step, we have calculated the strain energy in the grown layer based on the VFF model and found that 1) there is a minimum length above which dislocation can stably exist and 2) extra strain energy is generated when the dislocation crosses the step on the substrate surface. From the calculation results, we have indicated that the extra strain energy plays an important role to the increase of the critical thickness of the InAs grown on misoriented GaAs substrate.

The result that suppression of dislocation generation by substrate misorientation toward [110] direction is important information for realization of QD devices by InAs self-assembled island.

References

1) F. Houzay, C. Guille, J.M. Moisson, P. Henoc and F. Barthe, J. Cryst. Growth **81**, 67 (1987).

2) C.D'anterroches, J.Y. Marzin, G. Le Roux and L. Goldstein, J. Cryst. Growth **81**, 121 (1987).

3) S. Fujita, Y. Nakaoka, T. Uemura, M. Tabuchi, S. Noda and A. Sasaki, J. Cryst. Growth **95**, 224 (1989).

4) O. Brandt, L. Tapfer, K. Ploog, M. Hohenstein and F. Fillipp, J. Cryst. Growth **111**, 383 (1991).

5) X. Zhang, D.W. Pashly, J.H. Neave, J. Zhang and B.A. Joyce, J. Cryst. Growth **121**, 381 (1992).

6) M. Lentzen, D. Gerthsen, A. Forster, and K. Urban, Appl. Phys. Lett. **60**, 74 (1992).

7) Y. Nabetani, T. Ishikawa, S. Noda, and A. Sasaki, J. Appl. Phys. **76**, 347 (1994).

8) Y. Nabetani, N. Yamamoto, T. Tokuda, and A. Sasaki, J. Cryst. Growth **146**, 363 (1995).

9) M. Tabuchi, Y. Nabetani, S. Noda, and A. Sasaki, J. Cryst. Growth, to be published.

10) J.H. Van der Merwe, J. Appl. Phys. **34**, 117 (1963).

11) J.W. Matthews and A.E. Blakeslee, J. Cryst. Growth **27**, 118 (1974).

12) R. People and J.C. Bean, Appl. Phys. Lett **47**, 322 (1985).

13) M.B. Pashley, K.W. Haberern, and J.M. Gaines, Appl. Phys. Lett. **58**, 406

(1991).

14) I. Tanaka, S. Ohkouchi, and A. Hashimoto, Jpn. J. Appl. Phys. **31**, 2216 (1992).

15) P.N. Keating, Phys. Rev. **145**, 637 (1966).

16) R.M. Martin, Phys. Rev. B **1**, 4005 (1970).

17) M. Tabuchi, S. Noda, and A. Sasaki, J. Cryst. Growth **115**, 169 (1991).

18) Y. Nabetani, A. Wakahara, and A. Sasaki, J. Appl. Phys. **78**, 6461 (1995).

19) M. Tabuchi, Y. Nabetani, S. Noda, and A. Sasaki, J. Cryst. Growth, to be published.

20) L.T. Romano, J. Knall, R.D. Bringans, and D.K. Biegelsen, Appl. Phys. Lett. **65**, 869 (1994).

21) A. Trampert, E. Tournie, and K.H. Ploog, J. Cryst. Growth **146**, 368 (1995).

22) M.S. Abrahams, J. Blanc, and C.J. Buiocchi, Appl. Phys. Lett. **21**, 185 (1972).

23) G.H. Olsen, M.S. Abrahams, and T.J. Zamerowski, J. Electrcochem. Soc. **121**, 1650 (1974).

24) W.J. Bartels and W. Nijman, J. Cryst. Growth **37**, 204 (1977).

25) K.H. Kuesters, B.C.De cooman, and C.B. Carter, Phil. Mag. A **53**, 141 (1986).

26) K.L. Kavanagh, M.A. Capano, L.W. Hobbs, J.C. Barbour, P.M.J. Maree, W. Schaff, J.W. Mayer, D. Pettit, J.M. Woodall, J.A. Stroscio, and R.M. Feenstra, J. Appl. Phys. **64**, 4843 (1988).

27) T. Okada, R.V. Kruzelecky, G.C. Weatherly, D.A. Thompson, and B.J. Robinson, Appl. Phys. Lett. **63**, 3194 (1993).

Chapter 6

Growth of AlP/GaP ordered and disordered superlattices and their optical properties

6.1 Introduction

QW and SL are the most widely fabricated and investigated their optical properties among several kinds of quantum structures. In such structures, different materials are grown alternately to confine electrons and holes or to form subbands. Since potential is modulated in only one dimension in QWs and SLs, fabrication process is much easier than that of QWW or QD. On the contrary, the quantum effect induced in QW or SL is not so high comparing with QWW or QD. In such one dimensional quantum structures, it is usual to confine carriers in space where the potential is lower than other space. A. Sasaki et al. have proposed a completely different concept of quantum structure called disordered crystalline semiconductor to enhance the quantum effect [1]. A disordered superlattice(d-SL) is an example of disordered crystalline semiconductor. In d-SL, two constituent materials have a random arrangement in the layer thickness in contrast to the conventional ordered superlattice(o-SL) in which the arrange-

ment of two materials are regularly ordered. Thus far, experimental investigation of d-SL has revealed that d-SL has ability to improve the luminescence efficiency of indirect band gap semiconductors, such as SiGe, AlGaAs and AlGaP [2-11]. The enhanced luminescence efficiency by d-SL has been discussed in terms of carrier localization induced by the artificially disordered potential arrangement.

The carrier localization and enhanced luminescence efficiency caused by artificially disordered structure is not only unique and interesting physical phenomena but also important merits for device application. Since AlGaP alloy has the widest band gap in the zincblende structured III-V semiconductors(2.26~2.45eV, RT), this material is expected for light-emitting devices covering from orange to green colors. However, the band structure of AlGaP is indirect with the conduction band minimum at X point. Thus far, improvement of luminescence efficiency has been predicted by making short period SL in which zone-folding and band mixing effect occurs [12-16]. Several groups have grown AlP_n/GaP_n short period SLs [17-30]. They observed the luminescence and peak shift as the SL period changes. However, it has been also found that the luminescence intensity drastically decreases for $n \leq 3$ML. M. Kumagai et al. have calculated the band structure of AlP/GaP short period SLs and showed that the indirect-direct transition does not occur for $n \leq 5$ML [15]. C.H. Park et al. have also predicted that the band structure becomes indirect for $n \leq 3$ML [16]. Considering low luminescence efficiency of $AlP_n/GaP_n(n \leq 3)$ o-SL, it seems important to investigate optical property of short period d-SLs. Thus far, we have investigated AlP_m/GaP_n(m,n=3,6,9) d-SL in which m and n takes 3, 6 or 9ML randomly and have found that the PL and EL intensities are greater than those of the AlP_5/GaP_5 o-SL and $Al_{0.5}Ga_{0.5}P$ bulk [8,10]. However, the wavelength of AlP_m/GaP_n(m,n=3,6,9) was 600nm. If the luminescence wavelength of d-SL becomes shorter, green light-emitting device can be realized. Two methods are considered to obtain luminescence of shorter wavelength. One is to reduce the SL period and another is to change constituent material in which band gap is larger.

In this chapter, AlP/GaP short period o- and d-SLs were grown by OMVPE

Table 6-1 Typical growth condition of AlP/GaP SLs used in this study.

pressure	760Torr
H_2 flow	5slm
H_2 velocity	8.5cm/s
growth temperature	720°C
V/III	50
growth rate	1.40Å(GaP)
	1.47Å(AlP)
growth interruption	2s

using tertiarybuthylphosphine(TBP) where SL period was changed to investigate PL properties. PL properties of d-SLs are compared with those of o-SLs.

6.2 Growth procedure and experimental setup

The SLs were grown by atmospheric OMVPE. Schematic illustration of OMVPE system used in this study is shown in Fig.6-1. The phosphorous source was TBP. The decomposition temperature of TBP is several hundred °C lower than that of conventionally used PH_3, in addition to the fact that the toxicity of TBP is much lower than that of PH_3 [33,34]. Trimethylgallium(TMGa) and trimethylalminum(TMAl) were the group III sources. The substrates were S-doped GaP nominally (001) just-oriented. Impurity concentration of substrate is $5\times10^{17}/cm^3$. After etching by HNO_3:HCl:H_2O=1:2:2 at 55°C, the substrate was further dipped in the $(NH_4)_2S_x$ solution to passivate the surface by sulfur. By simultaneous use of TBP and $(NH_4)_2S_x$ treatment, the AlGaP epitaxial layer with a good surface morphology can be obtained at low growth temperature [31,32]. The smooth substrate surface and low growth temperature are essential to achieve abrupt SL interface. Typical growth condition is summarized in Table 6-1.

At first, 0.3μm-thick GaP buffer layers were grown on GaP substrate and then

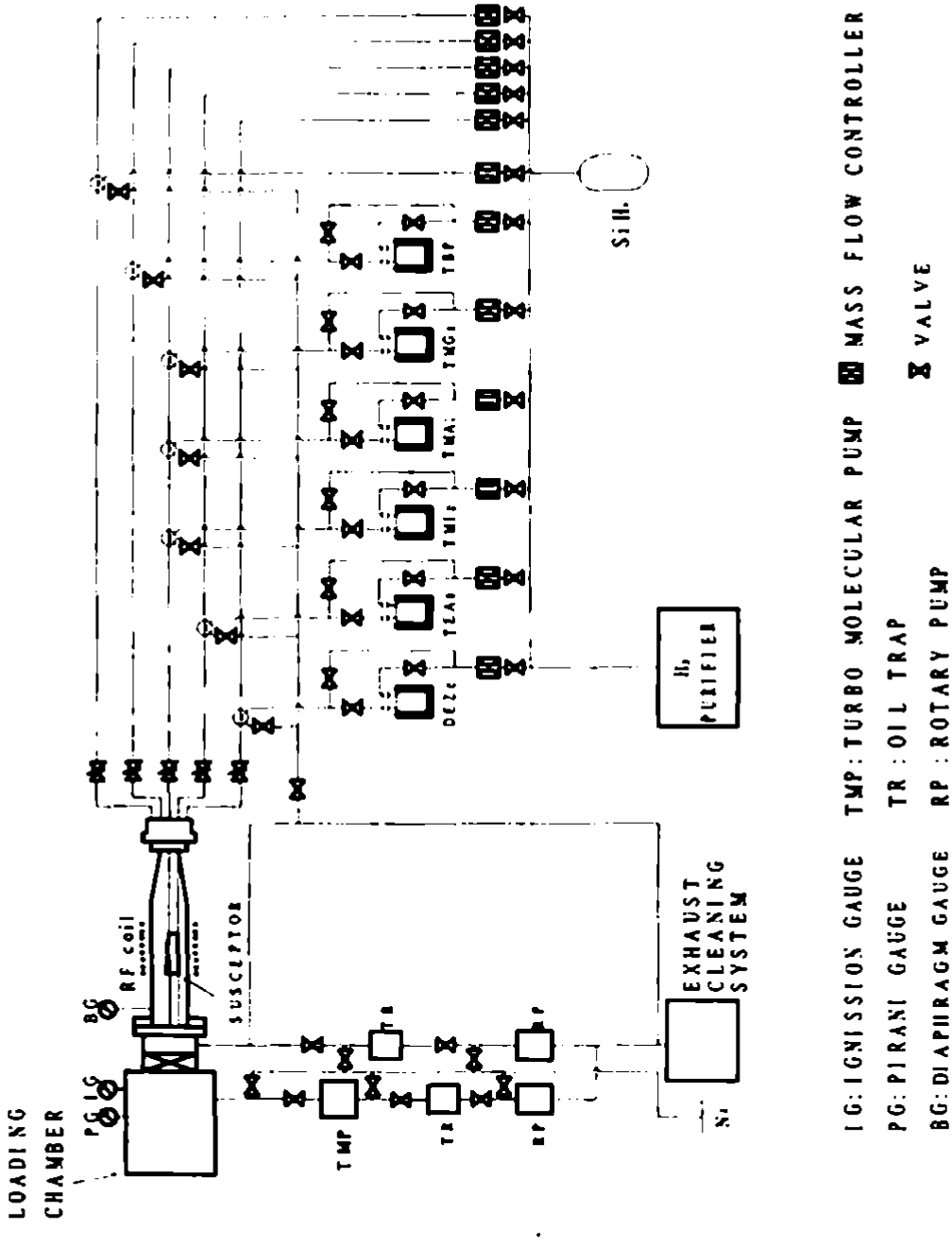

Fig.6-1 Schematic illustration of OMVPE system used in this study.

SL layers were grown 0.5μm. To achieve abrupt interface, the growth interruption of 2s was introduced at each interface. Finally, 300Å-thick GaP cap layers were grown. The SL periods were controlled by the gas flow time of group III source.

In the growth of AlP_m/GaP_n d-SL(m = h_1,k_1,l_1 and n = h_2,k_2,l_2), we adopted the linear congruential method to determine the layer thickness m and n as follows.

$$x_n = x_{n-1} \times 153 + 7391 (n = 1, 2, 3, \cdots) \tag{6-1a}$$

$$x_0 = 19 \tag{6-1b}$$

$$M = 576 \tag{6-1c}$$

$$x_n = mod(x_n/M) \tag{6-1d}$$

$$X_n = x_n/M \tag{6-1e}$$

where X_n represents a random value uniformly distributed between 0 and 1. Then, layer thickness is given by classifying X_n into three regions from following equations:

$$0 < X_n < \frac{1}{3} \cdots h_1, h_2 \tag{6-2a}$$

$$\frac{1}{3} < X_n < \frac{2}{3} \cdots k_1, k_2 \tag{6-2b}$$

$$\frac{2}{3} < X_n < 1 \cdots l_1, l_2 \tag{6-2c}$$

Using this process, we can get layer thickness of h_i, k_i, and l_i(i= 1,2) with equal appearance probabilities. The layer thickness combination of d-SLs was varied among (1,2,3), (2,4,6) and (3,6,9). In these combinations, average layer thickness is 2, 4 and 6ML, and deviations from average layer thickness becomes 1, 2 and 3ML, respectively. Thus, three kinds of d-SL such as AlP_m/GaP_n where m,n = (1,2,3), (2,4,6) and (3,6,9) have similar randomness in structure but only the periods are different. Example of disorder pattern generated by above sequence is shown as a conduction band structure in Fig.6-2.

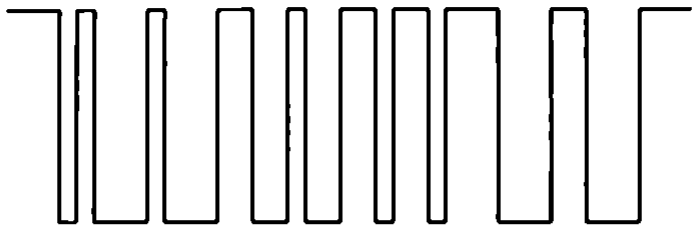

Fig.6-2 Example of disorder pattern as a potential of conduction band.

For comparison with d-SLs, AlP_n/GaP_n o-SLs where n=2, 4 and 6 were also grown.

The structural properties of the grown SLs were characterized by X-ray diffraction method. The optical properties were characterized by PL at low temperature. The excitation source was Ar-ion laser operating at UV-region(333.6-363.8nm). The excitation power density was 300mW/cm^2. Luminescence was detected by photo multiplier.

6.3 Experimental results and discussion

6.3.1 Structural characterization by X-ray diffraction

Figure 6-3 shows the θ-2θ X-ray diffraction patterns around (002) of AlP_m/GaP_n (m,n=1,2,3) d-SL and AlP_2/GaP_2 o-SL. The diffraction pattern of AlP_m/GaP_n (m,n=1,2,3) d-SL is characterized by many sharp peaks, whereas that of AlP_2/GaP_2 o-SL shows clear $\pm$1st order satellite peaks. The average heterointerface roughness of AlP_2/GaP_2 o-SL are estimated by following equation [35].

$$\delta\omega = \lambda\delta t(2\cos\theta_B\Lambda_{SL}^2)^{-1} \qquad (6\text{-}3)$$

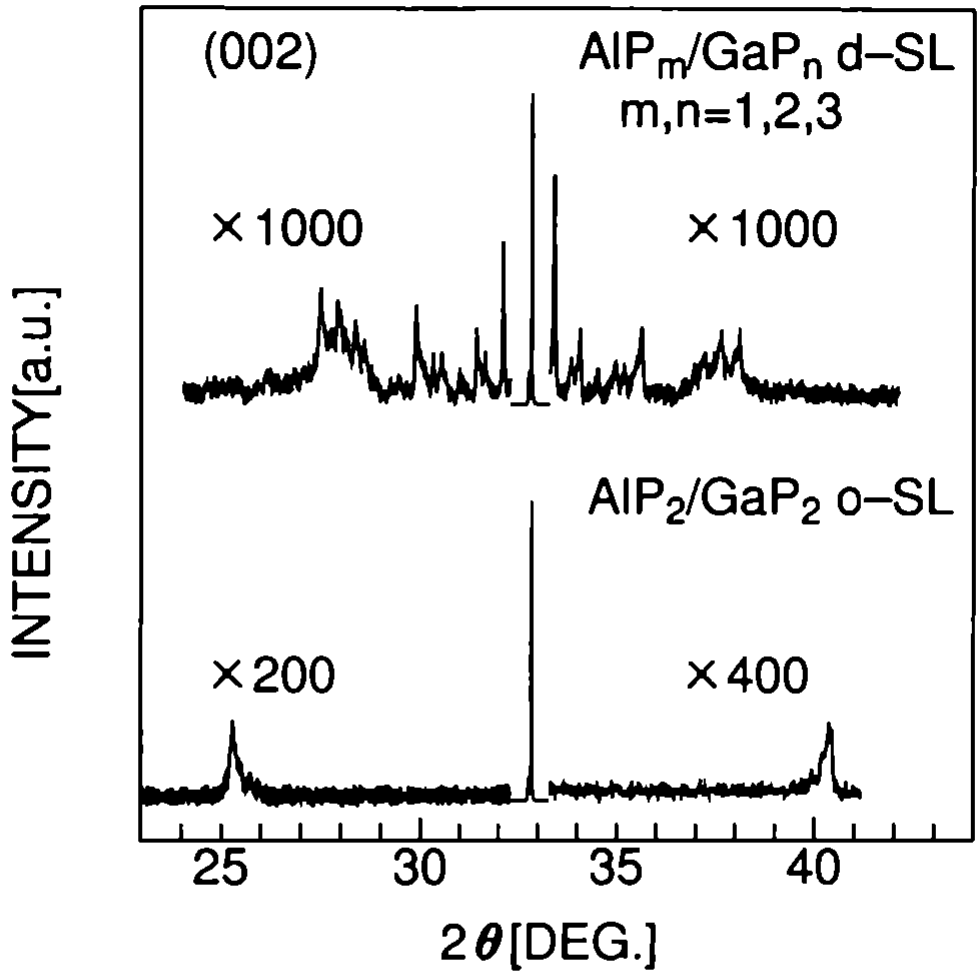

Fig.6-3 (002) θ-2θ diffraction patterns of AlP_m/GaP_n (m,n=1,2,3) d-SL and AlP_2/GaP_2 o-SL.

where δt is the average heterointerface roughness, $\delta\omega$ the FWHM of the satellite peak, λ the wavelength of X-ray, θ_B the Bragg angle of the substrate, and Λ_{SL} the SL period. From Fig.6-3, the FWHM of the -1st satellite peak of AlP_2/GaP_2 o-SL is 355arcsec which means that the average heterointerface roughness is 0.1ML. This value indicates the good quality of the hetrointerface. Although the characterizing method of heterointerface roughness for d-SL has not been established yet, the abruptness and homogeneity of heterointerface of d-SL are considered to be as excellent as those of o-SL, because the growth conditions and growth sequences are the same for all samples.

X-ray diffraction patterns of other o- and d-SLs show good abrupt heterointerfaces and crystalline qualities.

6.3.2 Photoluminescence spectroscopy

PL spectra of AlP/GaP o- and d-SLs are shown in Fig. 6-4. Sharp peaks were observed from each sample except for AlP_2/GaP_2 o-SL. It is clear that the peak wavelength decreases with reducing the SL period in both o- and d-SLs. However, the peak intensities also decrease. Comparing PL spectra of d-SLs with those of o-SLs which have the same average layer thickness as d-SLs, two features are seen: 1)the peak wavelength of d-SL is longer than that of o-SL and 2)the peak intensity of d-SL is stronger than that of o-SL. These features have been also observed with AlAs/GaAs o- and d-SLs [2].

At first, we consider the luminescence mechanism of o-SLs. It is noteworthy that the PL from AlP_2/GaP_2 o-SLs is very weak. The peak at 560nm of AlP_2/GaP_2 o-SL is inferred to be the DA pair recombination of S-C impurities [36]. S impurity may be introduced by TBP source. Since layer thickness is very short as 2ML, one may attribute the poor PL property of AlP_2/GaP_2 to the imperfection of the SL structure. However, the fluctuation of the heterointerface is 0.1ML as described above, then the heterointerface roughness is not responsible for the PL intensity. Next, band structure of short period o-SL should be consid-

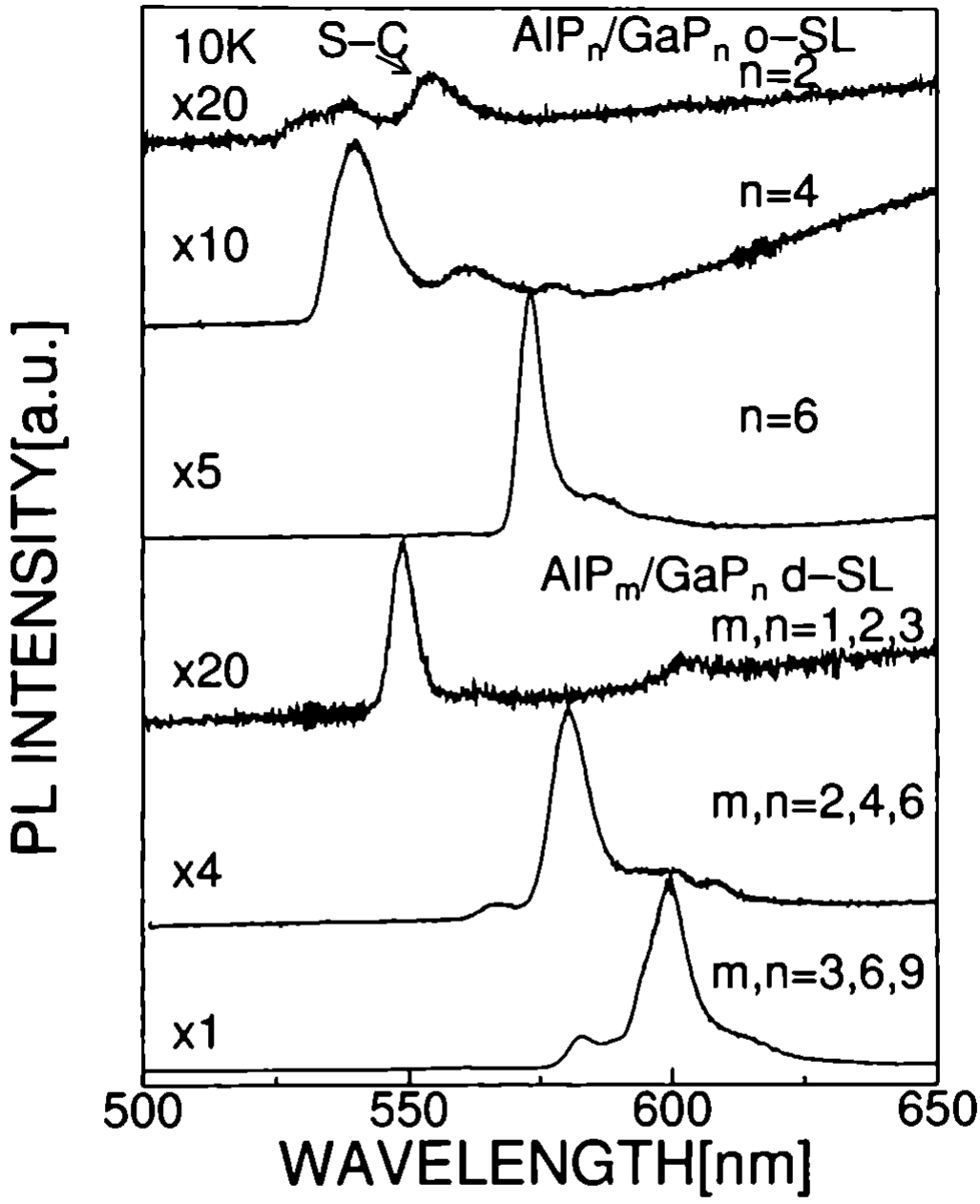

Fig.6-4 PL spectra of AlP_m/GaP_n d-SLs and AlP_n/GaP_n o-SLs.

ered. C.H. Parks et al. have calculated the band structures of AlP/GaP o-SL by tight binding method [16]. They have shown that the band structure of zone-folded AlP_n/GaP_n(n=1,2) is indirect and explained as follows. In zone-folded SL, there are five conduction minimum points, those are one $\Gamma(X_c)$ point which is folded from two X points in SL direction and four M_c points which are unfolded X points in the growth plane. When the layer thickness is considerably small, energy states repulsion at the heterointerface is significant. At Γ point, energy states repulsion mainly works between $\Gamma(X_c)$ and Γ_v which is valence band maximum and then $\Gamma(X_c)$ is raised. At the same time, repulsion also works between M_c points and another M points folded from <101> points. Contrast to Γ point, M_c is lowered in this case. As results, M_c becomes lower than $\Gamma(X_c)$ and the band structure remains indirect. However, we have no explicit proof that the luminescence from AlP/GaP o-SL is a result of indirect-direct transition induced by zone-folding, in spite of several intensive researches including other groups'.

In order to examine whether zone-folding occurs and it is responsible for the luminescence, we grew an AlP_4/GaP_3 o-SL and measured PL. When SL period m+n of AlP_m/GaP_n o-SL is an odd number, the folded X points does not come to Γ point [15], hence the band structure remains indirect even when the zone-folding occurs. Result is shown in Fig.6-5. Clear peak similar to AlP_4/GaP_4 and AlP_6/GaP_6 is seen. A broad peak beyond 580nm is probably related to complexes arising from S and Ga vacancy and also observed from S-doped GaP substrate [37]. From this experiment, it is considered that luminescence is not caused by zone-folding, furthermore it is suspicious that zone-folding itself really occurs.

Since zone-folding effect is found less concerned for luminescence, another reason of the luminescence from o-SL should be considered. From previous investigation of AlP/GaP o-SLs, PL at low temperature was related to exciton [25]. In this case, the weak luminescence from AlP_2/GaP_2 o-SL can be explained by the charge transfer at heterointerface of AlP and GaP [38]. Exciton is considered to be bound at the heterointerface, because SL structure of AlP/GaP is type-II [39].

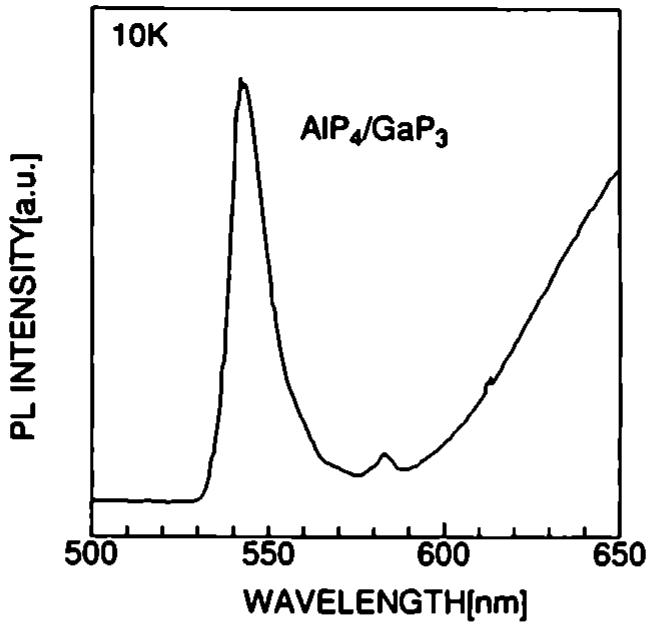

Fig.6-5 PL spectrum of AlP_4/GaP_3 o-SL.

In quite narrow layer such as 1 and 2ML, charge transfer phenomena smears the abrupt potential change between AlP and GaP and then the exciton does not bound which results in the disappearance of luminescence.

Contrast to the o-SLs, the strong luminescence from d-SLs indicates the enhancement of quantum effect. Remarkable difference between PL properties of o- and d-SLs is the fact that clear peak was observed from the AlP_m/GaP_n(m,n=1,2,3) d-SL, whereas that from the AlP_2/GaP_2 o-SL was not. Since AlP_m/GaP_n(m,n=1,2,3) d-SL contains 3ML-thick layer which is larger than 2ML, one might attribute the relatively large 3ML as a recombination center. However, as shown in Fig.6-4, the peak wavelength of AlP_m/GaP_n(m,n=1,2,3) d-SL is longer than that of AlP_4/GaP_4 o-SL in which the layer thickness is wider than 3ML. Therefore, luminescence is not from 3ML-thick layer. The precise mechanism is not clear, but localized states induced by artificially disordered potential arrangement is likely to formed. In such localized states, exciton is tightly bound. In Fig. 6-4, several

peaks are seen from d-SLs, and thus, several localized states in different energy levels are formed.

Next, we investigated the temperature dependence of PL from d-SLs. Figures 6-6 show the PL spectra of d-SLs with various temperatures. As can be seen, PL from d-SL becomes weak as increasing temperature. The longer wavelength peaks are the same as that observed in Fig.6-5.

To discuss PL temperature dependence more quantitatively, we plotted the integrated PL intensities of the main peaks as a function of the temperature and fitted by following equation as in the case of AlAs/GaAs d-SL [2].

$$I_{PL} = \frac{I_0}{1 + A \exp \frac{T}{T_0}} \tag{6-4}$$

Here, I_{PL} is the integrated PL intensity, I_0 a constant, A the ratio of probabilities of nonradiation recombination to radiation recombination at 0K, T the measurement temperature, and T_0 the characteristic temperature. Eq.6-4 is derived based on the assumption that the ratio of nonradiative recombination probability P_n to radiative recombination probability P_r increases exponentially: $P_n/P_r \propto \exp(T/T_0)$. The characteristic temperature T_0 indicates the degree of evanescence in luminescence intensity as temperature increases. Large T_0 means that the intensity of luminescence decreases gently as temperature increases. Figure 6-7 shows the fitted values of T_0 as a function of average layer thickness. X.W. Wang et al. have found that T_0 of d-SL is larger than that of o-SL [8]. Though the average layer thickness is reduced, the change in T_0 is small. Therefore, the result that T_0 does not change so much among three structures means that the ratio of the probabilities of nonradiative recombination to radiative recombination also does not change. The small change of T_0 may be attributed to the strong carrier localization in the d-SL.

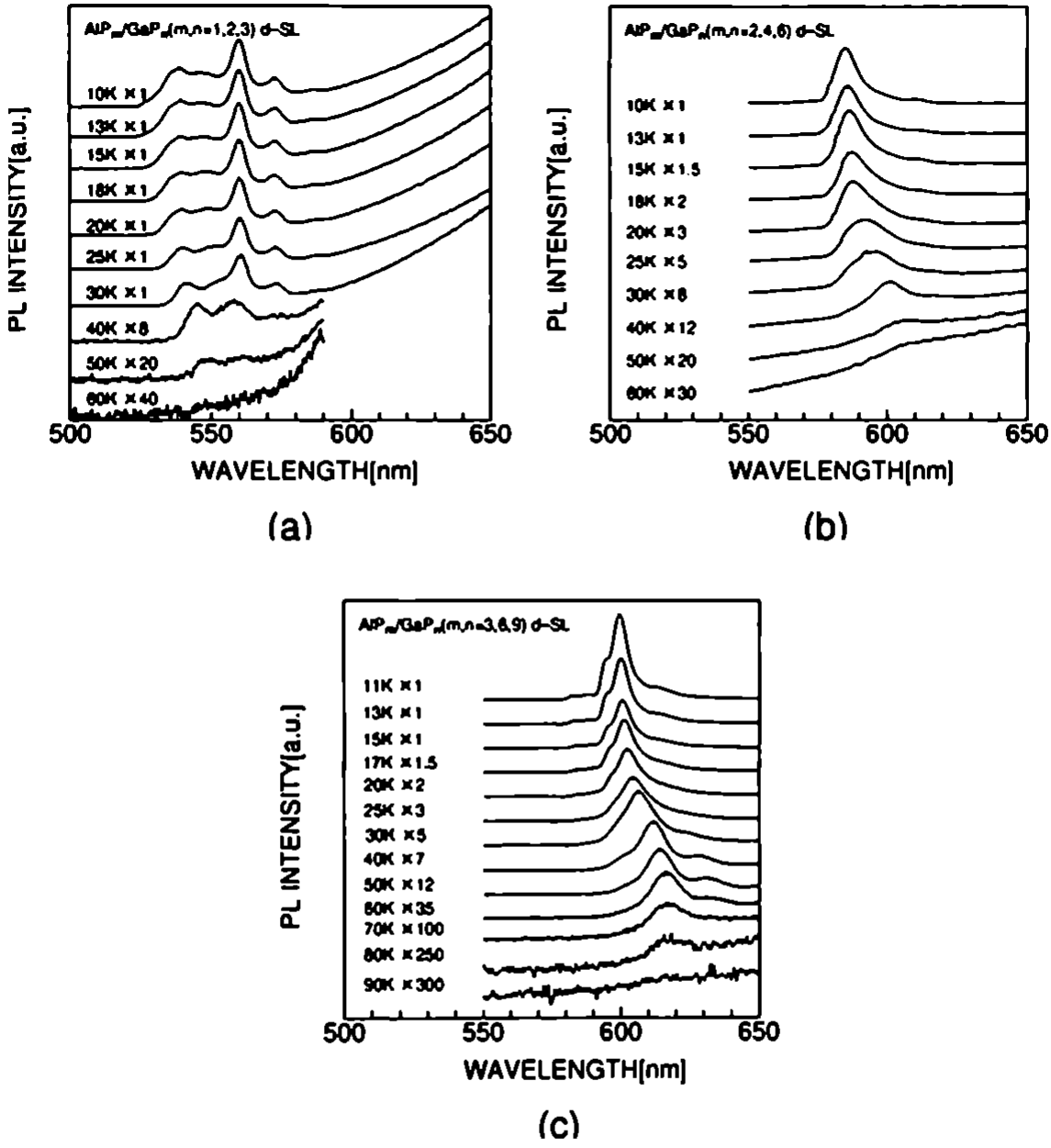

Fig.6-6 Temperature dependence of PL spectra of AlP_m/GaP_n d-SLs. SL period is (a)(m,n=1,2,3), (b)(m,n=2,4,6) and (c)(m,n=3,6,9).

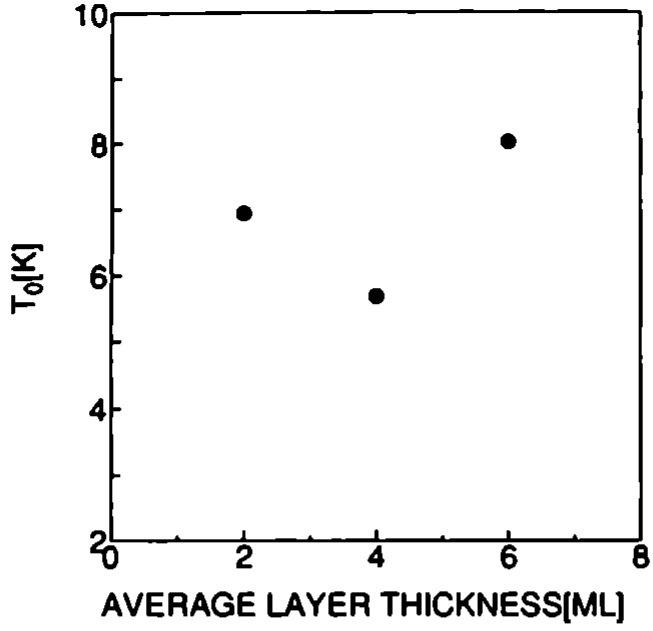

Fig.6-7 T_0 as a function of average layer thickness of d-SLs.

6.4 Summary

We have grown AlP/GaP o- and d-SLs by atmospheric OMVPE and investigated their PL properties. The PL peaks of AlP/GaP o- and d-SLs shift to shorter wavelength as the period decreases. The PL from AlP_m/GaP_n (m,n=1,2,3) d-SL have been clearly observed though that from AlP_2/GaP_2 o-SL which has the same average layer thickness as the d-SL was not observed. The clear peak has been observed up to 30K from AlP_m/GaP_n(m,n=1,2,3) d-SL as well as (m,n=2,4,6) and (m,n=3,6,9) d-SLs. The PL integrated intensity does not largely change by the reduction of the SL period. Though the luminescence wavelength of AlP_m/GaP_n(m,n=1,2,3)d-SL, which is the shortest wavelength from d-SLs, is little bit longer than that from AlP_4/GaP_4 o-SL, persistent luminescence property of d-SL was revealed.

References

1) A. Sasaki, M. Kasu, and S. Noda, Jpn. J. Appl. Phys. **28** (1989)L1249.
2) M. Kasu, T. Yamamoto, S. Noda, and A. Sasaki, Jpn. J. Appl. Phys. **29**, 828 (1990).
3) M. Kasu, T. Yamamoto, S. Noda, and A. Sasaki, Jpn. J. Appl. Phys. **29**, L1055 (1990).
4) M. Kasu, T. Yamamoto, S. Noda, and A. Sasaki, Jpn. J. Appl. Phys. **29**, L1588 (1990).
5) T. Yamamoto, M. Kasu, S. Noda, and A. Sasaki, J. Appl. Phys. **68**, 5318 (1990).
6) M. Kasu, T. Yamamoto, S. Noda, and A. Sasaki, Appl. Phys. Lett. **59**, 800 (1991).
7) A. Sasaki, J. Cryst. Growth **115**, 490 (1991).
8) X.L. Wang, A. Wakahara, and A. Sasaki, Appl Phys. Lett. **62**, 888 (1993).
9) A. Wakahara, T. Hasegawa, K. Kuramoto, K.K. Vong, and A. Sasaki, Appl. Phys. Lett. **64**, 1850 (1994).
10) A. Sasaki, X.L. Wang, and A. Wakahara, Appl. Phys. Lett. **64**, 2016 (1994).
11) K. Uno, S. Noda, and A. Sasaki, J. Appl. Phys. **77**, 4693 (1995).
12) U. Gnutzmann and K. Clausecker, Appl. Phys. **3**, 9 (1974).
13) J.Y. Kim and A. Madhukar, J. Vac. Sci. Technol. **21**, 528 (1982).
14) M.F.H. Schuurmans, H.W.A.M. Rompa, and R. Eppenga, J. Lumin. **37**, 269 (1987).
15) M. Kumagai, T. Takagahara, and E. Hanamura, Phys. Rev. **B37**, 898 (1988).

16) C.H. Park and K.J. Chang, Phys. Rev. **B47**, 12709 (1993).

17) H. Asahi, K. Asami, T. Watanabe, J.Y. Soon, T. Kaneko, S. Emura, and S. Gonda, Appl. Phys. Lett. **58**, 1407 (1991).

18) A. Morii, I. Ohno, A. Kanda, K. Arai, K. Tokudome, K. Hara, J. Yoshino, and H. Kukimoto, Jpn. J. Appl. Phys. **30**, L1244 (1991).

19) K. Asami, H. Asahi, T. Watanabe, S. Gonda, H. Okumura, and S. Yoshida, Surf. Sci. **267**, 450 (1992).

20) A. Morii, H. Okagawa, K. Hara, J. Yoshino, and H. Kukimoto, J. Cryst. Growth **124**, 772 (1992).

21) K. Asami, H. Asahi, T. Watanabe, M. Enokida, S. Gonda, and S. Fujita, Appl. Phys. Lett. **62**, 81 (1993).

22) H. Asahi, M. Enokida, K. Asami, J.H. Kim, T. Watanabe, R.K. Soni, and S. Gonda, J. Cryst. Growth **136**, 268 (1994).

23) A. Morii, T. Takano, J. Kitamura, K. Hara, H. Kukimoto, J.Yoshino, and T. Yasuda, Solid-State Electron. **37**, 649 (1994).

24) K. Asami, H. Asahi, S.G. Kim, J.H. Kim, A. Ishida, S. Takamuku, and S. Gonda, Appl. Phys. Lett. **64**, 2430 (1994).

25) X.L. Wang, A. Wakahara, and A. Sasaki, J. Appl. Phys. **76**, 524 (1994).

26) X.L. Wang, A. Wakahara, and A. Sasaki, Appl. Phys. Lett. **65**, 2096 (1994).

27) J.H. Kim, H. Asahi, K. Asami, K. Iwata, S.G. Kim, and S. Gonda, Appl. Surf. Sci. **82**, 76 (1994).

28) A. Wakahara, Y. Nabetani, X.L. Wang, and A. Sasaki, J. Cryst. Growth **145**, 187 (1994).

29) E.G. Wang and C.S. Ting, Appl. Phys. Lett. **66**, 1400 (1995).

30) F. Issiki, S. Fukatsu, and Y. Shiraki, Appl. Phys. Lett. **67**, 1048 (1995).

31) A. Wakahara, X.L. Wang, and A. Sasaki, J. Cryst. Growth **124**, 118 (1992).

32) X.L. Wang, A. Wakahara, and A. Sasaki, J. Cryst. Growth **129**, 289 (1993).

33) G.B. Stringfellow, *Organometallic Vapor Phase Epitaxy: Theory and Practice*, Academic Press, Inc. New York(1989).

34) D.S. Cao and G.B. Stringfellow, J. Electron. Matter. **20**, 97 (1991).

35) L. Tapfer, Physica Scripta **T25**, 45 (1989).

36) P.J. Dean, C.J. Frosch, and C.H. Henry, J. Appl. Phys. **39**, 5631 (1968).

37) X. Liu, S.G. Bishop, J.N. Bailargeon, and K.Y. Cheng, Appl. Phys. Lett **63**, 208 (1994).

38) S.H. Wei and A. Zunger, Phys. Rev. B**39**, 3279 (1989).

39) A. Morii, H. Okagawa, K. Hara, J. Yoshino, and H. Kukimoto, Jpn. J. Appl Phys. **31**, L1161 (1992).

Chapter 7

Growth of AlGaP/AlGaP ordered and disordered superlattices and their optical properties

7.1 Introduction

In previous chapter, it was found that the luminescence efficiency of AlP/GaP d-SL is higher than that of o-SL. The improved luminescence property was attributed to the localized states induced by artificially disordered material arrangement. Since d-SL is characterized by the disordered potential arrangement, it is interesting to investigate the optical property with respect to the band discontinuity.

In this chapter, $Al_xGa_{1-x}P$/GaP and AlP/$Al_yGa_{1-y}P$ o- and d-SLs were grown to investigate the PL properties with different band continuities. Because SL of AlP/GaP is type-II, the luminescence wavelengths from AlGaP/GaP and AlP/AlGaP SLs become shorter than those of corresponding AlP/GaP SLs as shown later. The luminescence of shorter wavelength(500~550nm) from AlGaP

system is expected for pure green light-emitting devices.

7.2 Growth and structural characterization

7.2.1 Growth procedure

Growth procedure of AlGaP/GaP and AlP/AlGaP SLs is the same as that of AlP/GaP SLs described in previous chapter. Here, only the modified point is described. Growth rates and V/III flow ratio are listed in Table 7-1. TMAl flow rate was decreased, since Al solid state composition in AlGaP becomes considerably higher than vapor phase composition TMAl/(TMAl+TMGa) [1]. Thus, growth rates are slower than those for AlP/GaP SLs, especially for AlGaP/AlP SLs. Source gas flow patterns are shown in Fig.7-1.

7.2.2 Structural characterization of AlGaP/GaP superlattices

In order to examine the structure of grown SLs, X-ray diffraction measurement was performed. Here, the structural characterization of o-SLs is described to simplify the discussion. Since o- and d-SLs were grown under the same conditions except for growth time, structure of d-SL can be understood by analogy with o-SL.

From X-ray diffraction measurement, we can obtain average Al composition from 0th order peak angle and SL period from satellite peak angles. In case of AlP/GaP, there are two parameters which characterize the SL structure, those are, 1) SL period or total of layer thickness in one period of AlP and GaP and 2) one of AlP or GaP layer thickness. Former parameter is obtained from satellite peak angle and latter is obtained from Al composition, in other words, 0th order peak angle. In case of AlGaP/GaP or AlP/AlGaP, however, SL structure cannot be determined as precisely from such two angles only. Al composition of AlGaP

Table 7-1 Growth rates and V/III flow ratio for AlGaP/GaP and AlP/AlGaP superlattices.

	AlGaP/GaP		AlP/AlGaP	
	AlGaP	GaP	AlP	AlGaP
growth rate(Å/s)	1.28	1.10	0.46	0.46~0.74
V/III	45	50	455	125~190

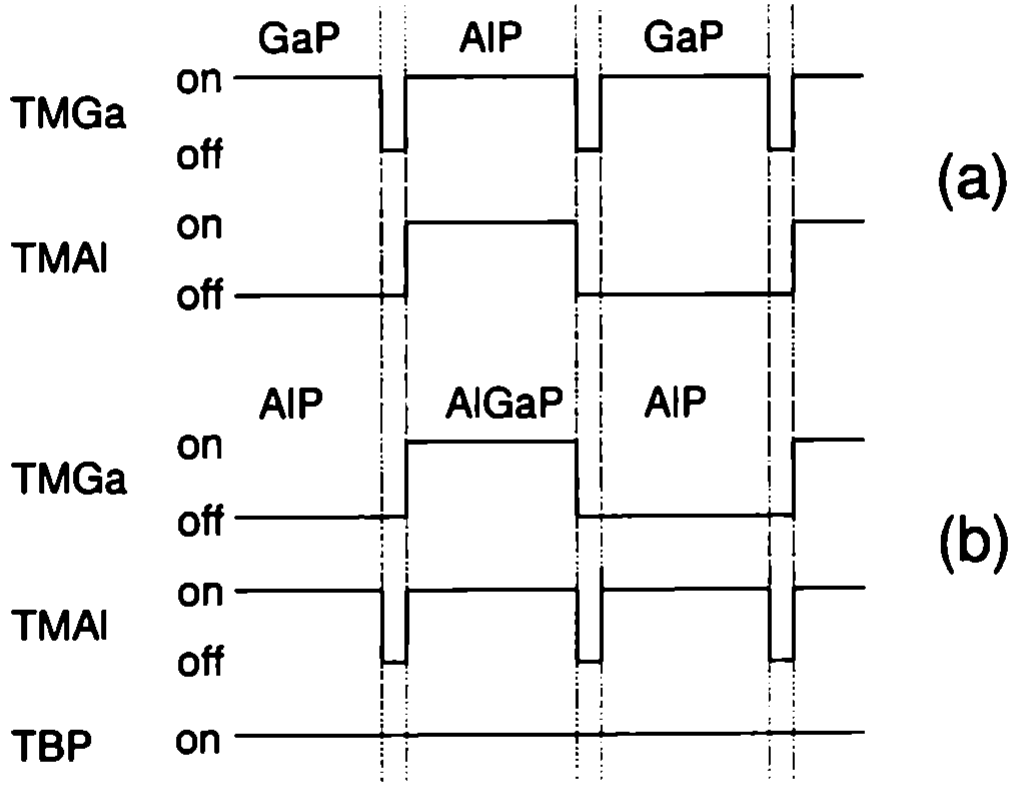

Fig.7-1 Source gas flow patterns for (a)AlGaP/GaP and (b)AlP/AlGaP SLs. TBP was supplied continuously.

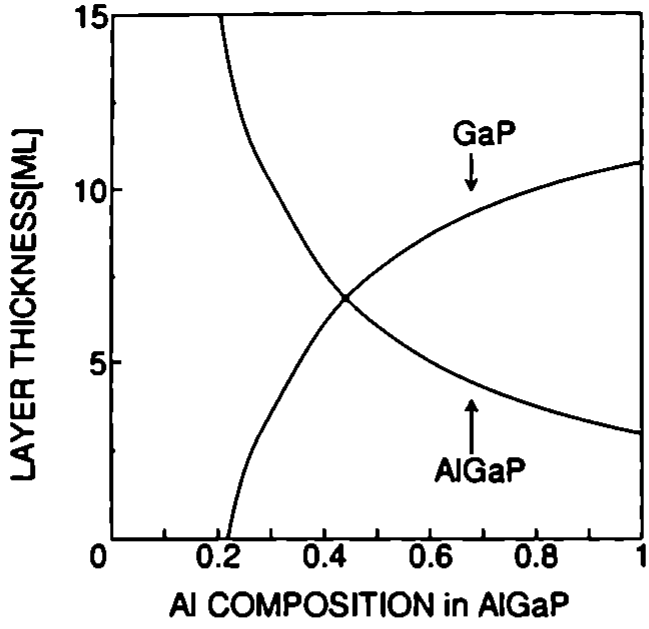

Fig.7-2 Combination of AlGaP and GaP layer thickness estimated by 0th and -1st order satellite peak angles for $(Al_{0.25}Ga_{0.75}P)_5/(GaP)_9$ o-SL. Layer thicknesses are shown as a function of Al composition in AlGaP layer.

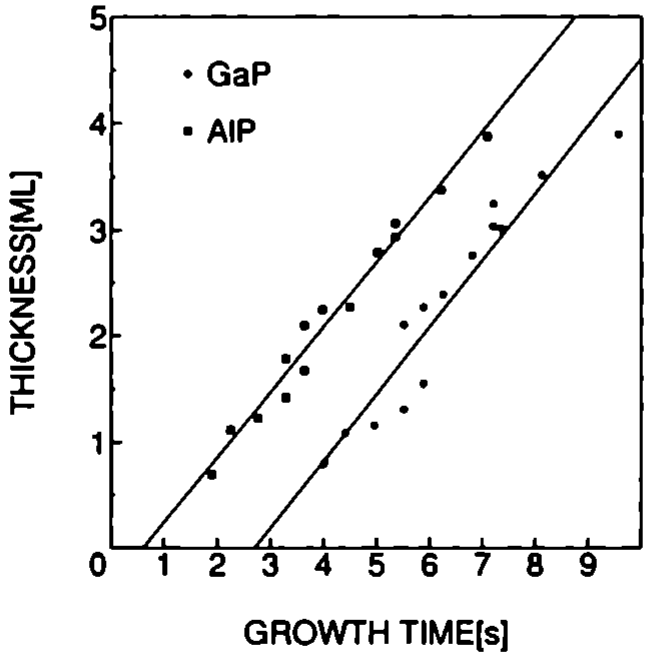

Fig.7-3 Relations between grown layer thickness and growth time of AlP and GaP layers determined by X-ray diffraction of AlP/GaP o-SL. Growth delay time is longer for GaP layer.

layer is also necessary besides average Al composition. Without third information, SL structure is estimated as certain combinations of GaP and AlGaP layer thickness with various Al composition in AlGaP layers. Figure 7-2 shows the combination of AlGaP and GaP layer thickness estimated from X-ray diffraction of a o-SL, in which the nominal designed structure is $(Al_{0.25}Ga_{0.75}P)_5/(GaP)_9$. Abscissa of Fig.7-2 represents the Al composition in AlGaP layer.

To specify Al composition of AlGaP layer, we adopted the growth rate of GaP as third information. The growth rate of GaP is already known from X-ray diffraction of AlP/GaP o-SLs as shown in Fig.7-3 and then, the layer thickness of GaP can be estimated with the growth time. As a result, Al composition of AlGaP layer is estimated as 0.75. This value is considerably higher than designed value of 0.25 which was confirmed by AlGaP alloy. Disagreement in Al composition arises from the fact that this approach assumes that the Al composition is uniform in one AlGaP layer. From the X-ray diffraction of AlP/GaP SLs, it was found that growths of AlP and GaP delay at the beginning of each layer and the delay time is longer for GaP as shown in Fig.7-3. These properties may arise from delay of group III source flow into the growth chamber. Therefore it is considered that the Al composition becomes higher at the beginning of AlGaP growth. We have carried out simulations of X-ray diffraction patterns of AlGaP/GaP o-SLs based on dynamical theory [2] assuming that thin AlP layer is inserted in front of AlGaP layer. Figure 7-4 compares the experimental diffraction pattern and simulated results. When no AlP layer is inserted, -2nd order satellite peak is not seen in simulated pattern, but experimental pattern shows. Comparing the integrated intensities of satellite peaks, we deduced that fractional layer of AlP is inserted between GaP and AlGaP layers.

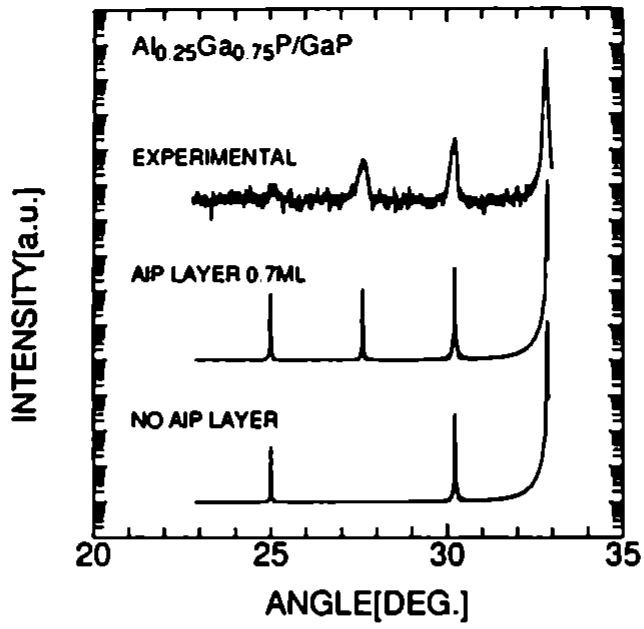

Fig.7-4 Comparison between experimental and simulation results of X-ray diffraction patterns. Simulation was based on dynamical theory. The SL period and average Al composition was determined by experimental results.

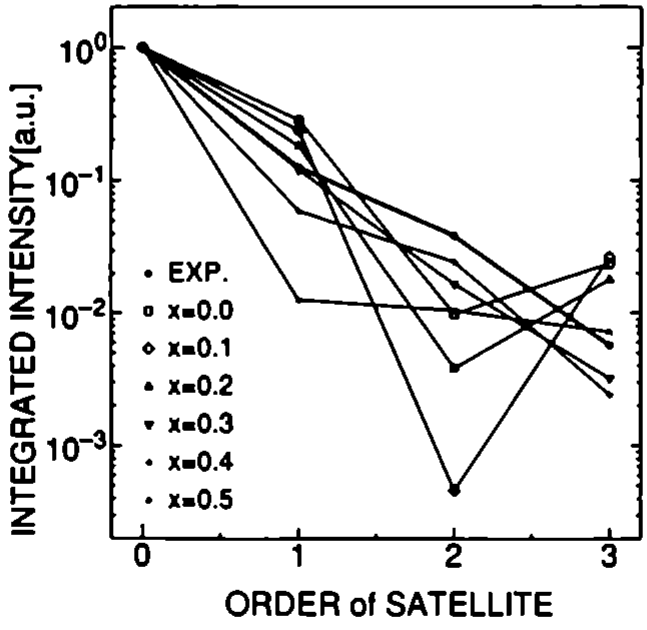

Fig.7-5 Integrated intensities of satellite peaks in X-ray diffraction patterns. All the intensities are normalized by intensities of 0th order peaks.

7.2.3 Structural characterization of AlP/AlGaP superlattices

From the structural characterization of AlGaP/GaP o-SLs, it was found that fractional layer of AlP is inserted in front of AlGaP layer. In case of AlP/AlGaP SLs, unintentional AlP layer does not cause serious structural change since AlP layer is one of the constituent layer of the SL. As a result, AlP layer thickness is slightly increased. However, there is still ambiguity in Al composition of AlGaP layer. This time, we have simulated X-ray diffraction patterns of several AlP/AlGaP o-SLs. The combination of AlP and AlGaP layer thicknesses and Al composition in AlGaP layer were determined by peak angles of experimental diffraction pattern similar to Fig.7-2. Figure 7-5 shows the integrated intensities of 0th through -3rd order satellite peaks. Intensities are normalized by 0th order peaks, respectively. One can see that the intensities of -1st order satellite peak decrease as Al composition increases. This is understood as follows. 0th order peak is related to the average Al composition in SL, and the intensity does not depend largely on Al composition. On the other hands, -1st order satellite peak arises from the difference in scattering factors of AlP and AlGaP. Since difference of scattering factor decreases and the satellite peak intensities becomes weak when Al composition in AlGaP is increased. Comparison of integrated intensity between experiment and simulation would be a good way to determine Al composition. In Fig.7-5, Al composition is deduced as 0.3.

7.3 Photoluminescence spectroscopy and discussion

7.3.1 AlGaP/GaP superlattices

PL spectra of $(Al_{0.33}Ga_{0.67}P)_5/(GaP)_9$ o-SL and $(Al_{0.33}Ga_{0.67}P)_m/(GaP)_n$ (m=2.5,5.0,7.5, n=4.5,9.0,13.5) d-SL are shown in Fig.7-6 together with AlP_5/GaP_9

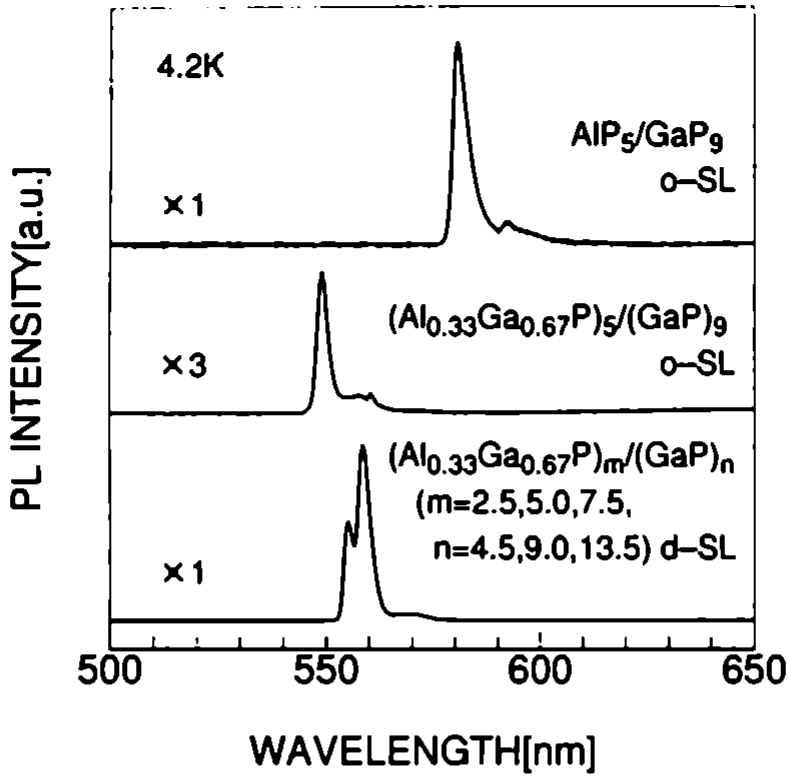

Fig.7-6 PL spectra of $(Al_{0.33}Ga_{0.67}P)_5/(GaP)_5$ o-SL and $(Al_{0.33}Ga_{0.67}P)_m/(GaP)_n$ (m=2.5,5.0,7.5, n=4.5,9.0,13.5) d-SL together with AlP_5/GaP_9 o-SL for comparison. Measurement temperature was 4.2K.

o-SL for comparison. It is clearly seen that the peak wavelength of AlGaP/GaP o-SL is considerably shorter than that of AlP/GaP o-SL, but intensity is four times weaker. On the other hands, the peak wavelength of AlGaP/GaP d-SL is longer than that of AlGaP/GaP o-SL, but still shorter than that of AlP/GaP o-SL. The peak intensity is stronger than that of AlGaP/GaP o-SL and almost the same as that of AlP/GaP o-SL. The full width at half maximums(FWHMs) of each main peaks are as sharp as 12.2, 13.6, and 15.2meV for AlGaP/GaP o-SL, AlGaP/GaP d-SL and AlP/GaP o-SL, respectively.

The shorter wavelength of AlGaP/GaP SLs is easily explained. Since AlP/GaP SL is type-II [3], electrons are confined in AlP layer while holes are confined in

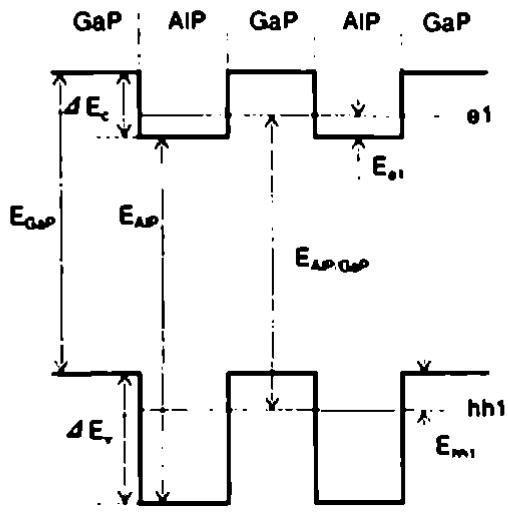

(a)

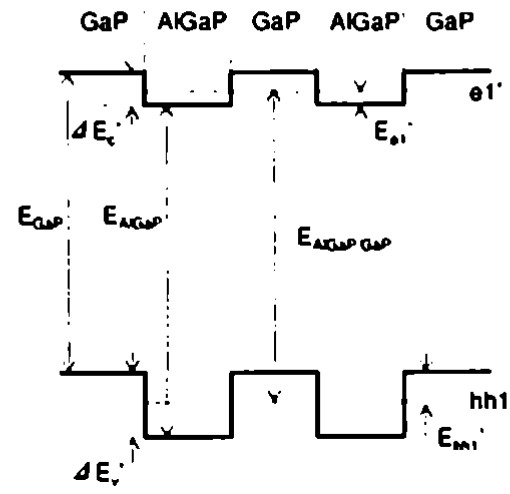

(b)

E_{GaP} = 2.29eV
E_{AlP} = 2.50eV
ΔE_v = 0.46eV
ΔE_c = 0.25eV
(10K)

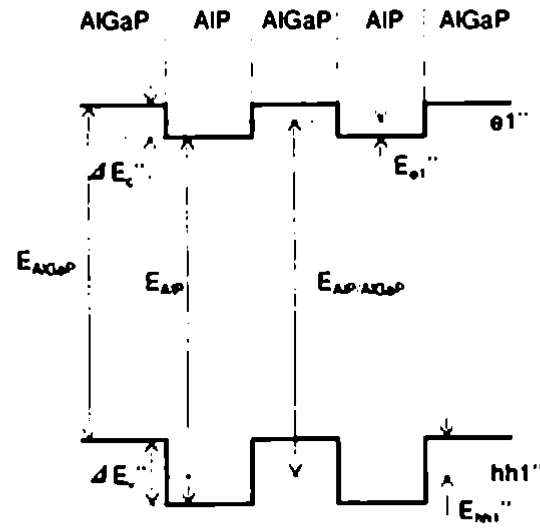

(c)

Fig.7-7 Band structures of (a)AlP/GaP, (b)AlGaP/GaP and (c)AlP/AlGaP SLs.

GaP layer. Although the band lineup of AlGaP/GaP nor AlP/AlGaP SLs are not experimentally confirmed, they are also type-II. Figures 7-7 shows the band structures of AlP/GaP, AlGaP/GaP, and AlP/AlGaP o-SLs. The effective band gap, $E_{AlP/GaP}$, in other words, the energy level difference between lowest subband in conduction band and highest subband in valence band, is given by following equations for AlP/GaP SL.

$$E_{AlP/GaP} = E_{GaP} - \Delta E_c + (E_{c1} + E_{hh1}) \quad (7\text{-}1a)$$

$$= E_{AlP} - \Delta E_v + (E_{c1} + E_{hh1}) \quad (7\text{-}1b)$$

where E_{GaP} and E_{AlP} denote the band gaps of GaP and AlP, respectively, ΔE_c ΔE_v band discontinuities in conduction and valence bands, respectively, E_{c1} and E_{hh1} the subband levels in conduction and valence bands, respectively. From Eqs.7-1, it is found that $E_{AlP/GaP}$ becomes smaller than E_{GaP} provided ΔE_c is larger than $E_{c1} + E_{hh1}$. This situation was seen in previous chapter(see Fig.6-4). Similar to Eqs.7-1, the effective band gaps for AlGaP/GaP and AlP/AlGaP SLs are given by following equations.

$$E_{AlGaP/GaP} = E_{GaP} - \Delta E'_c + (E'_{c1} + E'_{hh1}) \quad (7\text{-}2a)$$

$$= E_{AlGaP} - \Delta E'_v + (E'_{c1} + E'_{hh1}) \quad (7\text{-}2b)$$

$$E_{AlP/AlGaP} = E_{AlGaP} - \Delta E''_c + (E''_{c1} + E''_{hh1}) \quad (7\text{-}3a)$$

$$= E_{AlP} - \Delta E''_v + (E''_{c1} + E''_{hh1}) \quad (7\text{-}3b)$$

The symbols have the same meanings as in Figs.7-7. Comparing Eqs.7-1(a) and 7-2(a), we can find that $E_{AlGaP/GaP}$ is larger than $E_{AlP/GaP}$ since band discontinuity ΔE_c is larger in AlP/GaP SL. Similarly $E_{AlP/AlGaP}$ becomes larger than $E_{AlP/GaP}$. The subband levels also change when band discontinuities are changed.

however, the change in subband are not so large as that of band discontinuities. As results, the peak wavelengths of AlGaP/GaP and AlP/AlGaP SLs become shorter than that of corresponding AlP/GaP SL. Figure 7-8 shows the peak wavelength of $Al_xGa_{1-x}P$/GaP and AlP/$Al_yGa_{1-y}P$ o-SLs as a function of Al composition in AlGaP layer calculated by Kronig-Penny model. In the calculation, band gap of AlGaP alloy and band discontinuities in conduction and valence bands were linearly interpolated by those parameters of GaP and AlP. The peak wavelength is the longest at AlP/GaP as expected and approaches the band gap wavelength of GaP as Al composition decreases in AlGaP/GaP o-SLs, while wavelength approaches the band gap wavelength of AlP as Al composition increases in AlP/AlGaP o-SLs. The change in wavelength of AlGaP/AlGaP SL is remarkable as SL period becomes long, because subband levels are pushed up when the well width is narrow and the effective band gap of SL resembles that of AlGaP alloy.

The observed PL main peak wavelengths of AlGaP/GaP and AlP/GaP o-SLs shown in Fig.7-6 agree well with the calculation. It is considered that observed main peaks were not assisted by phonon emission from their strong intensities. Exciton binding energy may be neglected, since it is considerably small(~5meV). Besides main peaks, small peaks is seen at long wavelength in AlGaP/GaP o-SL. This peak is considered to be phonon replicas of main peak. The energy differences between small peak and main peak are 46.6meV. Although the phonon energy of AlP is unknown, the energy of LO-phonon in GaP is 45.6meV [4]. Here, we must remind that phonon dispersion relation is modified in growth direction. It is reported that zone-folding of phonon dispersion occurs in the SL structure [5]. Since SL is composed of 5ML-thick AlGaP and 9ML-thick GaP layers, the phonon dispersion between Γ and X points is 14 times folded. Then, energy of phonon along growth direction takes almost continuous values between minimum and maximum energy in bulk. However acoustical phonons such as TA- and LA-phonons, which have wide energy ranges, are less relative to the optical transitions, and LO-phonon is the dominant scattering factor. Energy dispersion of LO-phonon is almost constant between Γ and X points. Thus, phonon replica

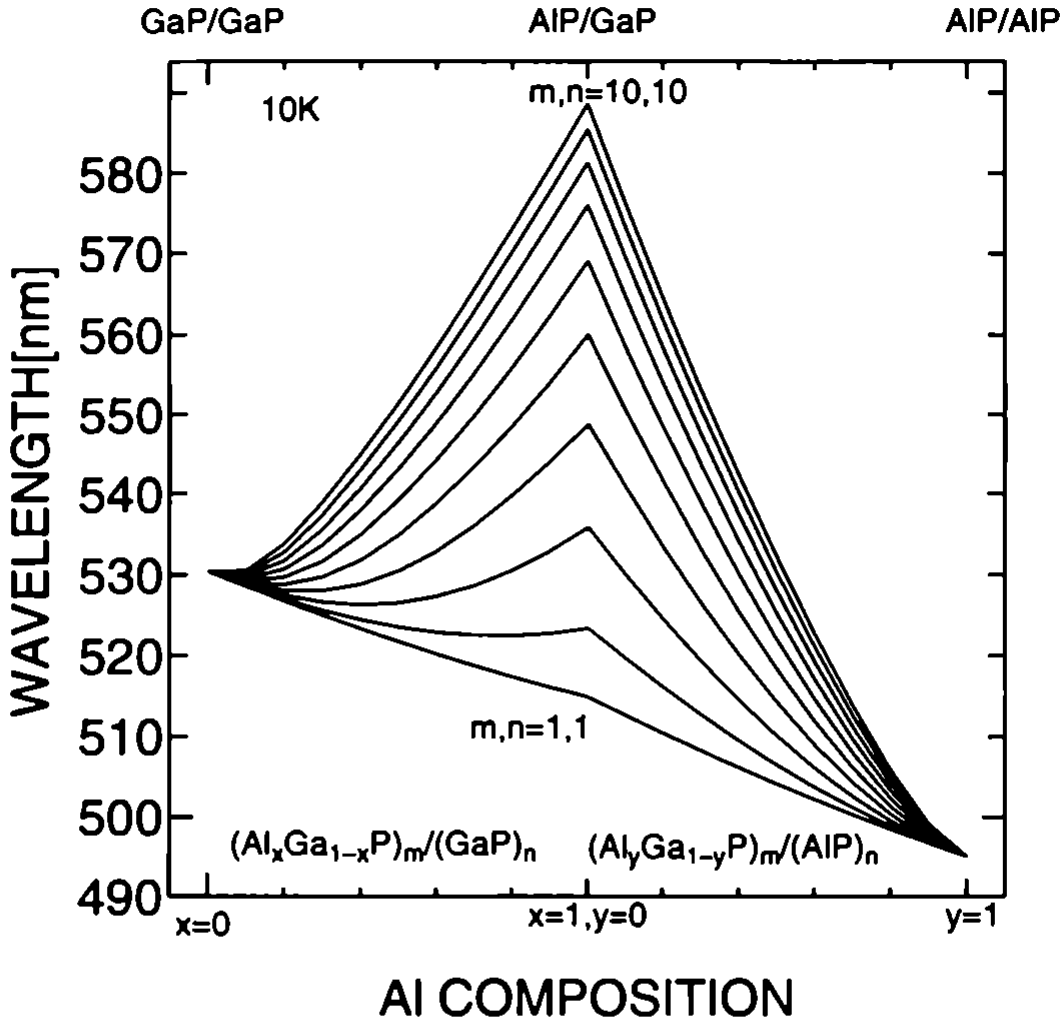

Fig.7-8 Peak wavelength of AlGaP/AlGaP o-SLs calculated by assuming Kronig-Penny model. Band gap of AlGaP and band discontinuities of AlGaP/GaP and AlP/AlGaP were linearly interpolated by those of AlP and GaP.

Table 7-2 Binding energies of typical impurities in GaP.

donor		acceptor	
impurity	E_b[meV]	impurity	E_b[meV]
Si	85	C	55
S	107	Zn	70
O	897	Si	210

with LO-phonon along growth direction must result in the same shift as with LO-phonon in lateral direction. Similar small peak is seen from AlP/GaP o-SL. However, the photon energy is 40.9meV lower from main peak and somewhat less than the LO-phonon energy. This peak can be attributed defect related recombination center as assigned by X.L. Wang et al. [6] rather than phonon replica. Contrary to the o-SLs, phonon replica is hardly seen in d-SL. The lack of phonon replica indicates the improved optical transition without phonon emission.

Temperature dependence of PL spectra of AlGaP/GaP o- and d-SLs are shown in Figs.7-9. As seen in Fig.7-9(a), the main peak at 549nm decreases quickly as temperature increases and disappears at 20K in AlGaP/GaP o-SL. The intensity of phonon replica also decreases. Another peak at 557nm becomes dominant. The energy difference with main peak is 32meV. The energy difference of 32meV is considerably smaller than binding energies of typical impurities in GaP summarized in Table 7-2. However, it is usual that the photon energy of DA par recombination emission becomes higher than the energy gap of donor and acceptor levels due to coulomb energy [7,8]. This peak is assigned as S-C DA pair recombination emission because similar peak was observed from S-doped GaP substrate.

Comparing o-SL, the temperature dependence of PL intensity from AlGaP/GaP d-SL is small. The main peak is clearly seen up to 30K in Fig.7-9(b). However, another peak located at 570nm becomes dominant beyond 40K. This peak is con-

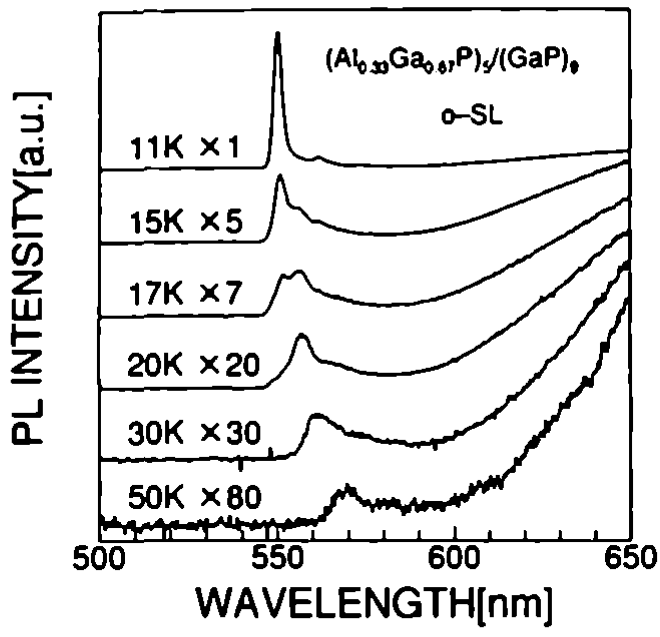

(a)

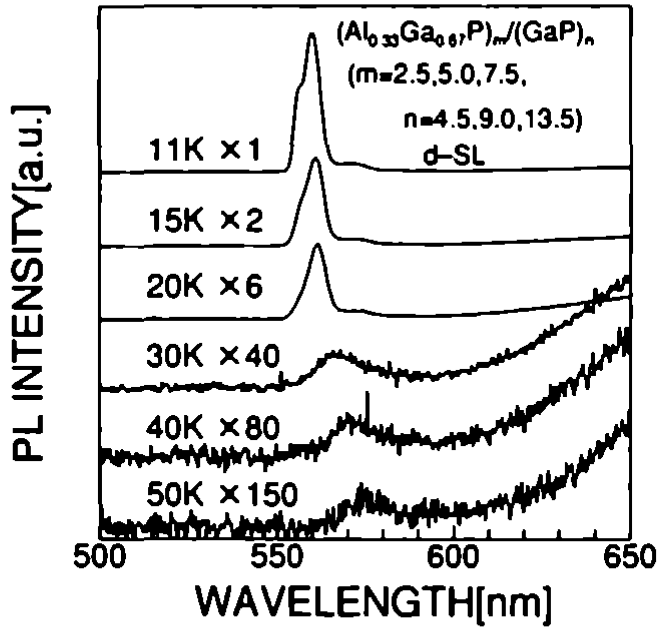

(b)

Fig.7-9 PL temperature dependence of (a)$(Al_{0.33}Ga_{0.67}P)_5/(GaP)_9$ o-SL and (b)$(Al_{0.33}Ga_{0.67}P)_m/(GaP)_n$ (m=2.5,5.0,7.5, n=4.5,9.0,13.5) d-SL.

sidered to be originated from impurities as that observed from o-SL. One can find that the small peak at slightly short wavelength from main peak decreases more quickly comparing main peak.

Figure 7-10 shows the integrated intensity of main peaks of AlGaP/GaP and AlP/GaP o- and d-SLs against temperature. Main peak of AlGaP/GaP d-SL were separated by assuming that the each peak is subjected to Gauss distribution. Although the SL period is different from others, PL temperature dependence of AlP_m/GaP_n (m,n=3,6,9) d-SL is also shown for comparison. From Fig.7-10, two important features are found, 1) PL integrated intensities of AlGaP/GaP o- and d-SLs decrease more quickly than those of AlP/GaP o- and d-SLs and 2)PL integrated intensities of AlGaP/GaP and AlP/GaP o-SLs decrease more quickly than those of d-SLs. These features become more evident by deriving characteristic temperature T_0 with Eq.6-4. Fitted T_0s are shown in Fig.7-11 as a function of Al composition in AlGaP layer. As expected, T_0s of AlGaP/GaP are less than those of AlP/GaP for both o- and d-SLs and T_0s of o-SLs are less than those of d-SLs.

Figure 7-11 indicates one more interesting feature. The difference of T_0 between o- and d-SLs is less in AlGaP/GaP than that in AlP/GaP. This is understood by the decrease of band discontinuity, in other words, barrier height. The distinction between o- and d-SLs is the arrangement of two constituent layer thickness, since disordered potential arrangement in d-SL causes certain localized states. If the chemical natures of two constituents are the same, o- and d-SLs would have the same properties. Thus, reducing Al composition in AlGaP layer weakens the carrier localization. As a result, the distinction between o- and d-SLs becomes small.

Finally we must consider the influence of unintentionally grown AlP layer found by X-ray diffraction measurements. Band structure taking fractional AlP layer into account is illustrated in Fig.7-12. Because of type-II structure, overlap of electron and hole wave functions are maximum at interface. Therefore carriers mainly recombinate at the interface to emit luminescence. In this case, AlP layer

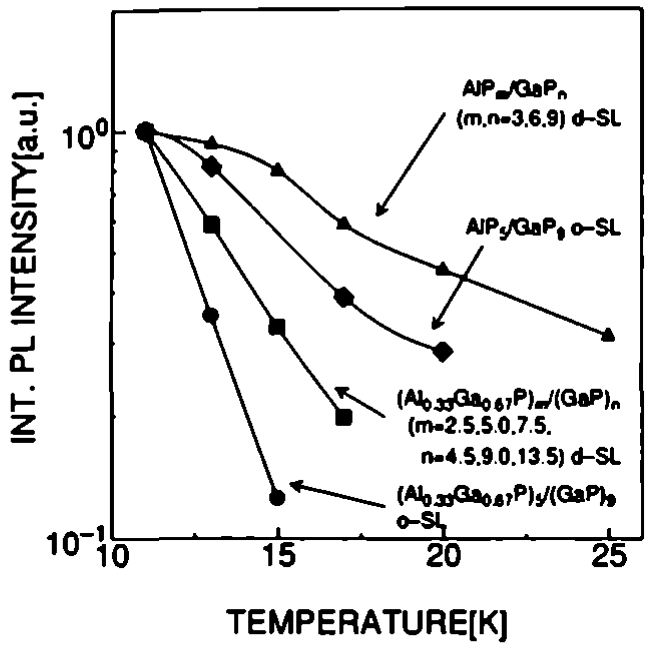

Fig.7-10 Integrated PL intensities of main peak of AlP_5/GaP_9 o-SL, AlP_m/GaP_n(m,n=3,6,9) d-SL, $(Al_{0.33}Ga_{0.67}P)_5/(GaP)_9$ o-SL and $(Al_{0.33}Ga_{0.67}P)_m/(GaP)_n$ (m=2.5,5.0,7.5, n=4.5,9.0,13.5) d-SL.

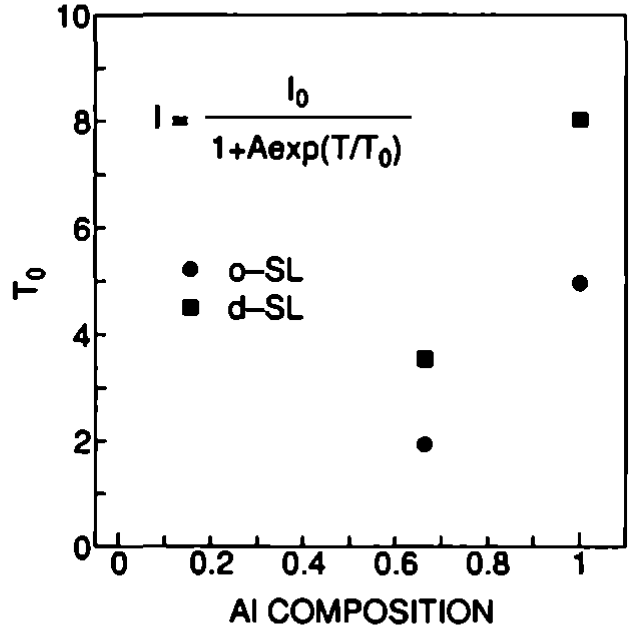

Fig.7-11 Characteristic temperature T_0s fitted by Eq.6-4.

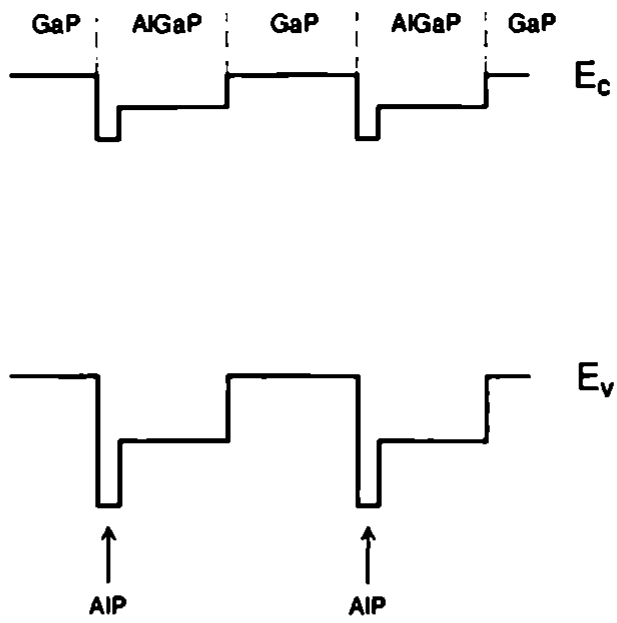

Fig.7-12 Band structure of AlGaP/GaP SL with unintentional AlP layer inserted at the interface of GaP and AlGaP.

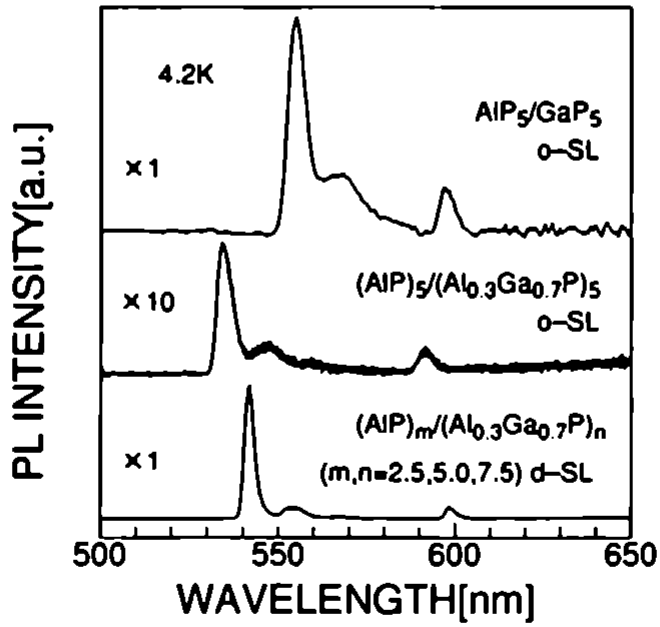

Fig.7-13 PL spectra of $(AlP)_5/(Al_{0.33}Ga_{0.67}P)_5$ o-SL and $(AlP)_m/(Al_{0.33}Ga_{0.67}P)_n$ (m,n=2.5,5.0,7.5) d-SL together with AlP_5/GaP_5 o-SL for comparison. Measurement temperature was 4.2K.

at the interface works as QW for electron since potential in AlP is lower than both GaP and AlGaP layers in conduction band. This situation seems to the quasi type-I structure and similar to neighboring confinement structure proposed by F. Isshiki et al [9]. They have grown AlP/GaP single heterostructure sandwiched by AlGaP layers. In their structure, AlGaP works as barrier for both electron and hole. Then the overlap of electron and hole wave functions becomes larger at the AlP/GaP interface and the luminescence efficiency is enhanced. Not only luminescence intensity, the effective band gap is also affected by the fractional AlP layer. However, significant discrepancy was not observed in PL wavelength between experimental and calculated results. Therefore, unintentional AlP layer may not cause strong enhancement of luminescence efficiency nor wavelength shift since the layer thickness is less than 1ML.

7.3.2 AlP/AlGaP superlattices

Observed PL spectra of AlP/AlGaP superlattices are shown in Fig.7-13 together with corresponding AlP/GaP o-SL. Peak wavelengths of $(AlP)_5/(Al_{0.3}Ga_{0.7}P)_5$ o-SL and $(AlP)_m/(Al_{0.3}Ga_{0.7}P)_n$ (m,n=2.5,5.0,7.5) d-SL are shorter than that of AlP/GaP o-SL as expected. The PL intensity of AlP/AlGaP d-SL is 10 times stronger than that of AlP/AlGaP o-SL but is 70% of AlP/GaP o-SL. The peak wavelengths of o-SLs agree consistently with the calculated results by assuming Kronig-Penny model. Similar to the AlGaP/GaP SLs in previous subsection, impurity related peaks are observed from all samples. Besides these small peaks, one can see other peaks at about 600nm. These peaks are assigned as defect related recombination [6].

The shortest PL wavelength among the grown AlP/AlGaP SLs was 532nm, which is from $(AlP)_5/(Al_{0.3}Ga_{0.7}P)_5$ o-SL. This wavelength is slightly longer than the wavelength of band edge luminescence of bulk GaP(530nm), but is shorter than the PL wavelength of N-doped bulk GaP(535nm). In order to shorten the luminescence wavelength, we have grown $(AlP)_5/(Al_{0.5}Ga_{0.5}P)_5$ o-SL and

$(AlP)_m/(Al_{0.5}Ga_{0.5}P)_n$ (m,n=2.5,5.0,7.5) d-SL. However, clear luminescence was not observed from both samples.

We also attempted to investigate the temperature dependence of PL, but, PL intensities decrease so quickly that the reliable data was not obtained.

The poor luminescence property of AlP/AlGaP SLs can be partly attributed to the small band discontinuity compared to AlP/GaP. Another reason is the high Al composition in the SL. Even the Al composition in AlGaP layer is 0.3, average Al composition in AlP/AlGaP SL becomes 0.65 when the layer thicknesses of AlP and AlGaP are equal. As for $AlP/Al_{0.5}Ga_{0.5}P$ SLs, average Al composition is 0.75. It is generally recognized that concentration of O increases with increasing Al composition in III -V semiconductors. Mostly, O impurity forms a deep donor level which works as a non-radiative recombination center by itself. One may consider that the Al composition in AlGaP layer does not crucially degrade the optical property, since SL composed of AlGaP system is type-II where electrons are confined in AlP layer in AlP/AlGaP SLs. However the lowest first subband in conduction band of $(AlP)_5/(Al_{0.3}Ga_{0.7}P)_5$ o-SL is estimated as 46meV from conduction band minimum of AlP. Considering that the band discontinuity in conduction band is 75meV, wave function of electron distributes not only in AlP layer but also in AlGaP layer. Then, the concentration of non-radiative center in AlGaP layer becomes less negligible, because the carriers recombinate mainly at the interface. D-SLs is advantageous when the deep impurity concentration is high, because the carriers are localized in certain space and cannot move freely and non-radiative recombination is suppressed.

7.4 Summary

In this chapter, we have grown AlGaP/GaP and AlP/AlGaP o- and d-SLs to investigate the relation between PL property and band discontinuity and to shorten the luminescence wavelength.

From X-ray diffraction measurement, it was found that fractional layer of AlP

was grown between GaP and AlGaP layers in AlGaP/GaP SLs by comparing experimental results and simulation based on dynamical theory. The origin of AlP layer was explained by delay of TMGa flow during AlGaP layer growth. On the contrary, unintentionally grown AlP layer does not become serious problem in AlP/AlGaP superlattices.

The PL intensity of AlGaP/GaP d-SL was four times stronger than that of AlGaP/GaP o-SL and almost the same as corresponding AlP/GaP o-SL. The PL wavelengths of AlGaP/GaP o- and d-SLs were shorter than that of AlP/GaP o-SLs. The wavelengths of AlGaP/GaP and AlP/GaP o-SLs agreed well with the calculated results based on Kronig-Penny model. The PL temperature dependence showed that the PL intensities of AlGaP/GaP o- and d-SLs decreased more quickly than those of AlP/GaP o- and d-SLs, though somewhat persistent luminescence was observed from d-SL. It was found that the band discontinuity plays important role, since difference of characteristic temperatures T_0 is less in AlGaP/GaP o- and d-SLs than that in AlP/GaP.

The PL wavelength of AlP/AlGaP o- and d-SL was considerably shorter than that of corresponding AlP/GaP o-SL. The pure green shortest wavelength of 532nm was observed from $(AlP)_5/(Al_{0.3}Ga_{0.7}P)_5$ o-SL. This wavelength is shorter than that of N-doped GaP bulk, 535nm at 4.2K. However, the luminescence property was degraded by deep level impurities with increase of Al composition.

For further study and device application, the luminescence intensity of d-SL should be quantitatively characterized, for example, by measurement of quantum efficiency.

References

1) X.L. Wang, A. Wakahara, and A. Sasaki, J. Cryst. Growth **129**, 289 (1993).
2) X.L. Wang, A. Wakahara, and A. Sasaki, Jpn. J. Appl. Phys. **33**, 5671 (1994).
3) A. Morii, H. Okagawa, K. Hara, J. Yoshino, and H. Kukimoto, Jpn. J. Appl. Phys. **31** L1161 (1992).
4) Landolt-Börnstein Numerical Data and Fundamental Relationshis in Science and Technology. Vol.17a Editted by O. Madelung(Springer-Verlag, Berlin, 1982).
5) M. Nakayama, K. Kubota, T. Kanata, H. Kato, and N. Sano, Jpn. J. Appl. Phys. **24**, 1331 (1985).
6) X.L. Wang, A. Wakahara, and A. Sasaki, J. Appl. Phys. **76**, 524 (1994).
7) J.I. Pankove, *Optical Processes in Semiconductors*(Dover, 1971).
8) P.J. Dean, C.J. Frosch, and C.H. Henry, J. Appl. Phys. **39**, 5631 (1968).
9) F. Issiki, S. Fukatsu, and Y. Shiraki, Appl. Phys. Lett. **67**, 1048 (1995).

Chapter 8

Conclusion

In this thesis, mesoscopic structures composed of III-V semiconductors has been investigated to obtain new quantum optical properties. Self-assembled QD was fabricated by lattice-mismatched heteroepitaxy of InAs/GaAs and investigated their optical property as a three-dimensional quantum structure, in other words, QD which has been difficult to fabricate. On the other hands, AlGaP/AlGaP d-SLs were investigated to enhance the quantum effect in one-dimensional quantum structure.

In chapter 2, InAs was grown on GaAs substrate by MBE and the structure of epitaxial InAs was characterized. *In-situ* RHEED observation showed that growth mode of InAs on GaAs changes from two-dimensionally to three-dimensionally at 1.8ML. From AFM observation, small island was formed abruptly at 1.8ML. The island size was 250Å in diameter and 30Å in height. Increasing InAs layer thickness, small islands coalesce each other to form large island of 400Å . TEM images of these samples have shown that no dislocations were found in the small island while Lomer-lock edge dislocations were generated in large island. The sizes of small island measured from TEM image were 150Å along [1$\bar{1}$0] direction and 133Å along [110] direction. The density was as high as $1.1\times10^{11}cm^{-2}$ in the growth plane.

In chapter 3, the transition thickness at which the growth mode changes was

calculated based on Wulff's theorem. As results, the calculated transition thicknesses of InGaAs/GaAs were somewhat smaller than experimental results. The discrepancy was attributed to the neglect of total energy in island and non-equilibrium growth condition. However, precise thickness was predicted by adding certain value to the strain energy. The strain distribution in island was also calculated. As results, strain distribution in embedded island in GaAs was considerably different from that in island with free surface.

The optical property of InAs on GaAs was widely investigated in chapter 4. From PL measurement, it was found that the luminescence spectra strongly depend on the structure of InAs; sharp peak was observed when InAs grew two-dimensionally, on the other hands, the FWHM became comparatively large as 80meV from InAs small islands. Luminescence from island was also observed from 1.5ML-thick InAs in which no island was confirmed by structural characterizations. The large FWHM was attributed to the fluctuation in the island size. Strong polarization was observed in luminescence from island, though the origin is unknown. Large island containing misfit dislocations was not concerned with luminescence. 1ML-thick InAs wetting layer was found when island was already formed by EL and PC measurement. Since wavelength of luminescence from island was much shorter than that calculated for SQW assuming the well width was equal to island height, InAs island has an ability of lateral carrier confinement.

In chapter 5, dislocation suppression on misoriented substrate was shown experimentally and theoretically. PL and plan-view TEM observations revealed that the critical thickness of InAs was increased to 5ML on substrate misoriented toward $[1\bar{1}0]$ direction, on the contrary, critical thickness on substrate misoriented toward [110] direction was 3ML and the same as that on just-oriented substrate. Increase of critical layer was partly explained by suppression of island coalescence on misoriented substrate. In order to investigate the interaction of dislocation and surface step, strain energy around the cross of dislocation and step was calculated by VFF model. As results, it was found that certain strain was generated at the step because of the unnatural slip plane connection.

In chapter 6, short period AlP/GaP o- and d-SLs were fabricated by OMVPE to enhance quantum effect in one-dimensional quantum structure. The PL wavelength became shorter as the SL period decreases for both o- and d-SLs. Clear peak was observed from AlP_m/GaP_n(m,n=1,2,3) d-SL while luminescence intensity was very weak from AlP_2/GaP_2 o-SL. Temperature dependence of PL intensity of AlP/GaP d-SLs was not sensitive to the average layer thickness.

In order to investigate the optical property of AlGaP SLs with respect to the band discontinuity, AlGaP/GaP and AlP/AlGaP o- and d-SLs were fabricated in chapter 7. From X-ray diffraction, it was found that unintentional fractional layer of AlP was grown at the beginning of AlGaP layer growth. The luminescence wavelength was shorter from AlGaP/GaP and AlP/AlGaP SLs than those from corresponding AlP/GaP SLs due to type-II structure. The shortest wavelength was obtained from $(AlP)_5/(Al_{0.3}Ga_{0.7}P)_5$ o-SL. PL intensities of d-SLs were stronger than those of corresponding o-SLs. PL from AlGaP/GaP o- and d-SLs quenched more rapidly than those from AlP/GaP o- and d-SLs, respectively and PL from AlGaP/GaP and AlP/GaP o-SLs quenched more rapidly than those from AlGaP/GaP and AlP/GaP d-SLs.

Although new quantum effect structures were proposed and realized in this thesis, some future works are still suggested as follows.

1) The size and position of island should be controlled to apply self-assembled QD to optical devices such as LD. As shown in chapter 5, step on substrate surface is a favorable site for the island formation. Therefore island growth on slightly misoriented substrate is intensively investigated recently. It is also reported that island are arrayed in the growth direction by stacking self-assembled QD plane with appropriate spacer layer similar to MQW; island in the upper layer is formed on island in the lower layer. Thus, strain distribution in surface plane plays important role for the island formation. In this case, however, the position of islands in each plane is determined by the position of island in the first plane. In order to control the position of island in the first plane, some substrate surface treatment is required, for example, certain amount of In atoms are selectively adsorbed on

substrate by manipulation technique of STM and then InAs layer is grown on it.
2) Energy state and wave function in QD should be theoretical calculated. Although there are some restrictions, effective mass approximation is the easiest calculation method for one-dimensional quantum structure such as QW. However, this approach is not applicable for two- and three-dimensional quantum structures with finite barrier height. One approach is that the wave function is expanded to a series of ortho-normalized plane waves and solve the boundary condition problem. However, as revealed in chapter 3, strain distribution in island is not uniform and this approach becomes complicated. Since we know the positions of all atoms, it is expected to elucidate the energy states by tight binding method.
3) Although the enhanced luminescence efficiency of d-SL was shown, the precise mechanism is not clarified. Because AlGaP alloy and SL composed by AlGaP system has suitable band gap for green to orange colored visible light, more precise investigation of band structure is expected. For example, photoluminescence excitation(PLE) or carrier life time measurements should be carried out. At the same time, the quantitative measurement of luminescence intensity such as quantum efficiency is required for device application.

ADDENDUM

Publications

A. Full papers

1. "Initial growth stage and optical properties of three-dimensional InAs structure on GaAs",
   Y. Nabetani, T. Ishikawa, S. Noda, and A. Sasaki,
   J. Appl. Phys. **76**, 347 (1994).

2. "Molecular beam epitaxy of InAs and its interaction with a GaAs overlayer on vicinal GaAs (001) substrates",
   X.W. Lin, Z. Liliental-Weber, J. Washburn, E.R. Weber, A. Sasaki, A. Wakahara, and Y. Nabetani,
   J. Vac. Sci. Technol. **B12**, 2562 (1994).

3. "Photoluminescence process in AlP/GaP short period superlattices grown by organometallic vapor phase epitaxy using tertiarybuthylphosphine",
   A. Wakahara, Y. Nabetani, X.L. Wang, and A. Sasaki,
   J. Cryst. Growth **145**, 187 (1994).

4. "Island formation of InAs grown on GaAs",
   Y. Nabetani, N. Yamamoto, T. Tokuda, and A. Sasaki,
   J. Cryst. Growth **146**, 363 (1995).

5. "Critical thickness of InAs grown on misoriented GaAs substrates",
   Y. Nabetani, A. Wakahara, and A. Sasaki,
   J. Appl. Phys. **78**, 6461 (1995).

6. "Photoluminescence properties of AlGaP superlattices",
   Y. Nabetani, A. Wakahara, and A. Sasaki,
   Mat. Sci. Eng. **B35**, 454 (1995).

7. "Growth and photoluminescence properties of AlGaP/AlGaP superlattices", Y. Nabetani, A. Wakahara, and A. Sasaki, J. Appl. Phys. to be submitted.

B. Letters

1. "Morphological transition of InAs islands on GaAs(001) upon deposition of a GaAs capping layer", X.W.Lin, J. Washburn, Z. Liliental-Weber, E.R. Weber, A. Sasaki, A. Wakahara, and Y. Nabetani, Appl. Phys. Lett. **65**, 1677 (1994).

2. "Electroluminescence from self-assembled InAs quantum dot grown on GaAs", Y. Nabetani, N. Yamamoto, T. Tokuda, S. Noda, and A. Sasaki, Appl. Phys. Lett. to be submitted.

3. "Calculation of transition layer thickness in InAs on GaAs", Y. Nabetani, A. Wakahara, and A. Sasaki, Appl. Phys. Lett. to be submitted.

C. International conferences

1. "Island formation of InAs grown on GaAs", Y. Nabetani, N. Yamamoto, T. Tokuda, and A. Sasaki, Eighth International Conference on Vapor Growth and Epitaxy(ICVGE8), Freiburg, Germany, 1994,

2. "Photoluminescence properties of AlGaP superlattices", Y. Nabetani, A. Wakahara, and A. Sasaki,

The First International Conference on Low Dimensional Structures & Devices(LDSD95), Singapore, 1995

3. "Photoluminescence properties of AlGaP/GaP superlattices",
Y. Nabetani, A. Wakahara, and A. Sasaki,
37th Electronic Materials Conference(EMC), Virginia, USA, 1995